UNIVERSITÀ DEGLI STUDI DI PALERMO
DIPARTIMENTO DI ENERGIA, INGEGNERIA DELL'INFORMAZIONE
E MODELLI MATEMATICI
Dottorato di Ricerca in Ingegneria Elettrica, Elettronica e delle Telecomunicazioni, Matematica e Automatica - indirizzo: Ingegneria Elettronica e delle Telecomunicazioni
Settore Scientifico Disciplinare ING-INF/01

Hybrid White Light Emitting Diodes: Study and Fabrication of Thin-Film and Nanowire-Based Devices

IL CANDIDATO
FULVIO CARUSO

IL COORDINATORE
PROF. MARIA STELLA MONGIOVÌ

IL TUTOR
ING. MAURO MOSCA

CICLO XXVI - ANNO CONSEGUIMENTO TITOLO: 2015

DOTTORATO

” I hope you'll be as lucky as I am. The world needs inventors – great ones. You can be one. If you love what you do and are willing to do what it takes, it's within your reach. And it'll be worth every minute you spend alone at night, thinking and thinking about what it is you want to design or build. It'll be worth it, I promise.

STEVE WOZNIAK

(Electronic Engineer and founder of Apple Computer Co.)

Abstract

Light emitting diodes are very compact and durable semiconductor devices that possess extraordinary physical properties for the generation of light. The white LED quietly moved from the middle of the 1990s to a point where, today, the lighting market is completely revolutionized. With the industry of solid state lighting demanding for always brighter and economic LEDs, the scientific research responds with innovative layouts and more efficient materials also mixed with applied nanotechnologies. Hybrid white light emitting diodes, for example, also use blue LEDs but replace the conventional inorganic material for color conversion with an organic dye that has a higher quantum conversion yield. The combination of a nanostructured blue light source with organic dyes can lead to another interesting structure that it is worth investigating on.

In this work, two layouts for novel hybrid white light emitting diodes were designed, fabricated and characterized. The first one consisted in a heterojunction ZnO/GaN nanowire-based hybrid device that showed an easy processing with a low-cost acqueous solution growth technique; the color conversion achieved with an organic perylene-based yellow dye coating led to the realization of a cold white hybrid LED. The second device exploited the properties of the organic conversion layer at the maximum of its capabilities with the use of an high-brightness GaN/InGaN blue pump source. Moreover, mixing yellow and red organic dyes resulted in the color tuning of the hybrid structure's emission. Finally, a detailed study of the conversion layer stability was also reported together with the solutions that can be adopted to obtain the best performances out of the hybrid white light emitting diode.

Sommario

I diodi ad emissione luminosa sono dei dispositivi a semiconduttore che posseggono straordinarie proprietà fisiche di generazione della luce. Il primo LED bianco si è mosso silenziosamente dalla metà degli anni 90 fino a un punto in cui, oggi, il mercato dell'illuminazione è stato totalmente rivoluzionato. A fronte dell'industria dell'illuminazione a stato solido che richiede LED sempre più luminosi ed economici, la ricerca scientifica risponde con strutture innovative, nuovi materiali più efficienti, anche combinati con l'uso delle nanotecnologie applicate. I diodi bianchi ibridi ad emissione luminosa, ad esempio, fanno anch'essi uso di un LED blu, come in un tradizionale diodo bianco, ma in essi il materiale inorganico convenzionale per la conversione del colore è sostituito da un colorante organico cha una maggiore resa quantica. La combinazione di una sorgente blu nanostrutturata con tali coloranti costituisce un'interessante struttura non ancora esaustivamente studiata in letteratura.

In questo lavoro, due strutture per diodi bianchi ibridi innovativi sono state progettate, fabbricate e caratterizzate. La prima consiste in un dispositivo a eterogiunzione ZnO/GaN, basato su nanofili di ossido di zinco, ottenuto con una tecnica di crescita in soluzione acquosa a basso costo; la conversione del colore, ottenuta tramite un colorante organico giallo a base di perilene, ha portato alla realizzazione di un LED ibrido bianco a luce fredda. Il secondo dispositivo ha sfruttato al massimo le proprietà dello strato organico di conversione del colore, facendo uso di una sorgente blu di pompa basata su una struttura GaN/InGaN ad alta luminosità. Inoltre, combinando opportunamente coloranti organici gialli e rossi, è possibile ottenere il controllo fine sul colore di emissione della struttura ibrida. Infine, viene presentato uno studio dettagliato sulla stabilità dello strato di conversione, insieme ad alcune soluzioni che possono essere adottate per ottenere le migliori prestazioni dal diodo ibrido bianco.

Ringraziamenti

La lista delle persone da ringraziare, incontrate lungo il percorso formativo del mio dottorato di ricerca -benché lunga- non riuscirebbe ad esprimere adeguatamente il ruolo fondamentale che esse hanno avuto nella stesura di questa tesi.

Immensa gratitudine va alla mia famiglia (mia madre Angela, mio padre Antonino e mio fratello Ciccio) che mi ha pazientemente sostenuto nelle mie scelte professionali e personali, mai mancando di comprensione e ascolto nei miei confronti. Uno speciale ringraziamento va alla mia fidanzata Valentina, che mi ha sempre spronato ad andare avanti per la mia strada senza porre limiti emotivi a tutto ciò che abbiamo pazientemente costruito insieme con amore e sacrificio.

Desidero inoltre ringraziare il mio tutor l'Ing. Mauro Mosca, per avermi guidato nel percorso di ricerca, credendo nel mio operato e dandomi saggi consigli utili a maturare l'esperienza necessaria al conseguimento del titolo di Dottore di Ricerca. Ringrazio inoltre l'Ing. Roberto Macaluso per il supporto datomi ogni giorno e per tutto il lavoro svolto insieme in laboratorio. Ringrazio il Prof. Claudio Calì, responsabile del Thin Films Laboratory, e il Prof. Giuseppe Lullo, responsabile della Clean Room, per l'aiuto e i preziosi insegnamenti nell'ambito delle tecnologie dei semiconduttori e della fotonica applicata. Grazie a Gineuve, Andrea e Vincenzo, colleghi ai quali auguro un brillante futuro per il loro percorso di dottorato.

Grazie al Dr. Eric Feltin di NOVAGAN Sàrl per tutto il materiale fornito senza il quale questa tesi sarebbe rimasta solamente un'idea incompiuta.

Grazie infinite al Dr. Jesús Zúñiga-Pérez per avermi dato l'opportunità di svolgere cinque mesi nell'affascinante struttura del CRHEA al CNRS di Valbonne, in Francia. Un profondo "grazie" al direttore del CRHEA, Jean-Yves Duboz, e agli altri ricercatori che mi hanno seguito in prima persona, Philippe De Mierry e Mathieu Leroux. Grazie anche ai tecnici dei laboratori ed allo staff informatico ed amministrativo del CRHEA. Un ringraziamento va ai colleghi dottorandi e stagisti francesi, nonché cari amici, Michelle, Gema, Esther, Alejandro, Stanislav, Roy, Samuel, Rami, Meletis, Florian, Rémi, Mathieu, Kevin, Chao, Christopher e François.

Ringrazio i colleghi del dipartimento DICAM dell'Università degli Studi di Palermo, il Prof. Francesco Di Quarto, la Prof. Monica Santamaria e l'Ing. Francesco Di Franco per la collaborazione e per l'utilizzo del SEM e dell'XRD.

Grazie al Dott. Filippo Saiano, del Dipartimento SAF dell'Università degli Studi di Palermo, per la collaborazione nell'acquisizione e nello studio degli spettri FT-IR e UV-VIS.

Grazie a tutto il personale del gruppo di Physical Chemistry of Building Materials dell'ETH di Zurigo che ha messo a disposizione un microscopio SEM per l'acquisizione di alcune immagini presenti in questa tesi.

Infine, mi preme ringraziare tutti i tesisti del TFL che ho avuto l'opportunità di seguire con piacere, regalandomi un'apprezzatissima formazione didattica di base. Ringrazio tutti i colleghi e amici del Nuovo Gruppo Universitario Informatico, anche per avermi aiutato ogniqualvolta si siano verificati problemi informatici.

A tutti quelli che non ho menzionato ma che comunque hanno contribuito con il loro supporto allo sviluppo di questo lavoro: un sincero "grazie".

Contents

Introduction

1

White Light-Emitting Diodes (LED) represent one of the most revolutionary electronic devices that have a direct impact in human life for their application in the field of illumination. In the past 25 years, the progress in the techniques for the development of high-efficiency LEDs have opened a window to achieve the goal of solid-state lighting (SSL): within this scenario, the concept of "energy saving" has become a key point in today's technology. Recent studies show that the lighting industry in the European Union uses 218 TWh/year, which corresponds to the 15% of the overall EU consumption for electricity [1]. A clever policy of reduction in the utilization of such energy has become mandatory: according to the Collaborating Labeling and Appliance Standards Program (CLASP), by adopting 200 millions LED units per year in the EU, the energy consumption would decrease to 79 TWh/year within 2030 [2]. Thus, since the global market has been demanding for more efficient light sources, the research interest in new semiconductor materials with remarkable optoelectronic properties has significantly increased.

Recently, nanoscale materials have attracted much enthusiasm because of their great potential in several disciplines of applied sciences. In particular, functional nanostructured semiconductor oxides like zinc oxide (ZnO) have unique properties for the realization of useful electronic devices e.g. sensors, energy harvesters, nanogenerators. Zinc oxide also proved to be a good material for blue/violet light emission due to its wide direct band gap, large exciton binding energy at room temperature and other interesting transport properties. There are several techniques that can be used to fabricate ZnO nanostructures: among them, with an acqueous chemical growth (ACG) it is possible to obtain nanorods at low temperature and using low-cost materials. ZnO nanorods have high electrical and thermal conductivity and take advantage of a natural light waveguiding structure.

Unfortunately, obtaining a high-quality *p*-type ZnO for the production of homojunction diodes has been a major concern for the scientific community in the last decades. Nonetheless, zinc oxide has intrinsic donor defects such as zinc interstitials and oxygen vacancies that make it a promising candidate as *n*-type semiconductor [3], [4].

During the second half of the 1990s, LEDs based on gallium nitride (GaN) have dominated the scene of SSL since when Nakamura *et al.* refined the GaN crystal growth technique and demonstrated a reliable *p*-doping process that brought to the realization of the first high-efficiency blue light-emitting source [5].

Both ZnO and GaN have the same wurtzite crystal structure with a lattice mismatch that is only 1.8% and an energy bandgap for the two materials that is quite similar (3.37 eV for ZnO, 3.39 eV for GaN).

In the first part of this research work, it has been explored the possibility to combine a nanostructured *n*-ZnO layer on a *p*-GaN substrate to form a heterojunction LED: such a structure is meant to replace the diode used as a pump source in the most common white LEDs where the blue light, produced by a GaN/InGaN diode, excites the luminescence of a phosphor that re-emits yellow light [6]. The second part of this dissertation analyzes the performances of an organic dye used in place of the inorganic phosphor. In such a structure, known as Hybrid White LED (HWLED), there are several benefits related with the use of organic materials for light conversion, but one of the most important features is the conversion efficiency close to 100%, whereas for conventional phosphors is slightly over 90%.

This work is presented as follows. Chapter 2 deals with the lighting technology, defining the “white light” and the physical quantities used for determining its specifications. The techniques used for obtaining white LEDs for SSL purposes are presented, along with the functional description of an HWLED. Chapter 3 describes extensively the technology used to obtain an HWLED: the growth technique for GaN and ZnO, along with used the characterization processes, are reported in detail; the investigation on the the organic dyes, and their encapsulating polymers, is discussed by the end of the chapter. In chapter 4 the attention is focused on the device performances of two categories of HWLEDs used in this work: the first exploiting the ZnO nanostructures combined with a GaN substrate to realize an innovative blue LED and the second using a standard GaN/InGaN blue source. The chapter ends with the study of the color tuning achieved with mixed dyes. Chapter 5 deals with the stability of the organic dye in its embedding matrix used for the HWLED, and the solutions proposed for the improvement of the lifetime of the device. Finally, Chapter 6 presents the conclusion and the outlook of this research work.

Lighting Technology

2

2.1 White Light Definition

Strange as it may seem, there is no rigorous definition of “white light”. Ideally, a source that is emitting white light has an optical spectrum represented by an equal combination of all of the wavelength components in the visible range, with the same radiant power. The biggest source of natural white light, the sun, has an uneven distribution of the intensities of its spectral components (Fig. 2.1).

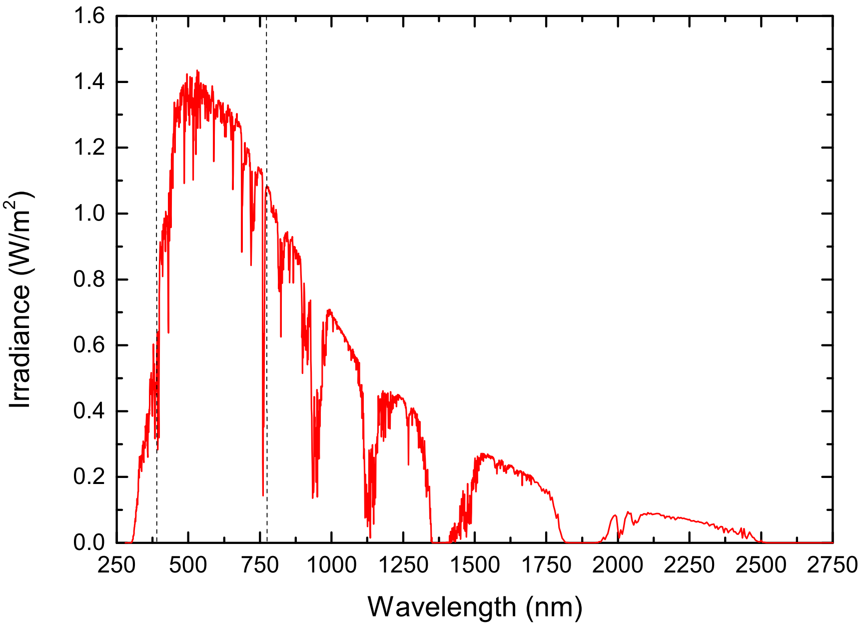

Fig. 2.1: Solar radiation spectrum at the sea level (according to ASTM G173-03): the range between the two dashed lines is the visible region.

One could notice that the solar spectrum has a relatively generous emission in the ultraviolet (UV) and in the infrared (IR), but since the human eye is not sensitive to these wavelengths, it is worthless trying to replicate the emission from the sun for general lighting purposes: basically, the spectrum of an artificial luminescent source needs to emit just in the visible range.

There are several techniques used to obtain a white-colored light from an LED (as it will be discussed more in detail in subsection 2.2.2), but all of them require a unique way to measure the optical power and the color of the source for illumination purposes.

2.1.1 Fundamental Photometric Quantities

Since light is an electromagnetic wave, the optical power of a radiating source requires to be studied with its appropriate theory: *radiometry* is the major field of physics that measures the electromagnetic radiation. Considering that the interaction of light with the human eye is limited to a specific portion of the electromagnetic spectrum, *photometry*, a subfield of radiometry, comes into help to define the light properties that humans can perceive.

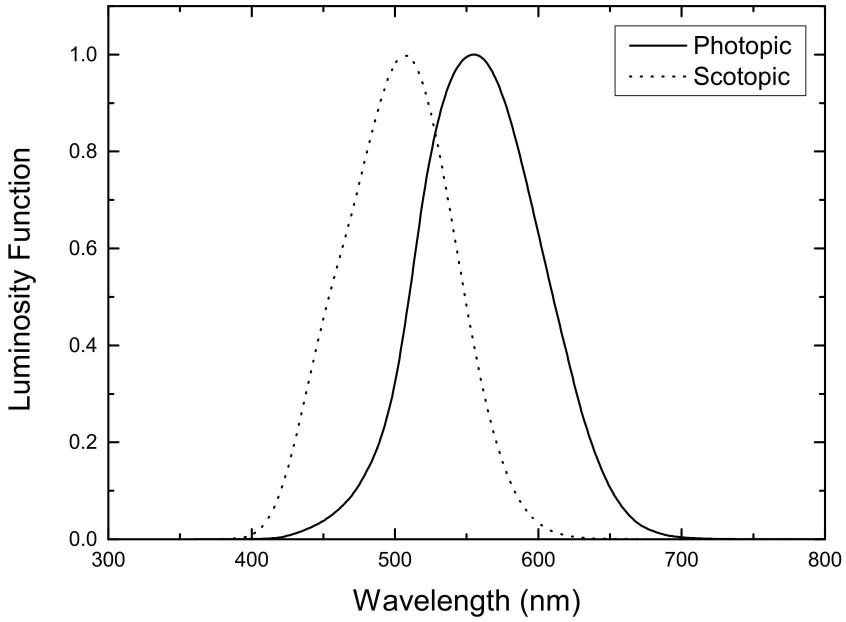

Fig. 2.2: Standard luminosity function for photopic (solid line) and scotopic (dotted line) vision.

Photometric quantities are used to measure the power of a source by keeping into account the sensitivity of the eye to different wavelengths. In 1924, the *Commission Internationale de l'Éclairage* (CIE) provided the data to form the luminosity functions that describe the human perception of brightness in light (photopic vision) and dark conditions (scotopic vision) [7]. The luminosity function, reported in Fig. 2.2, generated from different sets of data that were assembled together. Eventually, these data were slightly manipulated to symmetrize and smooth what some researchers claim to be “very divergent data” [8].

Nevertheless, the CIE 1924 function is today's most used curve to describe the physiological response of the eye to the light perceived. According to CIE, the luminosity function must be indicated with $V(\lambda)$.

All of the photometric quantities used to describe LED performances are mathematically related to the luminosity function. In the following sections, the most used quantities are presented and briefly described.

2.1.1.i Spectral Power Density

The spectral power density (SPD) represents the measured power per unit wavelength of a radiating source. In the case of LEDs, it is important to describe the absolute power of the emission spectra because they are not monochromatic sources. In this work, the SPD will be indicated with $P(\lambda)$.

2.1.1.ii Luminous Intensity and Luminous Flux

The luminous intensity is a measure of the optical power emitted by a source per unit wavelength and solid angle: this parameter must keep into account the luminosity function to weight the response of the human eye. The official definition of luminous intensity states that a monochromatic light at 555 nm emitting an optical power of (1/683) watt (W) into a solid angle of 1 steradian (sr) has a luminous intensity of 1 candela (cd). The calculation of this parameter requires the assumption of a point source or that, at least, its dimensions are negligible compared to the distance between the source and the detector used to measure the power. It has to be pointed out that the emission of light should also be isotropic or, more technically, *Lambertian*.

Although the luminous intensity is a physical quantity measured with one of the seven base units of the International System, the candela, the lighting industry rather prefers to adopt a parameter that considers the emission of a radiating source over a 4π solid angle: the luminous flux.

The formula for the calculation of the luminous flux is given by:

$$\Phi_v = K_m \int_\lambda V(\lambda) P(\lambda)\, d\lambda$$

where Φ_v is the luminous flux measured in lumen (lm) and K_m is a constant equal to 683 lm/W (dimensionally, 1 lm = 1 cd $\cdot$ sr).

2.1.1.iii Luminous Efficiency and Luminous Efficacy

There are different ways to estimate how well a radiating source is producing visible light but, due to the lack of an accepted standard, both in industry and in research there is still much confusion concerning the concepts of "luminous efficiency" and "luminous efficacy". While both of them are measured in (lm/W), the former defines the conversion from radiant optical power to luminous flux and the latter is an expression of how well the input electrical power of the device is converted to luminous flux. The definitions are the following:

$$\eta_e = \text{Luminous Efficiency} = \frac{\text{Luminous Flux}}{\text{Radiant Optical Power}} = \frac{\Phi_v}{P_{opt}} = \frac{\Phi_v}{\int_\lambda P(\lambda)\, d\lambda}$$

where P_{opt} is the total optical power of the source emitted in the whole electromagnetic spectrum, and:

$$\eta_v = \text{Luminous Efficacy} = \frac{\text{Luminous Flux}}{\text{Input Electrical Power}} = \frac{\Phi_v}{P_{el}} = \frac{\Phi_v}{I \cdot V}$$

where V and I are respectively the voltage and the current applied to the device. For the purposes of this work, only the luminous efficacy has been used.

2.1.2 Measuring Chromatic Properties of White Light

The science that studies the human color perception is named *colorimetry* and it can be considered as a specific subfield of photometry. The need for this applied science comes from actual physical considerations of the colors, like the angle of observation of the specimen or the illumination by an external source. Some other classifications originate from factors that are loosely related with optics or physics. Culturally speaking, for example, there is a wide debate about the proper words adopted for the color definition [9]: e.g. the work of *Brent and Kay* states that basic language systems only have a limited words for describing the colors, implicitly limiting the color gamut associated to that culture [10].

Of course, the lighting industry needs to adopt some parameters that could be measurable and reproducible by each light-emitting source manufacturer regardless of the cultural definition of that color or the entity of the source. In this section, the three most important chromatic quantities are defined to identify colors in a consistent way.

2.1.2.i Color Temperature and CCT

As mentioned in section 2.1, the solar radiation is not the most consistent source of white light that could be considered as a standard. Planck's black-body radiation spectrum, instead, can be used as a reference since its UV and IR components can be limited under certain conditions.

The black-body spectrum derived by Max Planck is given by the equation:

$$I(\lambda) = \frac{2hc^2}{\lambda^5 \left[exp\left(\frac{hc}{\lambda kT} \right) - 1 \right]}$$

The only parameter that defines the spectrum shape is the absolute temperature of the black-body (T) given in Kelvin; in Fig. 2.3 is shown the spectral intensity of the corresponding radiation.

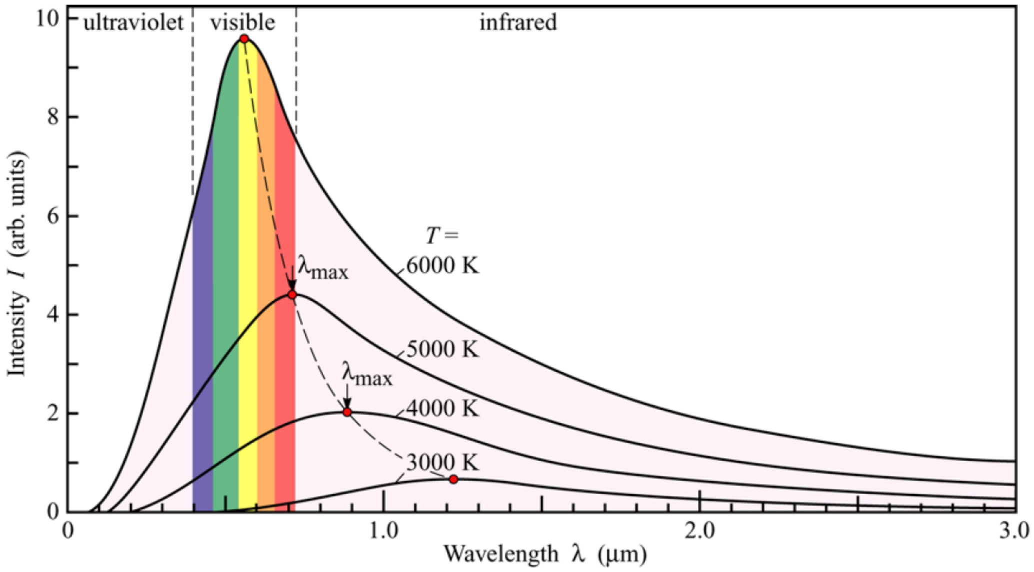

Fig. 2.3: Planckian black-body radiation as a function of wavelength for different temperatures [11].

Wien's Law describes the wavelength at which occurs the maximum intensity of the black-body spectrum, at a specific wavelength, as follows:

$$\lambda_{max} = \frac{2880}{T} \quad [\mu m]$$

Therefore, the color temperature of a white light source is referred to as the equivalent temperature of a black-body radiator that has the same chromatic properties as the analyzed source. It is usual for SSL devices not to have a white light emission for which the chromatic properties are exactly equivalent as those of Planck's black-body. Therefore the lighting industry has defined the correlated color temperature (CCT) as the temperature of the black-body radiator whose color is closest to the one of the analyzed source [12].

2.1.2.ii Color Rendering Index

Another useful measure for a white light source is its color rendering index (CRI). In other words, the ability of the source to render the true color of a physical objects illuminated by it. The higher the CRI, the better and more faithfully the color of the object are rendered in terms of vividness, whereas low-CRI sources can cause an object's color to look unnatural (Fig. 2.4). The calculation of the CRI is discussed in the next section.

Fig. 2.4: An example of (top) low-CRI source illumination and the same object when irradiated by a (bottom) high-CRI source. *(web source: www.digiolighting.com/cri - accessed on November 2015)*

2.1.2.iii CIE Chromatic Space

Like with the definition of the standard luminosity function, in 1931 the CIE has formulated a way to measure color with mathematical functions that represent the human perception of the three primary colors. The color-matching functions $\overline{x}(\lambda)$, $\overline{y}(\lambda)$, $\overline{z}(\lambda)$ (see Fig. 2.5) express the trichromacy character of the human eye's retina and are used for calculating the tristimulus values (X, Y, Z), which identify the color perception of a radiating source with a given $P(\lambda)$.

$$X = \int_{\lambda} \overline{x}(\lambda) P(\lambda) \, d(\lambda)$$
$$Y = \int_{\lambda} \overline{y}(\lambda) P(\lambda) \, d(\lambda)$$
$$Z = \int_{\lambda} \overline{z}(\lambda) P(\lambda) \, d(\lambda)$$

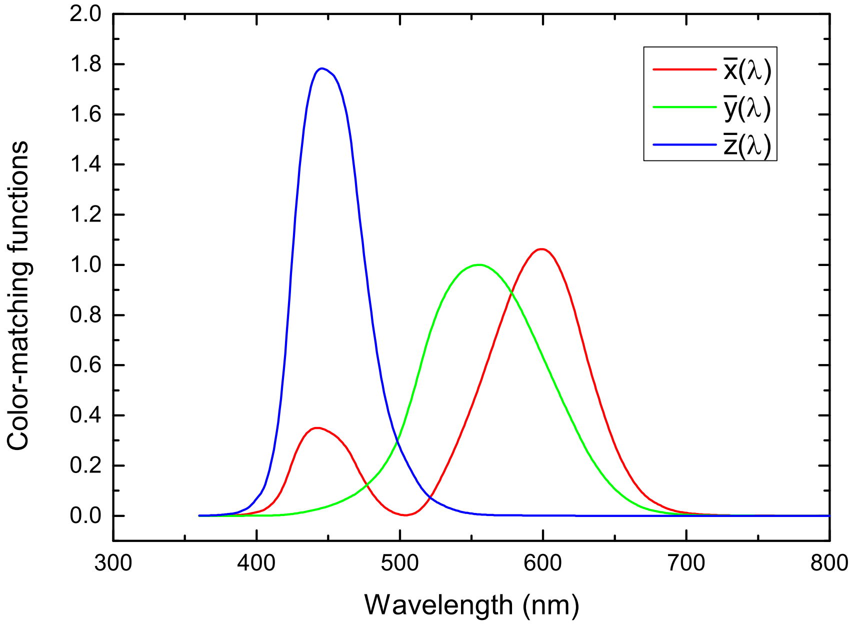

Fig. 2.5: CIE 1931 color-matching functions.

The tristmulus values, whose physical unit is Watt, can also be manipulated to become a dimensionless quantity suitable to be plotted on a graph that keeps into account two properties of the color: the dominant wavelength and the color purity. First, the chromaticity coordinates of a light source are calculated as follows:

$$x = \frac{X}{X+Y+Z}$$
$$y = \frac{Y}{X+Y+Z}$$
$$z = \frac{Z}{X+Y+Z} = 1 - x - y$$

then the resulting *(x;y)* point can be inserted in the CIE 1931 chromatic space (Fig. 2.6). A point on the border of the plot corresponds to a dominant wavelength which is identified by a monochromatic light source; as the point moves towards the center of the plot, the equal energy point *(x =1/3; y=1/3)*, the color purity varies accordingly (namely, the saturation of the color decreases).

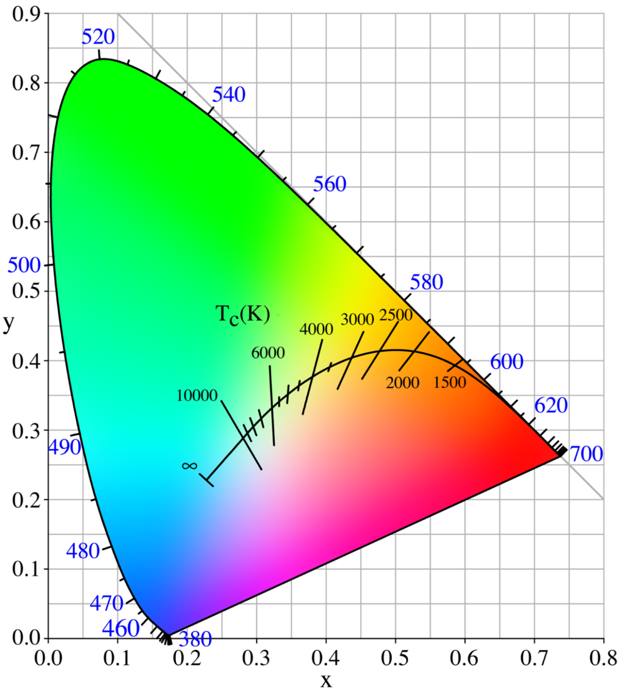

Fig. 2.6: CIE 1931 chromatic space. *(web source: https://it.wikipedia.org/wiki/Temperatura _di_colore - accessed on November 2015)*

From an electromagnetic point of view, on the border of the color space there are only spectral lines, whereas moving towards the center of the graph the spectrum broadens. A typical colored LED is not monochromatic, so the coordinates corresponding to its color stand very close to the border.

The curved line on the plot is known as the "planckian locus" and reflects the emission color of the black-body radiator for different temperatures. For white LEDs, the CCT is calculated as the temperature of the point on the planckian locus that is geometrically closer to the source's chromaticity coordinates. The CRI, instead, is defined as follows:

$$CRI = 100 - 4.6\,\Delta E^*$$

Where ΔE^* is the distance between the chromaticity coordinates of an object when illuminated by a reference source and when illuminated by the test source. Usually, the calculation of ΔE^* makes use of properly transformed coordinates in a chromatic space where geometrical distances between points are directly proportional to their chromatic difference, as recommended by CIE in 1976 [13].

2.2 Solid-State Lighting

The technologies of luminaires making use of incandescent and electrical discharge light bulbs have reached a point of evolution where their limits are very close. Despite the scientific progress in the field, these system have reached a maximum efficacy close to 100 lm/W leaving enough space for LEDs, with always increasing luminous efficacies, to offer better solutions. From the moment when high-brightness white LEDs became a reality in the optoelectronics semiconductor industry, the term "Solid-State Lighting" has marked a true revolution for the illumination companies that have now focused their research on the energetic and economic aspect of this technology.

Like Gordon Moore in 1965 defined a forecast for the processors' power to double approximately every two year [14], Ronald Haitz in 2003 observed that as the luminous flux generated by a single device should double every 18 to 24 months, the cost per lumen of said device should decrease (Fig. 2.7) [15].

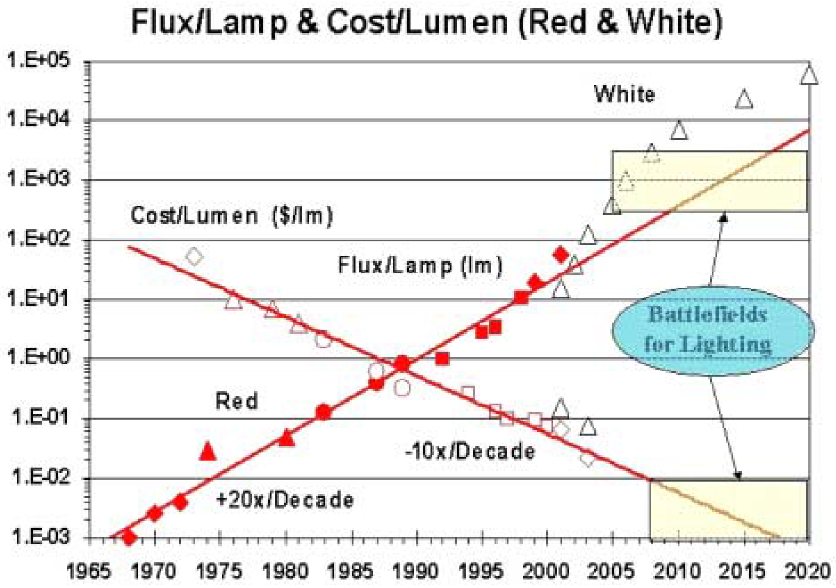

Fig. 2.7: "Haitz's Law" prediction for the luminous flux and the cost per lumen of an LED device [16].

At the beginning of this section, the comparisons between LED white light sources and the conventional luminaires were discussed, showing the physics and the techniques commonly adopted for generating white light from a diode. Then, the HWLED is briefly presented with a description of the difference between the two technologies and the motivations that push scientific research to develop innovative nanoscale light sources.

2.2.1 Comparison with Conventional White Light Sources

To better understand the efficiency properties of SSL, it is useful to give a simple example and make some calculations. A traditional 60 W incandescent light bulb has a luminous flux of 900 lm; if a standard high-power neutral white LED is considered, it typically delivers 90 lm at about 1 W. Then, to obtain the same luminous flux of the light bulb, it takes at least 10 LEDs, whose electrical power consumption is only 10 W.

Whereas the efficacy of LED systems is at least 5 to 6 times better than light bulbs, the cost of the luminaire has to keep into account the number of diodes employed to produce such an effective solution. Thus, the LED industry mainly focuses its attention on the development of high luminous efficacy sources to reduce the production costs. In Table 2.1, the characteristics of the most common lighting technologies on the market are summarized.

Tab. 2.1: Comparison between today's different lighting technologies [17].

Lamp Type	**Characteristics**				
	Luminous Efficacy (lm/W)	Lamp Life (h)	CRI	Cost of Installation	Cost of Operation
Incandescence	5-15	1000	100	Low	Very High
Halogen	12-35	2000-4000	100	Low	Very High
CFL	40-65	6000-12000	<85	Low	Low
Fluorescent tube	50-100	10000-16000	<95	Low	Low
High-pressure sodium	80-100	12000-16000	<30	High	Low
LED	20-120	20000-100000	>90	High	Low

2.2.2 Basics of LED Physics

LEDs are semiconductor devices that are based on the physical principle of the recombination of free carriers, injected in the depleted region of the diode, to form a quantum of light: the photon. The energy of the emitted photon is related to its wavelength by Planck's Law:

$$E = h\nu = \frac{hc}{\lambda}$$

where h is Planck's constant ($4.136 \cdot 10^{-15}$ eV·s), ν and λ are respectively the frequency and the wavelength of the photon, and c is the speed of light in vacuum.

The homojunction diode is composed by two pieces of the same semiconductor material that are oppositely doped: the *p*-type side is enriched by dopant atoms that cause an excess of free holes, wereas the *n*-type side has an excess of free electrons. When the two sides are brought into contact, the free charges diffuse from one side to the other where their concentration is lower, and a depletion region is formed beacuse the electrons coming from the *n*-side recombine with the holes in the *p*-type and vice-versa. Without an external bias, this process stops when the electric field, produced by the fixed ions of the depleted region, is strong enough to balance the effect of the diffusion and to generate a potential barrier that the free carriers have to overcome to reach the opposite neutral region. When a positive voltage is applied to the *p*-side (and, conversely, a negative voltage to the *n*-side), the barrier lowers and the free carriers can diffuse in the opposite region where they can recombine to emit a photon. The energy band diagram of the *p*-*n* junction with different bias conditions is outlined in Fig. 2.8.

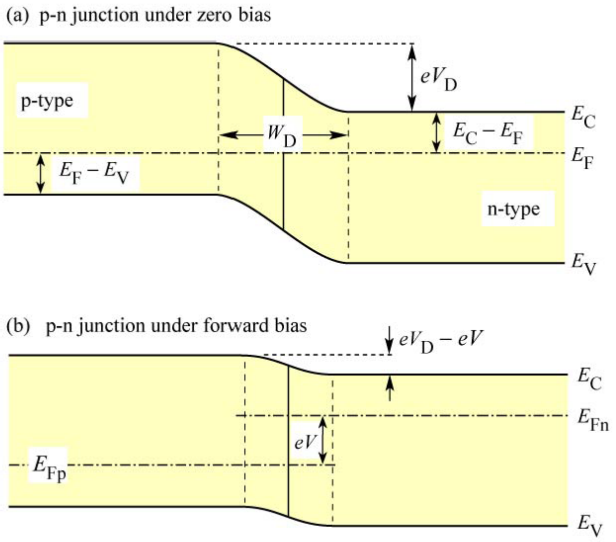

Fig. 2.8: Energy band diagram of a *p*-*n* junction with (a) no external bias and (b) a forward bias applied [11].

Independently of the applied bias, the energy bandgap (E_g) of the junction materials determines the wavelength of the emitted light. Thus, an ideal homojunction GaN diode would emit in the near UV region of the electromagnetic spectrum, being its bandgap close to 3.4 eV (and a corresponding emission wavelength around 365 nm). Other ternary compounds of GaN, like AlGaN or InGaN, can be exploited to obtain a more complex structure for the device and, at the same time, tuning the wavelength of the light emitted. GaN compounds that include aluminum (Al) have a higher energy bandgap with respect to pure GaN, whereas those containing indium (In) have a lower E_g (Fig. 2.9).

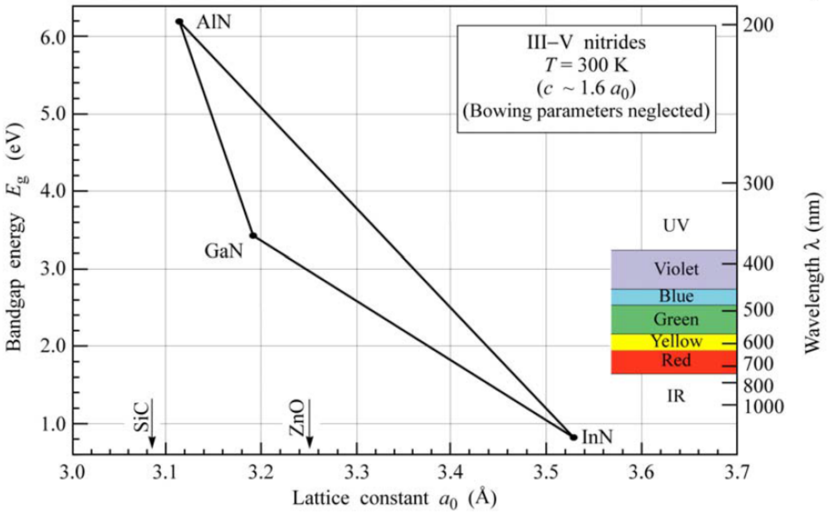

Fig. 2.9: Diagram of the energy bandgap for the AlGaN and InGaN ternary compounds [11].

Ideally, each electron injected in the depleted region recombines with a hole to produce a photon that is emitted in the free space, but this assumption is false in real diodes. For actual LEDs, the internal quantum efficiency (IQE) and the external quantum efficiency (EQE) are two important parameters that are defined as follows [11]:

$$IQE = \frac{\text{number of photons emitted from active region per second}}{\text{number of electrons injected into active region per second}}$$

$$EQE = \frac{\text{number of photons emitted into free space per second}}{\text{number of electrons injected into active region per second}}$$

The EQE must not be confused with the extraction efficiency η_{ext} that is defined as:

$$\eta_{ext} = \frac{\text{number of photons emitted into free space per second}}{\text{number of photons emitted from active region per second}}$$

And the relationship between the parameters is easily demonstrated:

$$EQE = IQE \cdot \eta_{ext}$$

2.2.3 Generation of White Light from LEDs

In this section, the working principles of the two techniques currently used in the LED technology industry to obtain white light are briefly described.

2.2.3.i Color Mixing

As mentioned in section 2.1, white light is generally intended as a combination of all wavelengths of the visible spectrum. Since LEDs produce monochromatic colors, the easiest way to obtain a white color is to mix the emissions of multiple diodes. This is generally achieved with two, three or four LEDs and -for this reasons- these devices are called dichromatic, trichromatic and tetrachromatic sources (Fig. 2.10).

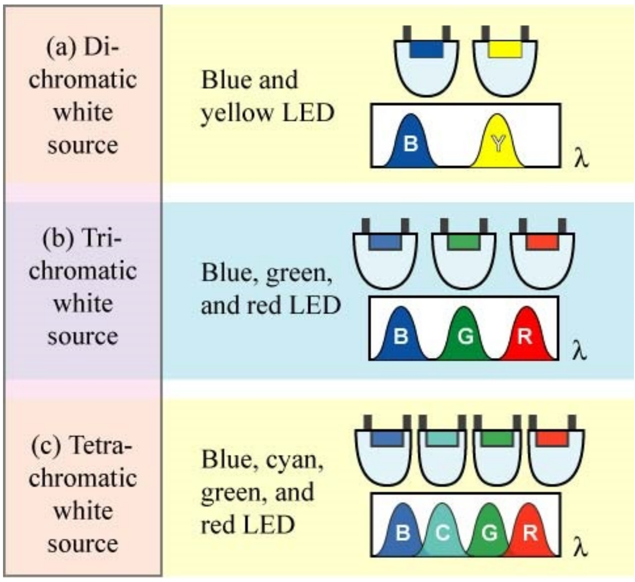

Fig. 2.10: Three approaches to obtain a color-mixed white LED: (a) dichromatic, (b) trichromatic and (c) tetrachromatic white sources [11].

Though dichromatic white sources are the less expensive solutions, the quality of the light is generally poor since the emission spectra of the single diodes have a relatively narrow band. In fact for simple LEDs, the full-width at half-maximum (FWHM) ranges from 20 nm up to 100 nm. The most common approach, in dichromatic sources, employs a blue and a yellow emission with a specific optical power ratio.

Trichromatic sources are the most common color mixed white LEDs that are found on the market and they are usually sold with the "RGB LED" label since the device incorporates a red (R), green (G), and a blue (B) light-emitting diode all in one package. In particular, Thornton [18] showed that the best combination of emission should use sources at 450 nm, 540 nm and 610 nm to obtain the best result in terms of CRI. However, the light of each diode can vary its intensity or even shift its emission wavelength when the operating temperature of the device increases.

Therefore, a specific electronic driver must be designed to keep into account the stability of the current fed to each LED.

Tetrachromatic white LEDs have, without any doubt, the best color-rendering performances but the luminous efficacy of polychromatic devices usually decreases with the increasing number of sources. Some tetrachromatic sources make use of an additional cyan or amber LED with respect to RGB devices.

2.2.3.ii Frequency Down-Conversion

To date, the most common technique adopted to obtain white LEDs is the frequency down-conversion: the device is made of an LED emitting at short wavelength (near-UV or blue) and a frequency converter material, which absorbs the light emitted by the source and re-emits it at a longer wavelength. The materials used for this purpose are known as “phosphors”: as an example, fluorescent lamps use an electrical discharge to excite mercury vapors that emit UV light, which is, in turn, absorbed by a coating made of europium (Eu) or terbium (Tb) inside the lamp tube and re-emitted between 400 nm and 700 nm.

While working at Nichia Corporation, Nakamura developed both the high-brightness blue LED and the first frequency down-converted white LED [6]. The phosphor that Nakamura used was an inorganic host (yttrium aluminum garnet, YAG) doped with cerium (Ce) which is a rare-earth element that acts as the optically active medium. The exact composition of the phosphor is still an intellectual property of Nichia. The device is based on a GaN/InGaN blue LED that is coated with a layer of Ce:YAG dispersed in a silicone or an epoxy resin (Fig. 2.11): the blue emission at 460 nm is absorbed and re-emitted in a broad-band between 500 nm and 650 nm.

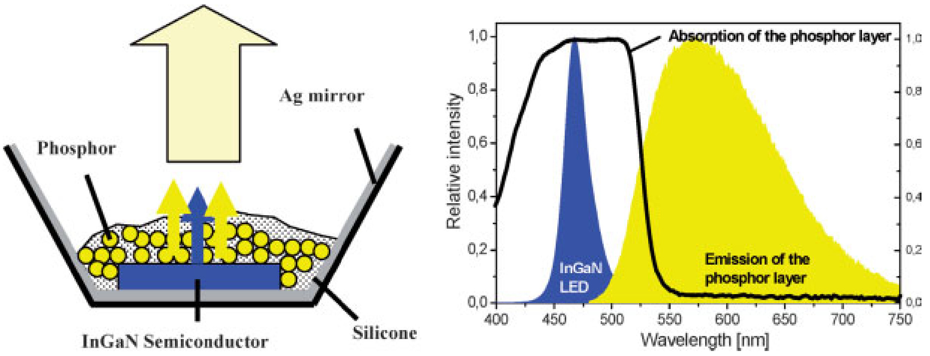

Fig. 2.11: Principle of operation in a phosphor down-converted white LED: (left) the device layout, (right) the emission and absorption spectra of the pump source and the phosphor [19].

The conversion efficiency of the first Ce:YAG phosphor employed was around 75% but an intensive research on host materials, and on alternative optically active elements, recently raised this value up to 90% and obtaining a high CRI [20]. In fact, a main drawback of using a single phosphor structure is the high color temperature of the produced white light (and the low value of CRI); to this problem there are other solutions commercially available today, like using an additional phosphor emitting in the red portion of the visible spectrum, or also changing the source pump replacing the blue diode with a near-UV LED which excites the emission of three blue, green and red phosphors.

An HWLED basically exploits the same device layout of the traditional frequency down-converted LED but, in this case, an organic dye replaces the inorganic phosphor as the wavelength converter. The conversion efficiency of a dye can show values close to 100% but several measures need to be taken into account to have a proper control of the light emission, the stability of the dye and a suitable encapsulation medium: the details about the preparation of an organic conversion layer, the performances of the HWLED and its stability will be discussed extensively in the next chapters of this work.

2.2.4 Motivations Beyond Nanoscale Light Sources

Besides adopting a more efficient frequency down-conversion material, the performances of a white LED may suffer of poor extraction efficiency that can seriously limit the EQE of the device. Several methods for improving the η_{ext} have been proposed during the years, like the use of double heterostructures, the shaping of the die or the texturing of the semiconductor surface: these last two methods have been intended to reduce the total internal reflection of the light emitted by the LED [11]. Nanoscale structures have extraordinary physical properties that can be adapted to the design of a high-efficiency light source. Nanorods, in particular, behave as a natural guiding cavity since the light's electromagnetic modes result well-confined in what can be considered as an ideal step-index waveguide. Unfortunately, obtaining nanostructures with controllable shape and position at low fabrication costs is still a major obstacle to the mass production of nanoscale optoelectronic devices.

However, the progresses in the study of the low-temperature aqueous chemical growth of zinc oxide nanorods [21] have opened wide application fields since ZnO is a good candidate for an heterojunction with GaN, considering their similar electronic and structural properties. Developing a nanorod/thin film structure has great potentials not only for lighting purposes but also for integrated optics and high resolution displays, thus there is a high interest in the industrial community for techniques capable of scaling up the process of nanofabrication.

3

Hybrid White Light Emitting Diodes Processing

3.1 Devices Layout

The configurations used for the design of an LED structure are somewhat limited. The main purpose of the technology adopted in III-nitride LED is to create a suitable device for the substrate adopted: in this case, sapphire (Al_2O_3) is the most common choice for growing GaN since it shows fairly high transparency and good thermal conductivity. All of the GaN part of the device processed in this work was indeed grown on sapphire substrate.

Whereas the GaN/InGaN HWLEDs have been designed with a flip-chip configuration, the nano-ZnO/GaN HWLEDs rely on a bottom-up structure, as shown in Fig. 3.1.

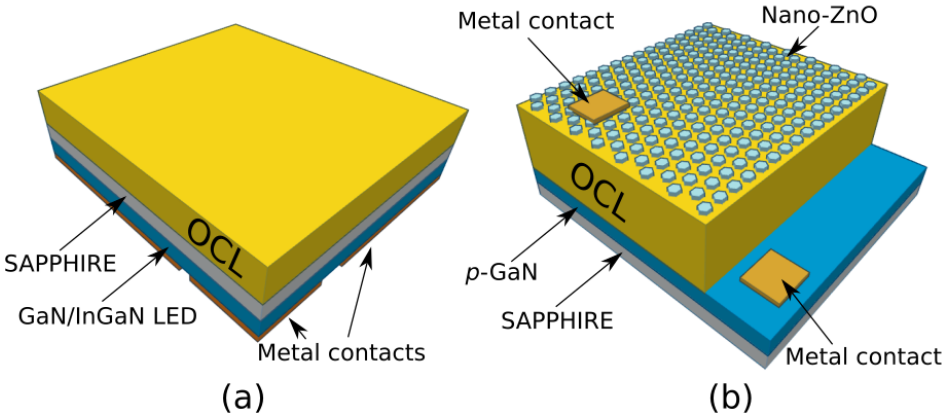

Fig. 3.1: Sketches of the two HWLEDs used in this work: (a) GaN/InGaN HWLED, (b) Nano-ZnO/GaN HWLED. Note that for both structures the same organic conversion layer (OCL) is used.

In the following sections, the processing of the materials used for the realization of the diodes analyzed in this work is described in detail, together with the characterization methods used to evaluate the quality of the samples.

3.2 GaN Thin Film Epitaxy

Gallium nitride is a fascinating material which imposed its value in a semiconductor world that, by the end of the ‘80s, was dominated by gallium arsenide (GaAs). At that time, the research focused on the development of II-VI materials like ZnSe or SiC because they showed very similar crystal structure and lattice constant as GaAs. Unfortunately, the growth temperature of II-VI compounds is not high enough to keep under control the formation of crystal defects. Many researchers reported a density of defects for ZnSe close to 10^4 cm^{-2} but this fact limited the lifetime of the devices to a few hundreds of hours [22]. One interesting thing is that, although GaN has a higher defect density than ZnSe, it works much better and has superior performances at almost any level.

Thus, to achieve the best GaN quality, a fine-tuned epitaxial growth technique is crucial. Today’s industry standard is, without any doubt, the metal-organic vapor phase epitaxy (MOVPE) technique which was perfected by Nakamura from its very first studies in 1990 and up to 1999. All of his (and his colleagues’) work led to the 2014 nobel prize in physics that was awarded to Isamu Akasaki, Hiroshi Amano and himself [23].

In this dissertation, all of the GaN-based devices have been processed with MOVPE reactors: the full GaN/InGaN diodes and most of the *p*-GaN templates were grown at NOVAGAN Sàrl in Lausanne (Switzerland), while other samples were processed at the Centre de Recherche sur l’Hétéro-Epitaxie et ses Application (CNRS-CRHEA) in Valbonne (France).

3.2.1 GaN Crystal Structure and Properties

Unlike other interesting materials for optoelectronic applications, like GaAs or InP, that are grown in the zincblende crystal structure, the nitride compounds grow as a stable phase in the hexagonal crystal, better known as wurtzite.

The lattice parameter for the crystal in Fig. 3.2 are a=3.189 Å and c=5.185 Å. Also the thermal expansion properties need to be taken into account since there is a large difference between the MOVPE growth temperature and the room temperature, and this causes a severe thermal stress for the GaN: the dilatation coefficient on the a lattice parameter is $3.1 \cdot 10^{-6} K^{-1}$, whereas for c is $2.8 \cdot 10^{-6} K^{-1}$. Similarly, the physical properties of the growth substrate must be analyzed with care because all these parameters contribute to the robustness of the final product, the defect population and give other important information to improve the technological

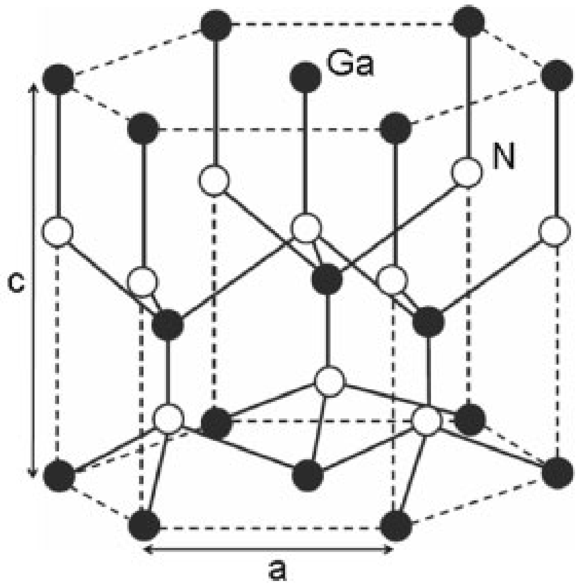

Fig. 3.2: The wurtzite crystal structure of GaN [24].

design. In section 3.2.2 the use of sapphire as substrate for the GaN epitaxy will be discussed.

GaNhas a spontaneous polarization on the [0001] growth axis (*c*-axis) since the wurtzite structure has an intrinsic polar behavior. This causes an internal electric field that can limit the performances of any GaN-based optoelectronic device: in fact the free charges injected in the active region can be separated by the action of the induced electric field and this could seriously limit the internal quantum efficiency of the diode. To attenuate the effect of the polar growth, the epitaxy of GaN can also be achieved with the c-axis disoriented with respect to the growth direction. When using c-oriented (0001) or a-oriented (11-20) sapphire, GaN grows on the c-axis. With r-oriented (1-102) sapphire, GaN grows in the non-polar a-direction <11-20>; m-oriented (10-10) sapphire causes the GaN to grow in the <11-22> direction, which is called “semi-polar”, and the c-axis forms a 32° angle with respect to the horizontal surface plane (see Fig. 3.3).

3.2.2 MOVPE Growth

The MOVPE, also known as metal-organic chemical vapour deposition (MOCVD), is a gas phase deposition method specially indicated to produce epitaxial growth for nitride compounds.

The process uses the chemical reaction of organometallic precursors in a chamber heated at high temperature and kept close to atmospheric pressure (between 10^4 Pa and 10^5 Pa). The gallium precursors used are typically trimethylgallium (TMGa)

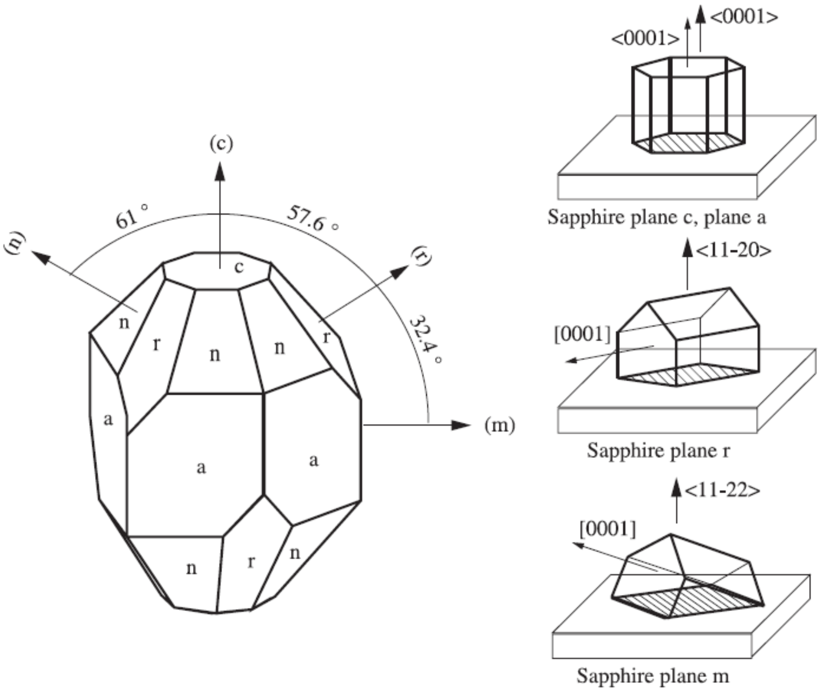

Fig. 3.3: Growth direction of GaN on sapphire: on the left are reported the orientation of sapphire, on the right are depicted the results of the GaN wurtzite crystal growth [25].

or triethylgallium (TEGa), whereas the source of nitrogen is ammonia (NH_3). The organometals are in liquid form and kept in special hermetic bottles in a thermostatic bath. Hydrogen flows in the liquid to carry it in a gas phase inside the growth chamber. In a vertical reactor, the gallium precursor and the ammonia are introduced via two different lines in the chamber, thus preventing unwanted reaction of the chemicals.

As mentioned previously, the most common substrate for GaN MOVPE growth is sapphire and it is brought at temperatures above 1000 °C on a graphite susceptor that is heated with a radiofrequency coil. Sapphire is the preferred material as substrate because it is a good thermal and electrical insulator. Nevertheless, the coefficient of thermal expansion for GaN is higher than the one of sapphire and for this reason care must be taken since, during the cooling stage of the growth, cracks may occur on the GaN layer. Thanks to the research of Amano *et al.* [26], nowadays it is quite common to include in the growth the formation of an aluminum nitride (AlN) buffer layer on the substrate to reduce the stresses of the lattice constant mismatch.

The precursors pyrolize on the substrate according to the general reaction:

$$\mathrm{Ga}_{(g)} + \mathrm{NH}_{3(g)} \rightarrow \mathrm{GaN}_{(s)} + \frac{3}{2}\mathrm{H}_{2(g)}$$

and the hydrocarbon by-products flow through the exhaust of the chamber. It should be pointed out that the environment is ammonia-rich because nitrogen evaporation occurs from the GaN surface due to the high temperature, so the ratio of the NH_3 precursor to the Ga precursor is around 1000:1. The growth rate is usually controlled using a laser reflectometry apparatus that focuses the beam of an He-Ne laser on the wafer and senses the oscillation of the reflected beam, caused by the difference in the refractive index at the film/substrate interface.

Fig. 3.4: A picture of the vertical reactor at CNRS-CRHEA.

The *p*-type doping of GaN is achieved with the introduction of magnesium atoms: this can be obtained using bis-cyclopentadienyl magnesium (Cp_2Mg) as its organometallic precursor. In MOVPE growth, the *p*-doping of GaN is not an easy task: contaminants in the reaction chamber, due to non-purified carrier gases or residues of other organometals, can easily be incorporated or passivate the magnesium atoms in gallium nitride obtaining narrow doping profiles or even unintentional *n*-type doping of the material.

In the following table are reported the process data of the *p*-GaN grown by MOVPE.

Tab. 3.1: Process data for the MOVPE of *p*-GaN: the first row corresponds to the first layer grown whereas the last row is the effective doped GaN layer.

	Thickness (nm)	Pressure (mbar)	Temperature (°C)	NH_3 (L/min)	TMGa (sccm)	TMAl (sccm)	Cp_2Mg (sccm)
GaN	200	300	1080	3.5	5	-	-
$Al_{0.1}Ga_{0.9}N$	10	300	1080	3.5	5	20	-
$Al_{0.1}Ga_{0.9}N$:Mg	50	300	1080	3.5	5	20	100
GaN:Mg	200	300	1080	3.5	5	-	100

To activate the magnesium (Mg) atoms an annealing process is required: this step is carried at 750 °C for 20 minutes at a higher pressure with respect to that of the growth (800 mbar).

3.2.2.i Doping Measurements on *p*-GaN

To quantify the doping level of the processed samples, the capacitance-voltage method (C-V) is a widely adopted technique, useful to determine semiconductor parameters both in academic research laboratories and industry. The method essentially measures the AC response to a DC bias, with a small AC voltage superimposed, applied on the semiconductor surface. To apply such a voltage, a special probe that puts in contact the material with liquid mercury is used. The response of the device is recorded by an LCR meter set to measure the capacitance of the depleted region of the wafer caused by the Schottky junction generated within the metal-semiconductor interface (see Fig. 3.5).

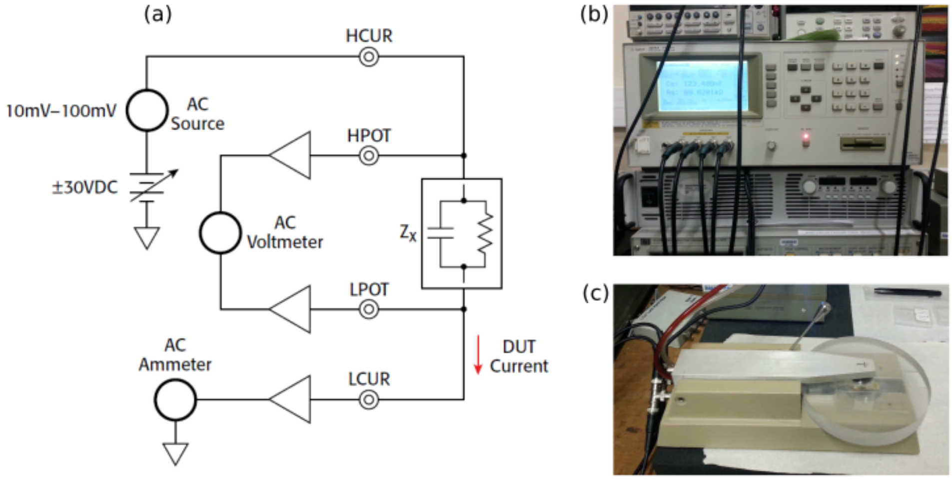

Fig. 3.5: Setup used to perform a C-V measurement: (a) the scheme of the measurement device, (b) Agilent LCR Meter (mod. 4284A), (c) MDC Mercury Probe.

Using the C-V measurement one can extrapolate the doping profile, since the concentration of the dopant atoms is related with the inverse of the square capacitance by the relation:

$$N_{dopant} = N_A - N_D = \frac{2}{q\epsilon_s A^2 \frac{d(\frac{1}{C^2})}{dV}}$$

where N_A and N_D are the acceptor and the donor concentrations, ϵ_s is the semiconductor electrical permittivity and A is the surface of the contacted area (in the case of the mercury probe, it is a dot contact with a diameter of 760 μm). The plot in Fig. 3.6 shows a typical doping profile generated by a C-V measurement.

The method is trustworthy until the level of doping recorded is too high. In that case, there might be a leakage of free carriers by tunneling and the measurement gives an erroneous value of the concentration [27]. Thus, Hall Effect measurements are always needed to have a complete vision of the doping process. Hall results on a well-processed *p*-GaN thin film give a concentration of free holes around 10^{17} cm^{-3}; it should be noted that, because of the high Mg ionization energy (around 200 meV), concentration of dopants around 10^{19} - 10^{20} cm^{-3} are needed.

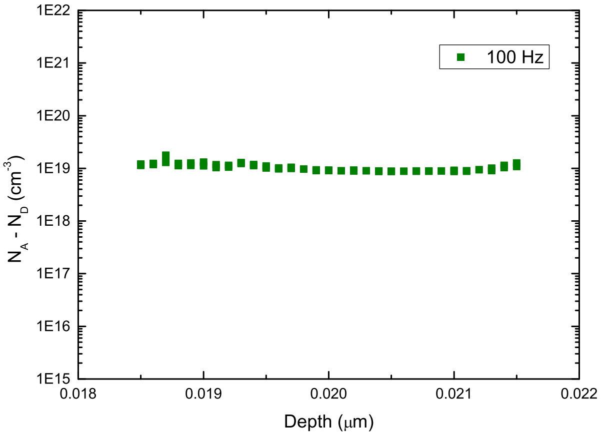

Fig. 3.6: Doping profile of a *p*-GaN sample obtained by extrapolation of a C-V plot.

3.2.3 Microscope Analysis of GaN

A microscopic analysis of the *p*-GaN thin film is generally not a step included during the processing of nitride-based devices but, since in this work one of the proposed diodes is based on a heterostructure with a different material, it is recommended to have information on the surface morphology of the semiconductor. Therefore, the use of the atomic force microscope (AFM) helps to better understand what to expect in terms of surface roughness after the epitaxial growth.

The AFM system consists of a cantilever with a sharp tip that is specially designed to run on the surface of a sample with minimal damage, since the tip senses the atomic forces with the surface (Van der Waals, dipole-dipole interaction, etc.). A laser is focused on the back of the tip and its reflection is recorded by a photodiode, thus transforming the height variation of the tip in a position variation of the reflected beam's spot. The instrument used in this work is a Veeco Dimension 3100 (Fig. 3.7) and is set to operate in tapping mode. In other words, the tip is forced to oscillate close to its resonant frequency and it is driven by a piezoelectric element that moves the cantilever up and down. The system is equipped with an electronic system, which provides feedback control to a servo that helps the cantilever to mantain a constant oscillation amplitude.

Fig. 3.7: Veeco Dimension 3100 at CNRS-CRHEA.

There are two images for each AFM scan: the topographical image records the height difference of the tip when tracing a line and the derivative image records the variation of the voltage amplitude that drives the servo to keep the oscillation condition. While the former is used to measure the profile of the sample, the latter detects sudden variations of the surface allowing the user to distinguish features otherwise unseen in the topographical image.

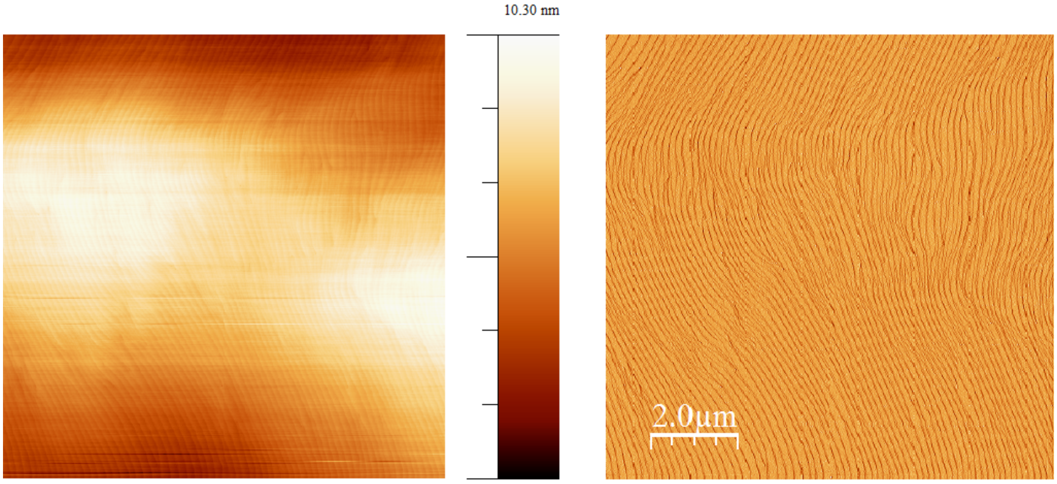

Fig. 3.8: (10 μm×10 μm) AFM image of a GaN template: (left) topographical image, (right) derivative image.

In Fig. 3.8 is reported a (10 μm×10 μm) AFM image of an undoped GaN sample. The atomic steps of the growth are clearly visible in the topographical image, while in the derivative image some details may arise, like those marked in Fig. 3.9.

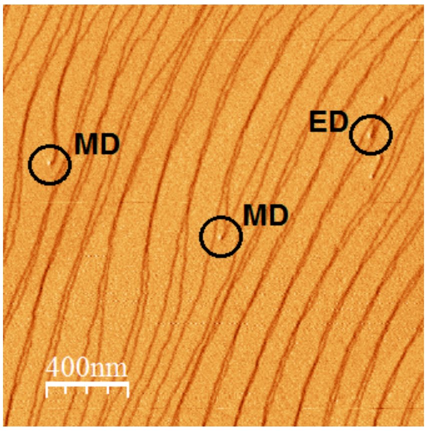

Fig. 3.9: (2 μm×2 μm) AFM image of a GaN template: an edge dislocation (ED) and two mixed dislocations (MD) are marked with a circle.

After the MOVPE growth of the *p*-GaN layer, the surface profile is deeply affected. A spontaneous formation of truncated hexagonal pyramids is evidenced in the AFM images (Fig. 3.10).

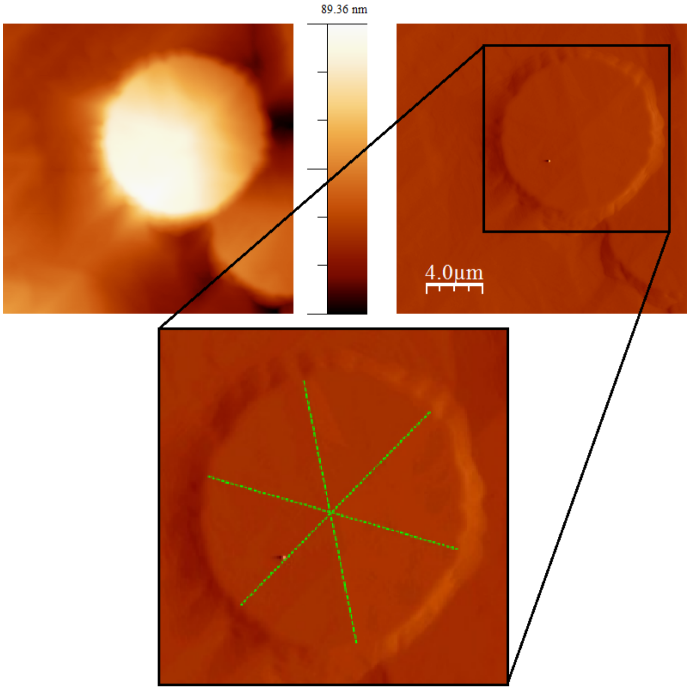

Fig. 3.10: AFM image of the *p*-GaN surface: the magnified portion of the derivative image shows, with dashed green lines, the ridges of the truncated hexagonal pyramid.

The wafer is quite populated with these formations that are clearly visible even under the optical microscope (Fig. 3.11). The density of the pyramids is approximately 10^5 cm^{-2}.

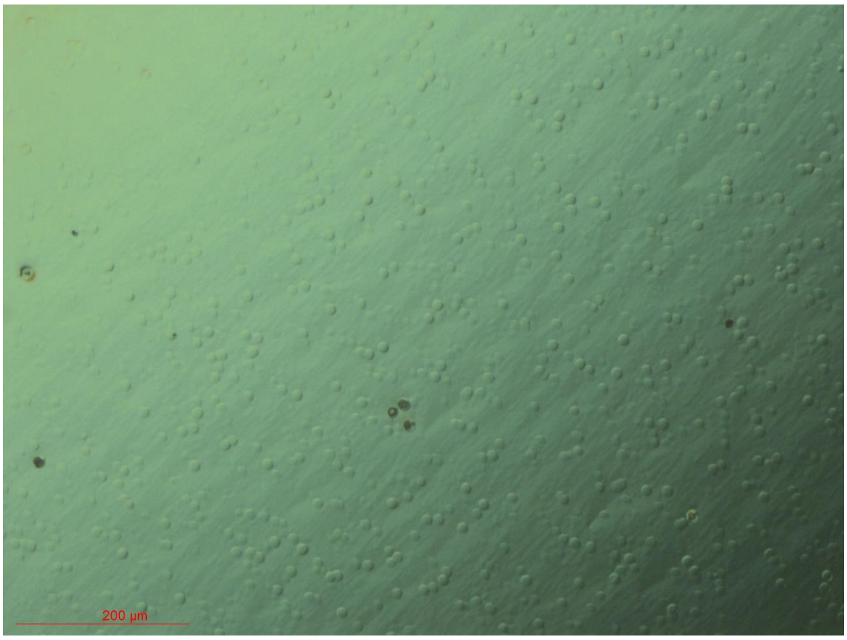

Fig. 3.11: Optical microscope image of the p-GaN surface.

Though this phenomenon may be seen as quite a major disadvantage for any subsequent growth of other epitaxial layer, its usefulness will be discussed in the section relative to the growth of the nanostructured layer.

3.2.4 Photoluminescence of GaN

Most of the information related with the optical properties of semiconductors can be obtained by a careful analysis of the photoluminescence (PL) spectra of the materials. In PL, the thermal equilibrium of a semiconductor, like GaN, is perturbed by the optical excitation provided by a laser. The electrons in the GaN are excited from the valence band to the conduction band and, in order for the system to return to its ground state, a recombination process occurs emitting light. The recombination can be achieved with band-to-band transitions or via other transitions within discrete levels inside the band gap of the material: these levels are related with dopants and defects [28]. The emission spectrum (the PL spectrum) is captured with very sensitive optical devices and every peak of the graph can be ascribed to a different energy transition.

To excite the electrons, the laser must be more energetic with respect to the band-gap of the semiconductor. For the analysis of GaN samples, He-Cd lasers emitting at 325 nm are often used as pump sources. Since the optical absorption coefficient (α) of GaN is over 10^5 cm^{-1}, the penetration depth (D) of the incident laser is less than 100 nm (being $D = 1/\alpha$) so only a thin layer close to the surface is excited. The sample is placed under high vacuum inside a cryostat, then liquid helium can be pumped in to record the spectra at low temperatures.

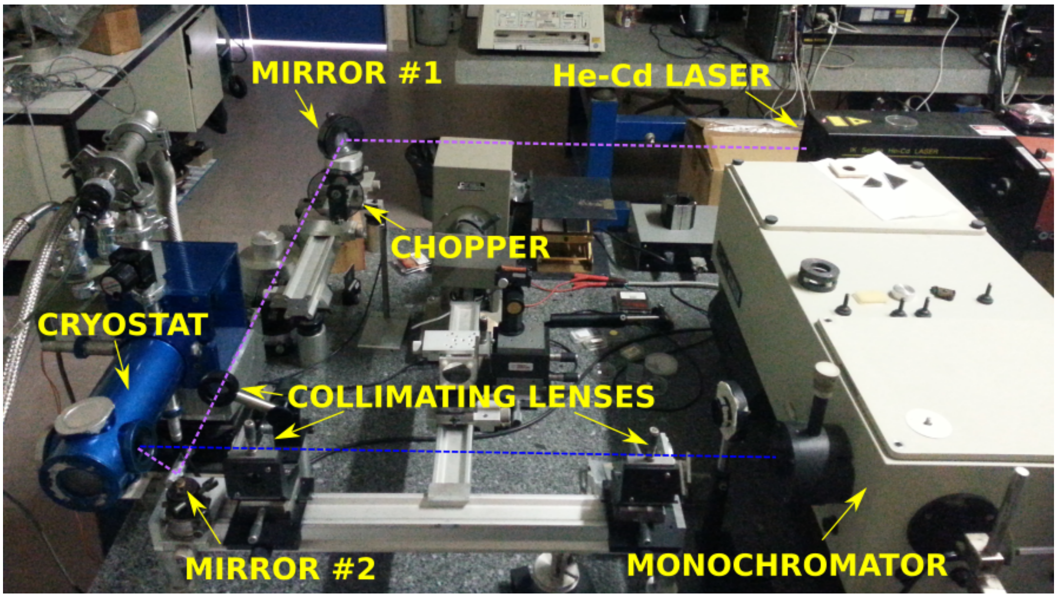

Fig. 3.12: PL setup equipped with a He-Cd laser and a monochromator at CNRS-CRHEA.

The interpretation of PL spectra of Mg-doped GaN is quite difficult. It is still not clear which levels are introduced by which defects in GaN, but past research confirms that this kind of *p*-doping introduces shallow acceptors with ionization energy around 200 meV [28]. It is also well documented that, in the low-temperature PL spectra, a peak around 3.27 eV shows up [29] and it is typical of neutral donor-acceptor pair recombination. Sometimes, this peak transforms into a broad band for very high concentrations of Mg. In all of the processed GaN samples, a band peaked at 3.27 eV is always present, confirming the presence of Mg in the doping (see Fig. 3.13).

3.3 ZnO Synthesis

ZnO is a II-VI semiconductor material that has interesting properties for optoelectronics and photonics applications. Due to its wide band-gap (3.37 eV) and a fairly large free-exciton binding energy (60 meV), ZnO represents a valid alternative to other nitride compounds for the realization of commercial LED luminaires. Even though research focusing on ZnO started on the first half of the twentieth century, only more recently there have been a renewed interest due to the possibility to realize low-cost optoelectronic devices and high-quality substrates: this brought to numerous, controversial, research papers that claim to have obtained *p*-type doping [3].

The first studies on the lattice parameters of ZnO date back to 1935 [30], whereas a more in-depth study of its optical properties came out in 1954 [31]; some early

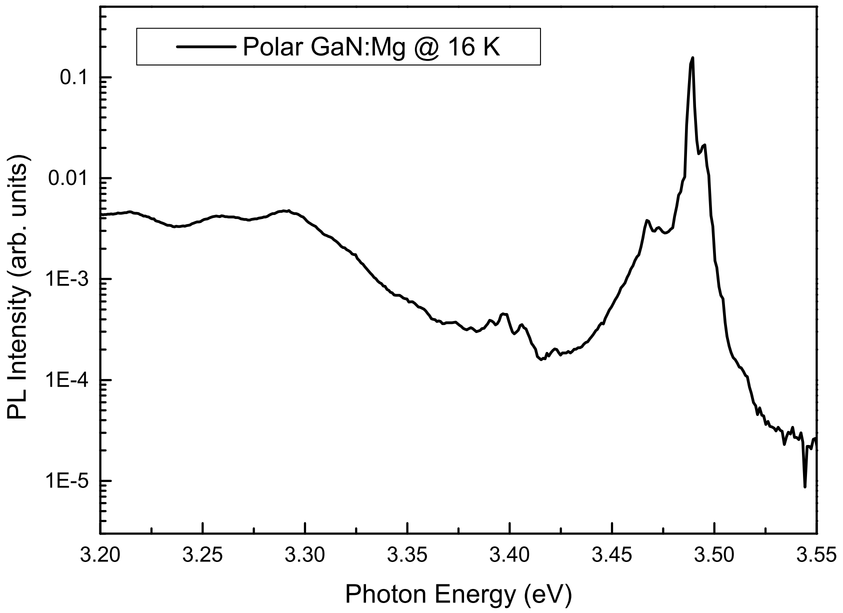

Fig. 3.13: Low temperature, near band-edge PL spectrum of Mg doped GaN.

attempts in processing a *p-n* junction with zinc telluride showed up in 1975 [32] and three years later appeared a study on the metal contacting of ZnO [33].

Then, in 2001, the discovery of nanobelts of semiconducting oxides marked a breakthrough in nanotechnology [34]. Since when this result came out, it has paved the way to research novel nanostructures of functional oxides with applications in optoelectronics. ZnO is a material with the highest number of configurations than any other existing nanomaterial, including carbon nanotubes; not to mention that zinc oxide is also environmentally friendly. With an incredible acceleration on technology, nanorings [35], nanohelixes and nanosprings [36] have been realized within just a couple years one from each other. Most importantly, the growth of aligned structures like nanorods found applications also in sensing and field emission thanks to its piezoelectric feature. But the nanorods are, first of all, natural optical cavities that have a 2D confined space which can lead to a one-directional output of light; of course, LED structures that have directional emission already exist but they benefit of specially designed quantum wells or shaped semiconductor dies. The reduced size of ZnO nanorods makes easy to think of optoelectronic devices that could match their features with integrated optics.

Many are the growth techniques known to obtain aligned ZnO nanorods but most of them exploit catalysts or are operated at high temperatures, like the gas-phase synthesis methods. A solution-phase approach, adopted in this work, allows for an easier control of the process and requires a low-cost equipment. In this section, the theory of both growth techniques are described, along with the description of ZnO properties and the accurate report of the ACG of ZnO. The nanostructures have been grown at the Thin Films Laboratory, in the DEIM department of the Università degli Studi di Palermo.

3.3.1 ZnO Crystal Structure and Properties

Like most of the II-VI compounds, ZnO crystallizes in either zincblende or wurtzite structure: under ambient conditions the stable phase is wurtzite, otherwise ZnO crystallizes in zincblende only when grown on cubic substrates. The measured lattice parameters in the wurtzite ZnO are a=3.249 Å and c=5.206 Å: it must be noted that only a 1.8% lattice mismatch occurs between GaN and ZnO crystals. The thermal dilatation coefficient on the a lattice parameter is $4.3 \cdot 10^{-6} K^{-1}$, whereas for c is $2.5 \cdot 10^{-6} K^{-1}$.

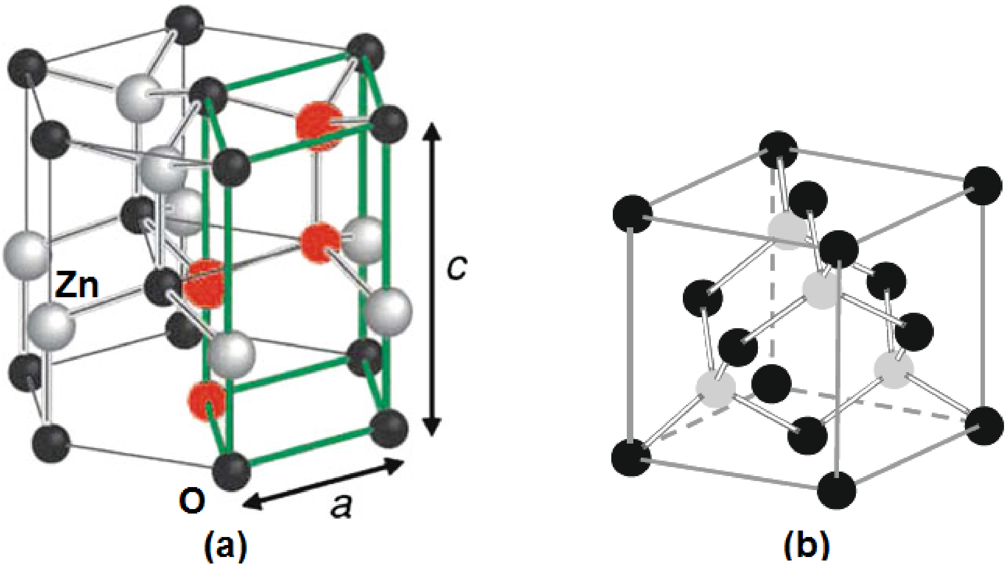

Fig. 3.14: (a) Wurtzite and (b) zincblende crystal structures for zinc oxide. Note that, in the wurtzite structure, the unit cell is shown in green [37].

Because of the strong bond polarity of ZnO, the wurtzite crystal has faces with pronounces polar character. The electric field induced by the polarity on the <0001> direction is intense enough to slightly distort the bonds on the c-axis. Among all of the wurtzite polar semiconductors, ZnO is the one that has the highest degree of distortion from the ideal structure. This polarity behavior, with a non-central symmetric crystal, causes ZnO to be piezoelectric and make it suitable for electromechanical coupling applications at the nanoscale level. New terms like "piezotronic devices" or "piezo-phototronics" have recently been coined to strengthen the physics concepts behind these interesting research themes [38].

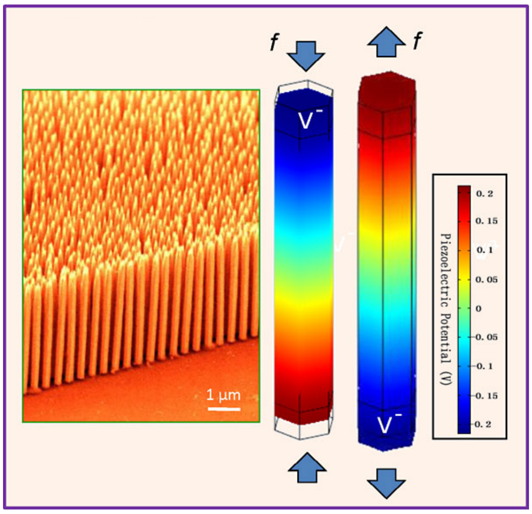

Fig. 3.15: Distribution of the piezoelectric potential along a ZnO nanowire under external strain applied [38].

3.3.2 High-Temperature Synthesis

The vast number of synthesis techniques of ZnO nanostructures at high-temperatures allows researchers with a consolidated experience in specific growth technologies to adapt their knowledge to this new material.

So far, this category of synthesis includes the following growth methods: vapor-liquid-solid (VLS), MOVPE, molecular beam epitaxy (MBE), pulsed laser deposition (PLD), etc. In this section are briefly described the working principles of two major techniques used in industry: VLS and MOVPE.

In the VLS technique, a substrate is sputtered with gold and placed in a quartz tube inside a furnace. In the same tube, an alumina boat with a mixture of graphite and ZnO powder is placed, then the temperature is ramped up between 800 °C and 1000 °C. The high temperature causes the reduction of the ZnO and lets the evaporated Zn to be transported by an oxygen gas carrier onto the surface of the substrate: here, the gold melts in tiny droplets and acts as a catalyst, forming a liquid alloy with the zinc vapor. When the droplet saturates, the zinc precipitates and reacts with the oxygen in the tube to form ZnO nanorods. The reaction continues until there is no more gold on the tip of the nanorod. This method allows the formation of very well aligned nanostructures but the control of the reaction remains challenging [39].

Similarly to the GaN, in the MOVPE of ZnO organometals like diethylzinc (DEZn) or dimethylzinc (DMZn) are used to perform the growth. This technique is one of the most indicated to replicate the growth direction of the substrate. The main difference with the MOVPE of nitride compounds is that gas-phase reaction can occurr far from the substrate surface, since oxygen precursors used to obtain ZnO are usually very reactive. Therefore, one solution could be to reduce the oxygen precursor pressure in the reactor but, at that point, the formation of ZnO is very difficult. Other alternative less reactive precursors are still subject of study [40]. In all cases, a high-temperature stress for certain kind of substrates is not always indicated: processed *p*-GaN substrates can suffer thermal stress under prolonged heating.

3.3.3 Hydrothermal Growth of ZnO

The aqueous chemical growth of zinc oxide was first reported in 2001 [41] and it is an inexpensive method to fabricate nanorod arrays from a solution of a zinc salt in water at low temperature. This technique can be easily scaled-up and adapted to almost any kind of substrate. Tuning some parameters of the growth, other nanostructures like nanotubes, nanoflowers, nanoplates, nano-urchins, etc. can be obtained [42, 43]. The method used in this work has been tailored to obtain nanorod arrays within a specific range of dimensions.

The mechanism of reaction, in the hydrothermal synthesis of ZnO, exploits the decomposition of zinc nitrate ($Zn(NO_3)_2$) in water: here, Zn^{2+} ions react with the hydroxyl ions obtained by the thermal degradation ($< 90°C$) of hexamethylenetetramine (HMTA, $(CH_2)_6N_4$), a water soluble amine. The process can be summarized as follows:

$$\begin{gathered}
(\mathrm{CH_2})_6\mathrm{N_4} + 6\mathrm{H_2O} \rightleftharpoons 6\mathrm{HCHO} + 4\mathrm{NH_3}, \\
\mathrm{NH_3} + \mathrm{H_2O} \rightleftharpoons \mathrm{NH_4^+} + \mathrm{OH^-}, \\
2\mathrm{OH^-} + \mathrm{Zn^{2+}} \longrightarrow \mathrm{ZnO} + \mathrm{H_2O}.
\end{gathered}$$

It is generally accepted that the main function of the HMTA is to provide the hydroxyl group for the reaction with zinc ions [44, 45], although some researchers have proposed the theory that the compound could also attach to the non-polar facets of the ZnO nanorod crystal allowing it to grow only along the c-axis [46]. Most of the past research papers report on the use of a ZnO seed layer to promote the nucleation of oriented structures on the desired substrate [47, 48, 49, 50]. In section 3.3.4, the results of the hydrothermal growth on various substrates are reported, some of them with a seed layer and others without. Then, the growth of well-aligned ZnO nanorods on a *p*-GaN substrate without the use of a seed layer is shown.

Many recipes are available in literature to prepare the hydrothermal growth solution [48, 51, 52]. According to their expertise, researchers suggest to prepare an equimolar solution of zinc nitrate hexahydrate and HMTA in deionized water with a concentration between 5 mM and 50 mM: a value of 20 mM is chosen as starting point. The influence of the concentration on the final result will be discussed in the following sections. Every solution was stirred for a couple of hours without heating, and the residual particles were filtered with a syringe filter. The solutions were stored in hermetic bottles and kept for possible use for 1 week maximum.

3.3.4 SEM Analysis of ZnO

The scanning electron microscope (SEM) is an instrument capable of acquiring high-resolution images of inorganic and organic samples. A specimen, which is placed inside a high vacuum chamber, is scanned with a focused, very energetic, beam of electrons that interacts with the electrons of its surface: the raster scan pattern produces secondary electrons (SE) which are collected by a SE detector. A computer then takes the conditioned signals from the detector and transforms them into graphical data containing the images information. In conventional systems, it is important for every specimen to be conductive, otherwise the accumulation of electrostatic charge at the surface will result in a distorted or very fuzzy image: samples that are not conductive can be sputter-coated with a layer of gold. The resolution of a SEM is limited by the detector performances and not by the power of the objective lens: this is the main difference with a simple optical microscope (see Fig. 3.16).

The first set of ZnO nanorods analyzed are grown on different substrates to compare the relationship between the underlying material and the morphology of the nanostructures. The substrates are completely immersed in the nutrient solution while being heated at a temperature between 70 °C and 90 °C. After 3 hours, the heater is turned off and the samples are left in the solution to cool spontaneously to room temperature. No annealing is performed on the nanostructures. Finally, the samples are rinsed with distilled water to remove any trace of precipitate.

The image reported in Fig. 3.17 shows an array of nanorods grown on a layer of indium-tin-oxide (ITO) on glass. The ITO is a transparent conductive oxide (TCO) commonly used to realize contacts on ZnO-based devices. The hexagonal shape of the elements protruding from the surface immediately confirms the effective presence of ZnO. Also, the absence of a specific order is typical of the growth on poorly crystalline or disordered films. A very similar result is obtained when the nanorods are grown on a layer of fluorine-tin-oxide (FTO) on glass, another type of TCO (Fig. 3.18). In both cases, the diameters of the nanorods are between 50 nm and 200 nm.

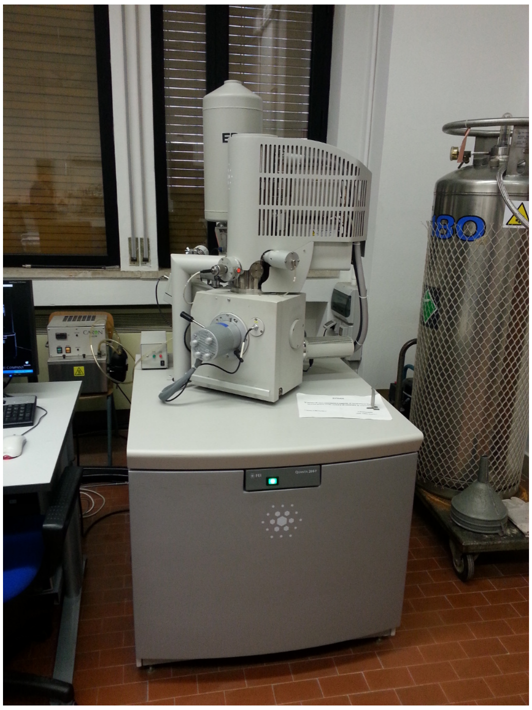

Fig. 3.16: The FEI Quanta 200F in the SEM laboratory of DICAM at Università degli Studi di Palermo.

A peculiar result is produced when growing ZnO nanostructures on a bare plastic flexible substrate like polyethylene terephthalate (PET) (see Fig. 3.19). The rods are fully disordered and facing in random directions, showing that in this case there was effectively no growth: the rods that have formed in the solution have been attracted to the insulating substrate by electrostatic forces, probably caused by residual impurities on the PET. This interpratation could explain why some of the rods are vertical (the polar face of the rod is attracted by the electrostatic charge on the plastic). Though the density of ZnO nanorods is lower than the one in the previous samples, their dimensions are generous: almost all of the rods have diameters between 1 μm and 2 μm, the length ranging from 8 μm to 15 μm.

For the sample in Fig. 3.20, a thin film of ZnO (around 200 nm) is deposited with a PLD system on c-sapphire. The resulting wafer is then processed with the hydrothermal growth of ZnO nanorods. The degree of orientation of the rods on this sample is between the ones processed on the TCOs and the one on PET, whereas their shape is much more defined. Although the quality of the ZnO film deposited with the PLD system is very high (almost no impurities incorporated), unfortunately the control of the crystalline order is quite tricky when using sapphire as a substrate, and the result of the PLD of ZnO thin film is a layer composed of randomly oriented grains. This phenomenon is reflected on the highly disordered growth of the nanorods; also, a large number of pillars penetrated in each other (see Fig. 3.21). It is interesting to notice that in a small portion of the sample, a number of nano-threads appear on the top of the nanorod layer (Fig. 3.22). This formation was casual and never showed in other growths. The diameter of the grown nanostructures ranges from 500 nm to 800 nm.

Next, a thin film of p-GaN on sapphire is used as the substrate for the growth of ZnO nanorods. It must be noted that, for this growth, the concentration of the reagents has been temporarily raised to 35 mM because the substrate is bigger than the others used (one sixth of a 2” wafer). The result is visible in Fig. 3.23. A formation of ZnO nanorods shows up with well aligned growth direction on the c-axis. The more compact zone on the top left of the image represents a zone of high coalescence of the rods, which is typical for nutrient solutions of medium-high concentrations. On the bottom part of the image is clearly visible a portion of a big residue, probably carried by an air bubble during the growth; other tiny bubbles stuck on the surface, instead, form “holes” in the nanorod layer.

Lastly, three growths at different values of concentration of the hydrothermal solution were performed to compare the morpholgy results of the nano-ZnO layer. The sample in Fig. 3.24 was grown with a solution at 20 mM; for the sample showed in Fig. 3.25, a 30 mM solution was used; in the case of the sample in Fig. 3.26, the concentration of the solution was raised to 40 mM. The coalescence of the nanorods increases when using solutions with higher concentration. The growth time does not influence much the density of the nanostructures but contributes to form wider and longer pillars. For photonics’ research purposes, where the control of light through a single structure is desirable, the sample grown from a 20 mM solution represents the best result since it allows to well discriminate the nanorods. Furthermore, the resulting images suggest that the truncated pyramid morphology of the p-GaN surface probably acts as nucleation pattern for the ZnO nanorods. A lower control of the layer’s arrangement is achievable with the 30 mM solution, since it shows an alternation between more and less coalesced zones, similar to the case of Fig. 3.23. In the last case, the sample grown in the 40 mM hydrothermal bath forms a very dense layer of rods thus proving that a proper choice of the concentration can lead to an estimation of the compactness of the layer. The following table summarizes the range of the nanorods diameter size obtained for the last three samples.

Tab. 3.2: Diameter of the ZnO nanorods for different hydrothermal solution concentrations.

Hydrothermal Solution Concentration (mM)	Nanorod Diameter (nm)
20	150 - 350
30	250 - 700
40	400 - 800

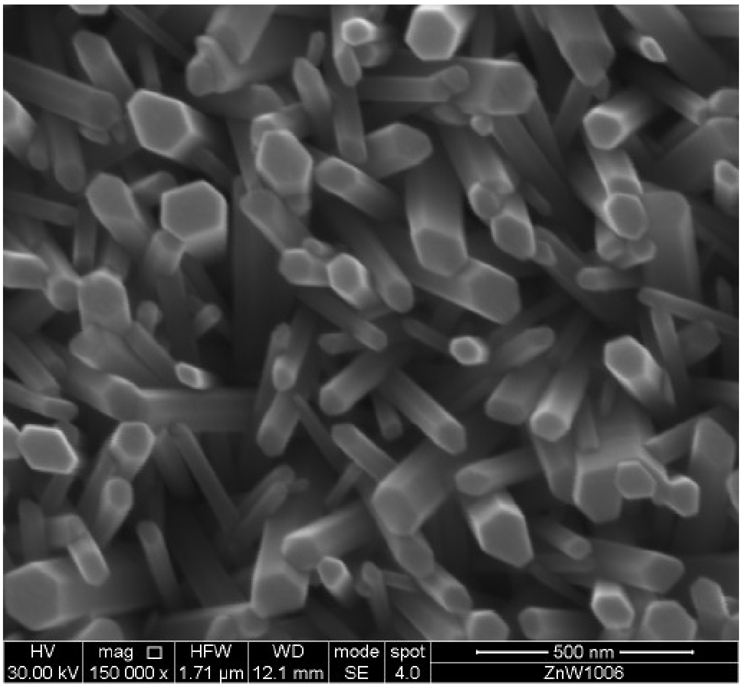

Fig. 3.17: SEM image of ZnO nanorods grown on ITO-on-glass.

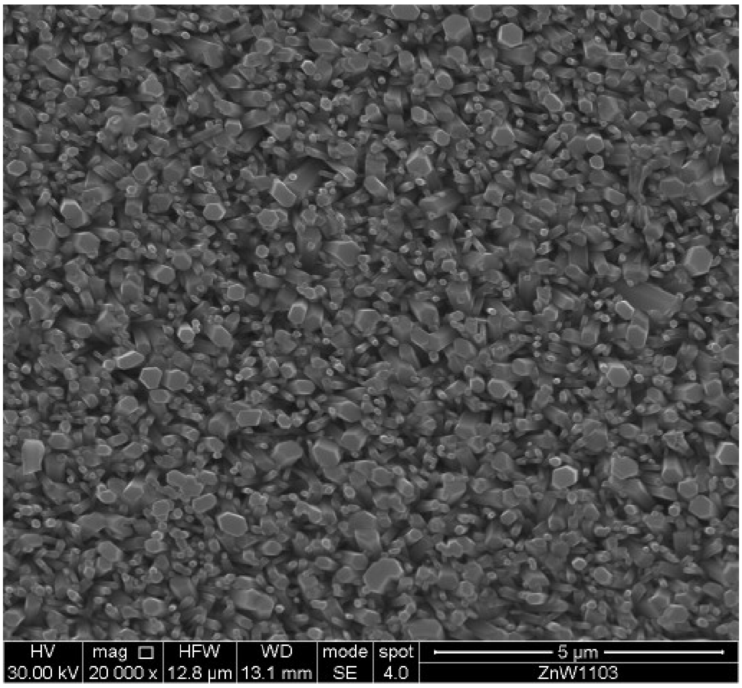

Fig. 3.18: SEM image of ZnO nanorods grown on FTO-on-glass.

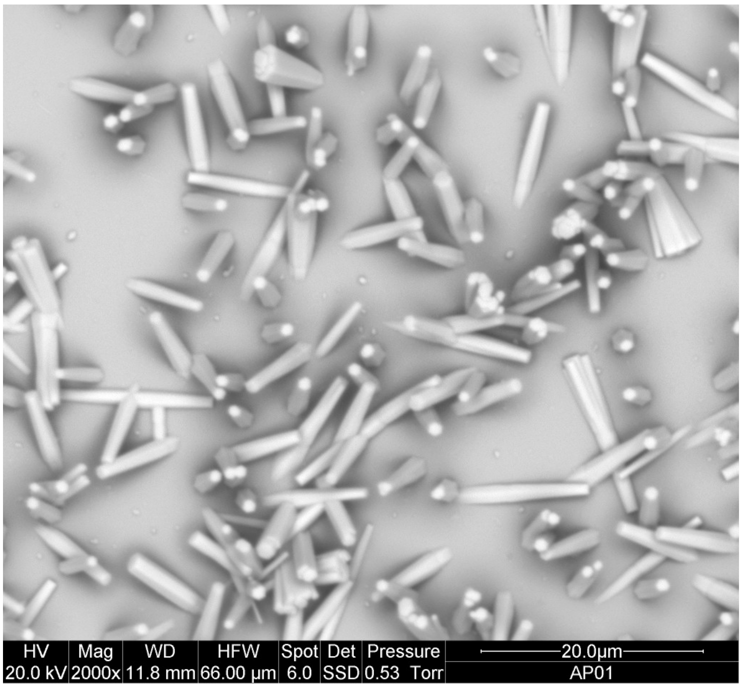

Fig. 3.19: SEM image of ZnO nanorods grown on PET.

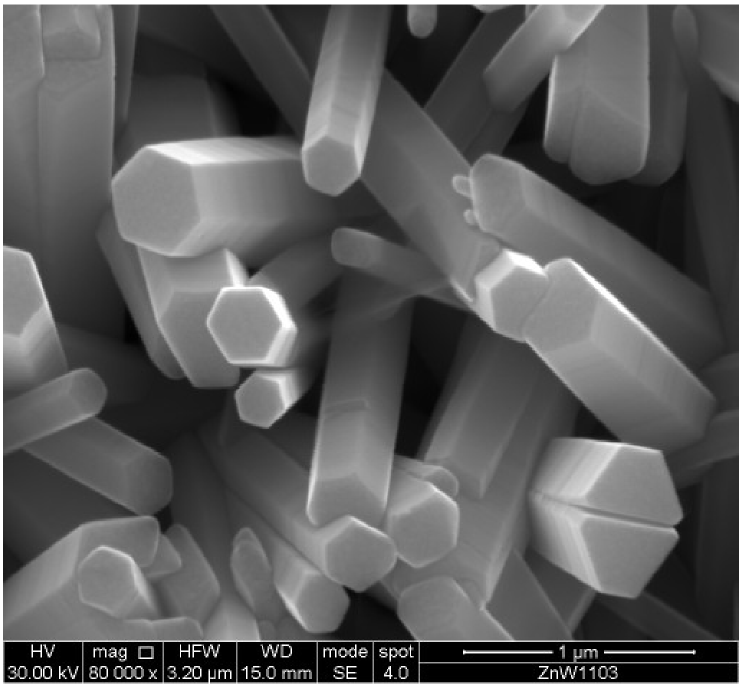

Fig. 3.20: SEM image of ZnO nanorods grown on a ZnO thin film-on-sapphire grown with PLD (zoomed view).

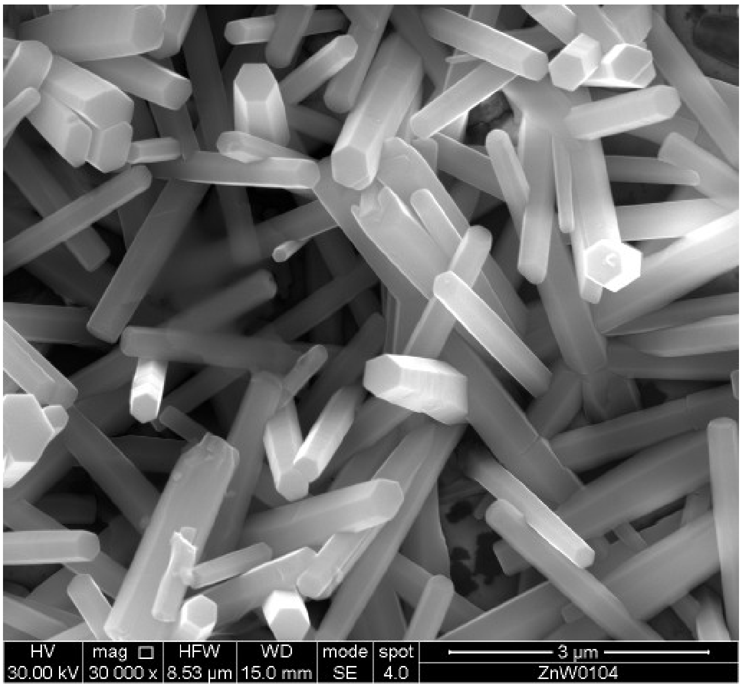

Fig. 3.21: SEM image of ZnO nanorods grown on a ZnO thin film-on-sapphire grown with PLD (large area view).

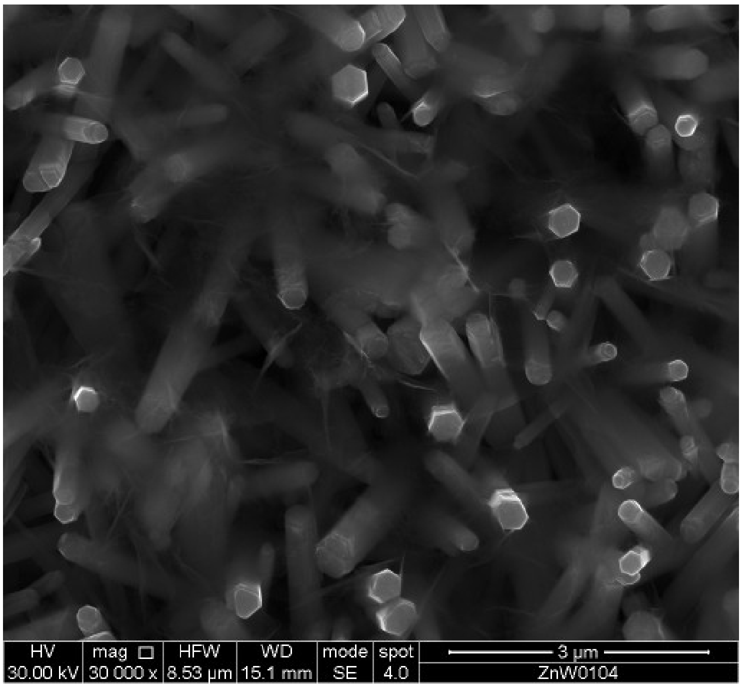

Fig. 3.22: SEM image of another portion of the sample of Fig. 3.20: here nano-threads spontaneously grew on top of the ZnO nanorods layer.

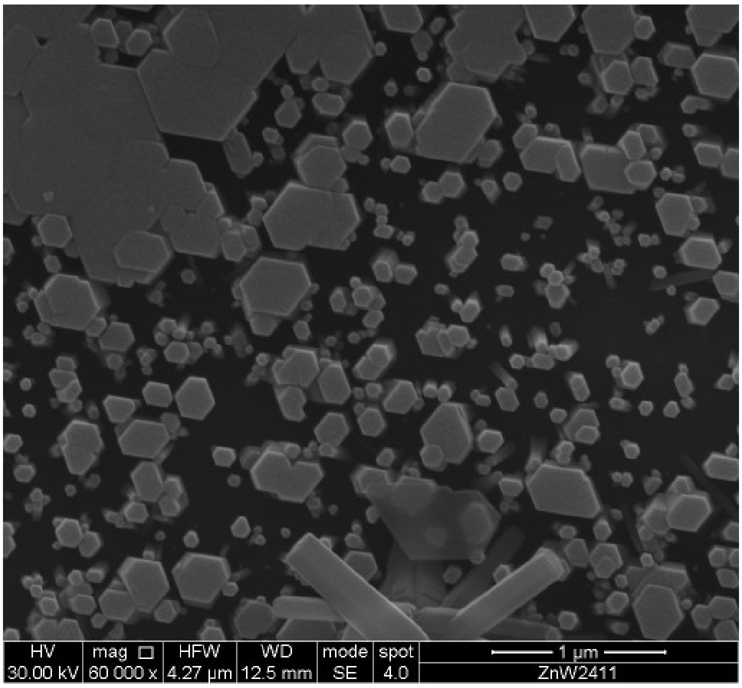

Fig. 3.23: SEM image of ZnO nanorods grown on *p*-GaN: the tips of the rods are all facing up confirming the growth along the c-axis.

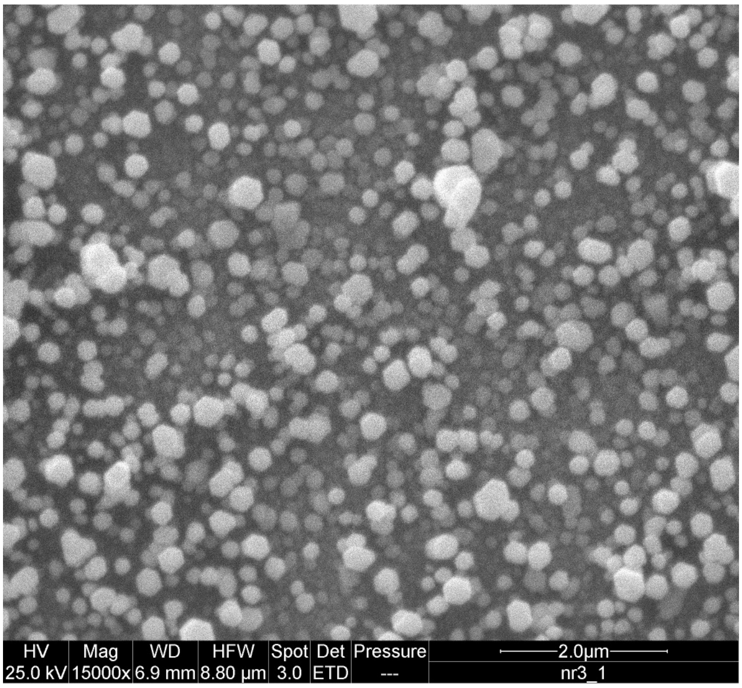

Fig. 3.24: SEM images of the ZnO nanorod layer grown from a 20 mM hydrothermal solution.

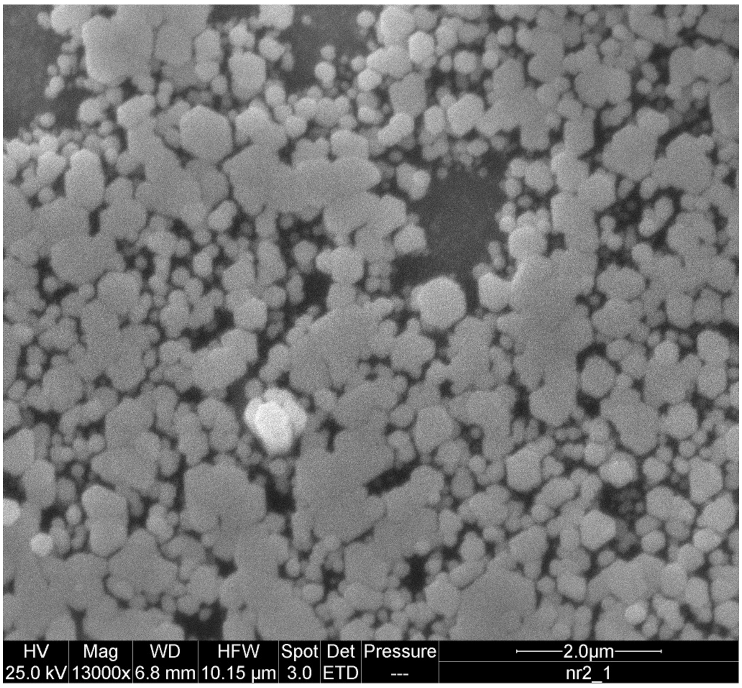

Fig. 3.25: SEM images of the ZnO nanorod layer grown from a 30 mM hydrothermal solution.

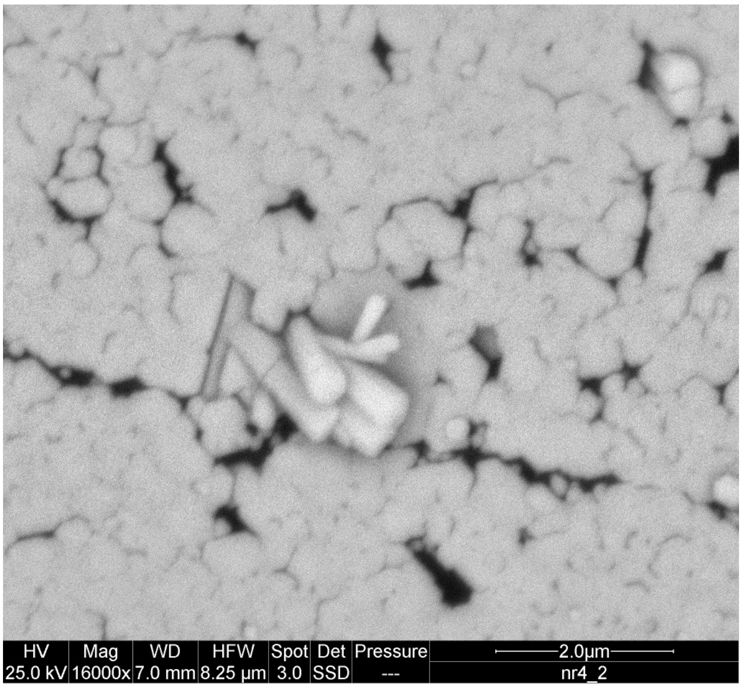

Fig. 3.26: SEM images of the ZnO nanorod layer grown from a 40mM hydrothermal solution.

3.3.5 XRD Analysis of ZnO

X-ray diffraction (XRD) is a non-destructive technique that can be used to analyze the properties of a crystalline material. Whether it is a semiconductor or an insulator, in an XRD system a regular array of atoms is needed to get structural information on the specimen to be analyzed. In an XRD instrument, a focused source of X-rays illuminates a crystalline sample placed in a goniometer (a mount with selectable angle orientations) and the elastic scattering of the X-rays with electrons of the crystal's atoms form constructive or destructive interference according to Bragg's law:

$$2d\, sin\theta = n\lambda$$

where d is the spacing between crystal planes, θ is the Bragg's angle, n is an integer representing the order of diffraction and λ is the wavelength of the X-ray source. Rotating the goniometer causes the angle of the incident beam to vary and, as the detector rotates as well, the diffraction pattern is fomed and can be investigated. An XRD pattern provides information about the degree of order inside a, supposedly crystalline, material. For simple nanostructures, the XRD pattern needs to be very clear with narrow peaks on the diffractogram to indicate oriented growth.

To characterize the crystalline structure of the ZnO nanorods grown, an XRD pattern was taken with a PANalytical Empyrean diffraction system. A θ-2θ scan on a vertical goniometer is performed with Cu K-α radiation (λ = 1,5405980 Å), a generator voltage of 40 kV and a tube current of 30 mA. In Fig. 3.28 is reported the XRD pattern of a sample grown from the 20 mM solution.

Fig. 3.27: PANalytical XRD diffractometer at x-ray laboratory of DICAM at Università degli Studi di Palermo.

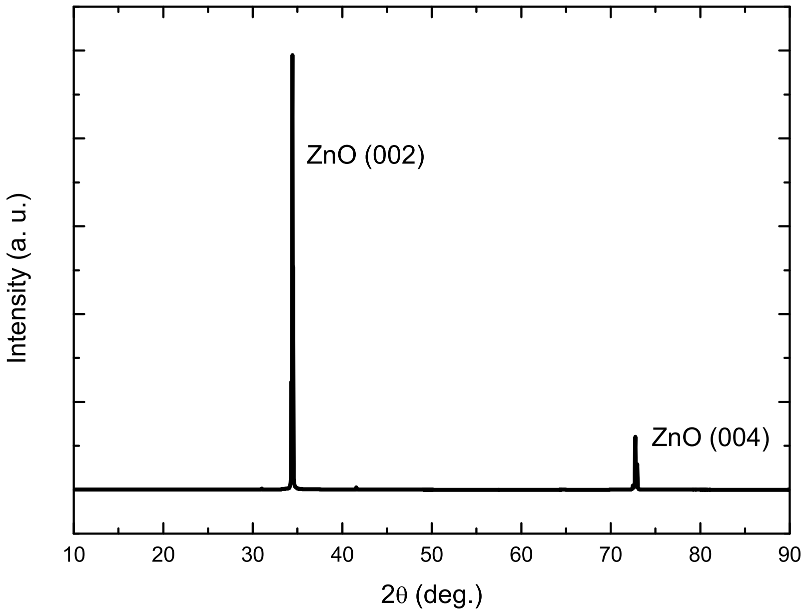

Fig. 3.28: XRD pattern of the zinc oxide nanorod layer grown from the 20 mM solution.

The strong diffraction peaks which are located at 34.4° and 72.7° are in good correspondence with those reported for ZnO (002) and ZnO (004) planes in JCPDS #36-1451. This result confirms that the hydrothermal growth technique leads to wurtzite nanostructures with marked vertical orientation.

3.4 Organic Conversion Layer Preparation and Deposition

The conversion layer used in HWLEDs is composed of an organic dye and a polymer matrix that could build up a solid structure for the dye. The choice of both element must respond to some features that are needed for the industrial standards of mass production. A list of possible requirements should include:

- low cost;
- easy processability and the possibility to cover large areas by inexpensive deposition techniques;
- a way to tune the optical properties;
- robustness to natural deteriorating agent;
- low toxicity and an environmental-friendly disposal process . . .

In this section, the materials used for the preparation of the organic conversion layer (OCL) and the methods used to deposit it for the specific application in this work are briefly described.

3.4.1 Poly(Methyl-Methacrylate) Embedding Matrix

Poly(methyl-methacrylate) (PMMA) is an organic polymer well known because it is widely used in semiconductor lithographic processes [53]. PMMA is the polymer of th methyl-methacrylate (MMA), which is the ester of the metacrylic acid (MAA); it is a strong, lightweight material and, most importantly, is almost transparent in the visible range of the electromagnetic spectrum (92% transmission). This features allow PMMA to be often used as an alternative to glass.

The chemical formula of PMMA is $(C_5H_8O_2)_n$ and its structure is shown in Fig. 3.29.

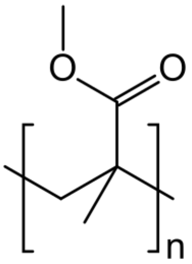

Fig. 3.29: Chemical structure of the repeating unit of PMMA.

Since different compositions for the industrial PMMA exist, there is no absolute glass transition temperature: nonetheless, in literature are reported values ranging from 45 °C to 140 °C [54] are reported. For this reason, PMMA appears like a solid glass at room temperature.

Usually, PMMA is obtained by radical polymerization of MMA but in this work the material used is in powder form and dissolved in an organic solvent for easier handling during the casting process. Among all of the known solvents that can be used [55], ethyl acetate (Sigma-Aldrich, 99.8%) has been chosen for two reasons: one is that for its volatility it is suitable for casting processes where fast drying is required, and the other because it is one of the less dangerous alcohol-based solvent.

Two types of PMMA (Sigma-Aldrich) are used in this work: one at 350,000 average M_W and the other at 996,000 average M_W.

Fig. 3.30: A picture of the chemicals used for the preparation of the OCL.

3.4.2 BASF Lumogen F Dyes

As discussed previously, using phosphors made of rare-earth mixtures (e.g., Ce:YAG, etc.) as wavelength converters, is a well consolidated process but still in some cases very expensive and with relatively poor balance between color rendering properties and luminous efficiency. The use of organic dyes can offer a better conversion efficiency (CE) and higher degree of color tunability. It is reported that the CE of some organic dyes can reach values higher than 95% [56], whereas inorganic dyes have CE around 90% (see Table 3.3).

Tab. 3.3: Conversion efficiency of some commercial phosphors [57].

Phosphor	Abbreviation	CE (%)
$Mg_4GeO_{5.5}F:Mn$	MGM	80
$(Sr,Mg)_3(PO_4)_2:Sn$	SPS	80
$Y_3Al_5O_{12}:Ce$	YAG	80
$Y(V,B,P)O_4:Eu$	YVE	85
$BaMgAl_{10}O_{17}:Eu$	BAM	90
$(Ce,Tb)MgAl_{11}O_{19}$	CAT	90
$(Ce,Gd,Tb)MgB_5O_{10}$	CBT	90

In this work, organic luminescent dyes based on a perylene molecule were used. These materials were supplied by BASF SE and commercialized under the name "Lumogen F series". The Lumogen dyes have high resistance to weathering and show low migration phenomena; they can resist to temperatures up to 300°C (in PMMA) and they can also be disperded very easily. Differently from other organic dyes used for lighting applications, Lumogen is in powder form and can be dissolved in common organic solvents [58].

Fig. 3.31: A picture of Lumogen F Yellow 083 powder.

Previous works on the use of Lumogen for color conversion applications [59] and as fluorescent solar collector [60] have been published, proving that its use can be fitted to visible light-emitting devices.

A dye for frequency down-conversion must have its absorption spectrum that completely overlaps with the emission spectrum of the pump source: Lumogen dyes have a wide absorbtion spectrum and this also allows the user to have much freedom in the choice of the pump wavelength. For example, the absorption range of Lumogen F Yellow 083 shown in Fig. 3.32, it can be seen that one could choose pump LEDs emitting from 400 nm to 450 nm, whereas care must be taken when using higher wavelength sources because of the overlapping with the emission spectrum of the dye that could cause self-absorption phenomena.

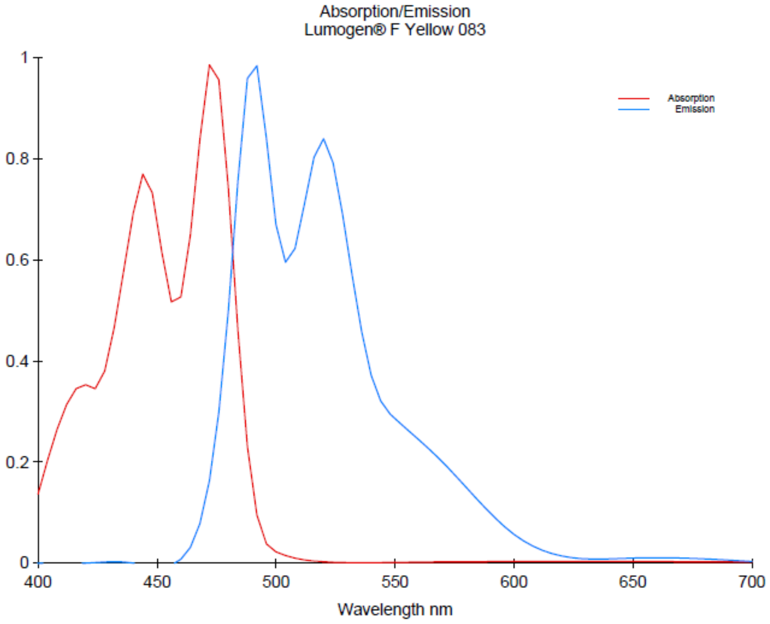

Fig. 3.32: Absorption and emission spectra of Lumogen F Yellow 083. *(source: BASF Lumogen F Yellow 083 Technical Datasheet)*.

3.4.3 Deposition of the Conversion Layer

To obtain an HWLED, different organic conversion solutions can be prepared choosing either the concentration of the chemicals or the molar mass of the PMMA incorporated. In any case, the density of the solution is affected but, when choosing two solutions with the same viscosity, the dye shows more resistance to to dissolve in the solution using the PMMA with the higher molecular weight. Ethyl acetate solutions at 11% (w/w) prepared with PMMA at M_W = 350,000 and 0.5 g/L of Lumogen F Yellow are obtained by stirring the materials in small bottles without any heating for one night, with no direct natural or artificial light source shining on the solution. The bottles are then stored in air tight containers in a dark area.

The deposition technique of the conversion layer depends on the coating profile that is required for the white LED. For special conversion layer configurations, like remote coating or conformal coating, complex instruments may be required. Conventional coating in a traditional white LED is obtained by dispensing a droplet of the phosphor, dispersed in a silicone resin, onto the packaged device [11].

Fig. 3.33: Cammax Precima spin-coater at the Thin Films Laboratory of DEIM of Università degli Studi di Palermo

In flip-chip HWLEDs the deposition of the OCL can be obtained by spin-coating the material on the sapphire bare side of the LED. A spin coater is an instrument with a rotating disk, named "chuck", that is used to spread a liquid coating on a sample with the centrifugal force of the rotation. The rotational speed can be set to a specific value, while vacuum is applied through the center of the disk to help keeping the sample steady and flat against the chuck (see Fig. 3.33). For liquids with moderate viscosity, a precise control of the thickness of the spin-coated material can be achieved [61]. High-viscosity liquids are more difficult to spin, since the drying process of the solvent could end before the polymer lays evenly on the device surface. For nanostructured HWLEDs, the OCL can also be spin-coated but, according to the technique adopted, the deposition can be performed before or after the processing of the metal contacts of the device.

Since a spin coater can have several setting parameters, it is easier to have specific control of the OCL thickness (and, therefore, of the color obtained for the HWLED); in this way, the binning of the white LED can be reduced to obtain commercial devices with a lower spread on color emission characteristics.

4

Device Performances and Comparisons

In this chapter, the performances of the HWLEDs processed are analyzed. First, the device that makes use of the nanostructured ZnO on a GaN thin film is shown; the layout process and the measurements are explained in detail. Afterwards, the HWLED obtained with a standard GaN/InGaN blue LED is tested, along with the possibility to obtain a tuning of the emission color by incorporation of mixed dyes in the polymer matrix of the OCL.

4.1 Nano-ZnO/GaN HWLED

4.1.1 Device Fabrication

For a better understanding of the fabrication process it is useful to show the proposed geometry for the device to be fabricated as in Fig. 4.1.

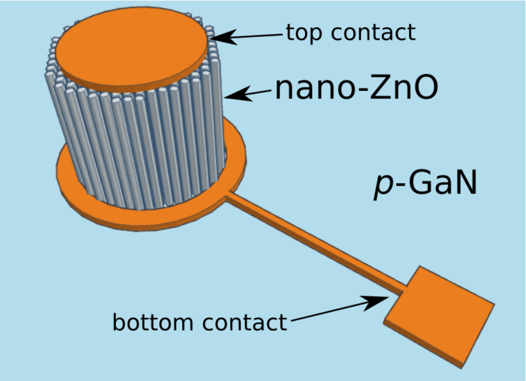

Fig. 4.1: Sketch of the nano-ZnO/GaN diode.

The *p*-GaN film, grown by MOVPE, is cleaned with acetone and isopropanol in a ultrasonic bath for 15 minutes. At the end of the cleaning the sample is dried with compressed air. Then, the sample is spin-coated with Shipley Microposit S1805 photoresist for 60 s at 2700 rpm and placed in a laser direct writing machine for the anular bottom contact lithographic definition. After the writing, the sample is developed with MF319 for 75 s. Once the metal contacts for the bottom contacts are deposited, the lift-off process of the residual photoresist is carried on with acetone.

Then, a new lithography process is required to open the circular windows for the growth of ZnO nanorods (see Fig. 4.2).

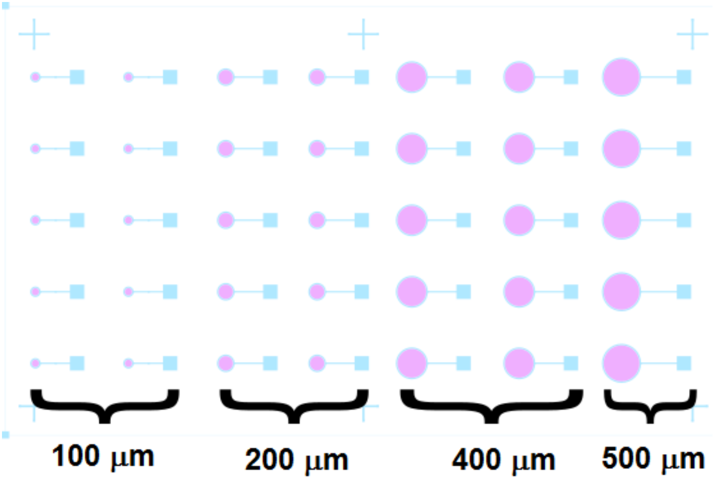

Fig. 4.2: Lithographic mask engineered with Electric VLSI Design System: in the lower part of the figure the diameters of the circular contact for the ZnO nanorods are reported.

After developing the sample, it is placed in a beaker with the hydrothermal solution and heated for 4 hours to obtain around 10 μm long nanorods. At the end of the growth, the sample is rinsed with bi-distilled water and blown dried with compressed air. Finally, the metal top contact is deposited and the lift-off process reveals the final device, shown in Fig. 4.3.

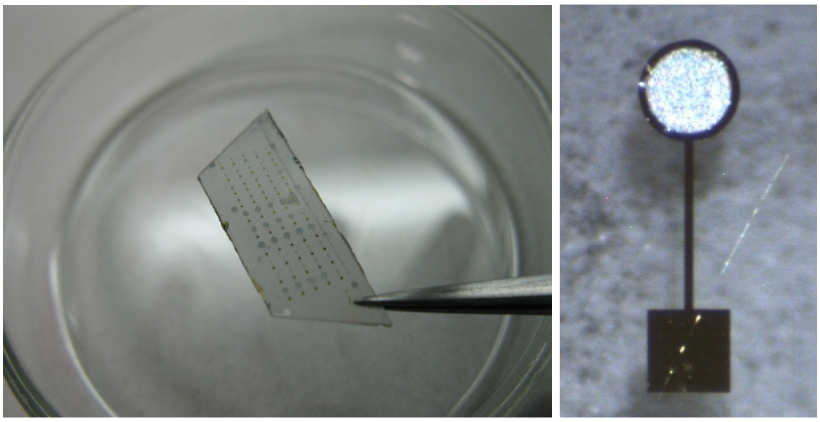

Fig. 4.3: (Left) picture of the finished sample; (right) optical microscope picture of the nano-ZnO/GaN diode: the top contact has a diameter of 200 μm and the spacing between the top and bottom contact is 3 μm; the pad for GaN probing of the device is a (200 x 200) μm square.

The metal contacts can be evaporated with two techniques: for metals with low melting point, a thermal evaporator (also CO_2 laser-assisted) is used, for other metals with higher values of melting point an electron beam evaporator comes into help.

For the deposition of the OCL, a drop of the PMMA solution with the dye is placed on the sample about 1 cm away from the device and then spin-coated at 2000 rpm for 30 s; the zone with the square pad on GaN is cleaned with a cotton swab dipped in acetone, whereas the nanorod zone remains filled with the dyed polymer.

4.1.2 Characterization and Analysis

The device is placed on a probe station equipped with two micromanipulators (Electroglas Inc.) with tungsten probes, and the manipulators are connected to an external power supply (see Fig. 4.4). The emission of the diode is collected with 50 μm core optical fiber and directed to a USB spectrometer (Ocean Optics HR4000) connected to a laptop. The software for the acquisition of the spectra and the chromatic coordinates is Ocean Optics Spectra Suite.

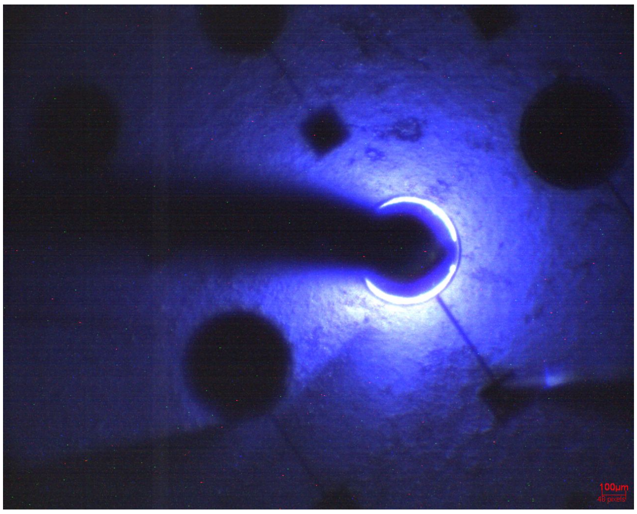

Fig. 4.4: Optical microscope picture of an operating nano-ZnO/GaN device.

At the beginning of the analysis, a couple of devices without the OCL are considered. The first noticeable feature is deduced by the current-voltage curves of the LEDs (see Figg. 4.5 and 4.6). All of the devices show a diode exponential characteristic but with a fairly high forward voltage value of about 6-7 V. The first reason of this behaviour is of course the metal used for contacting the GaN: in this case, Ti/Au is used whereas for *p*-GaN the suggested couple should be Ni/Au. Unfortunately, the facilities used could not provide the deposition of the desired metals, therefore the injection characteristics can be definitely improved. The other reason for the high forward voltage could be the absence of doping in ZnO: on this work the intrinsic *n*-type properties of ZnO were exploited because there is still no advance in literature concerning the hydrothermal doping of ZnO. For example Croxall *et al.* in 1974 proved that incorporation of lithium is possible [62], but so far there is no evidence that this method leads to the spontaneous formation of aligned nanorods; besides, and most importantly, lithium is not a donor.

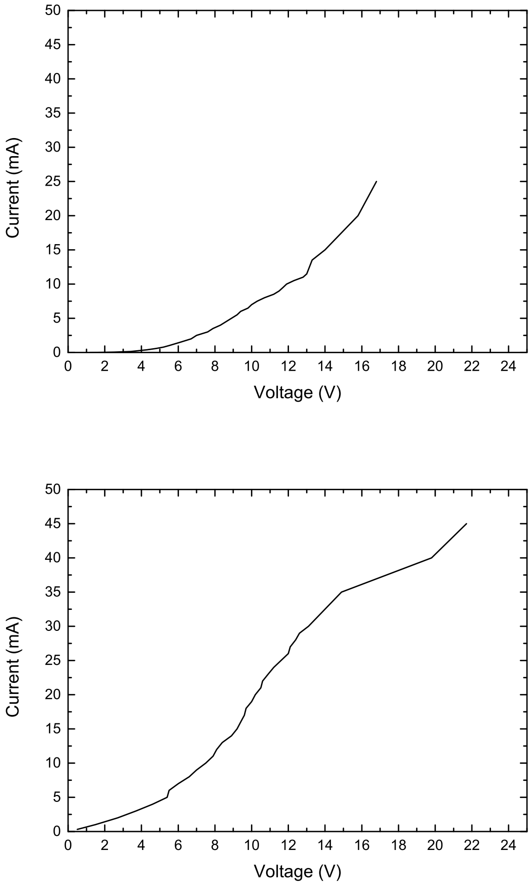

Fig. 4.5: V-I curves of the nano-ZnO/GaN diode with (top) a 100 μm top contact and (bottom) a 200 μm top contact.

It is also noticeable that most of the curves do not have an abrupt turn-on voltage and also start bending at around 14 V. These non-idealities can be identified as follows:

- for the sub-threshold conduction, a current can be due to transport through surface states of the ZnO nanorods. This can be modeled with a shunt resistance, parallel to the diode.
- the curve bending effect at high voltages is mainly due to high-injection of carriers which cause a voltage drop in the quasi-neutral regions. This is modeled with a series resistance to the diode.

The inspection of the emission spectra reveals an interesting result. As light is emitted, with increasing driving current, there is a blue-shift of the emission curve (Fig. 4.7): this could be attributed to the fact that the recombination process at low injection current is dominated by conduction-acceptor transitions in p-GaN (typical at 440 nm emission) and, as the current increases, the luminescence approaches to

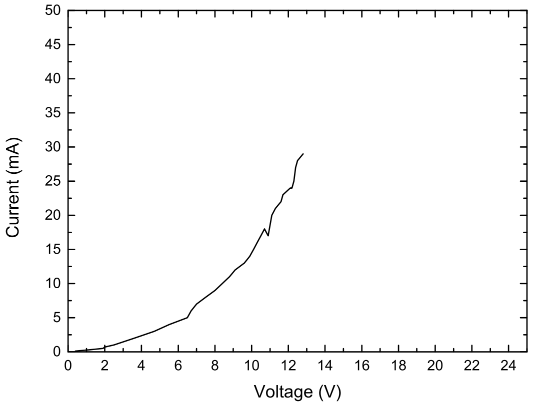

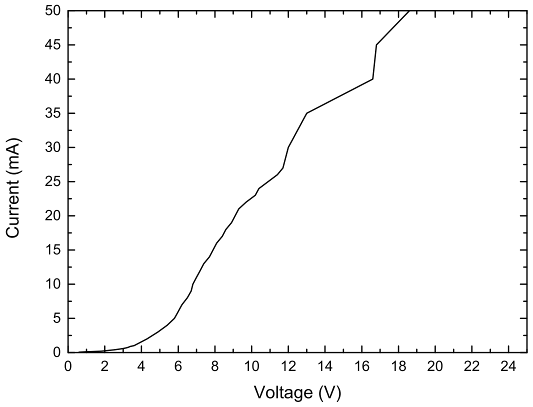

Fig. 4.6: V-I curves of the nano-ZnO/GaN diode with (top) a 200 μm top contact and (bottom) a 500 μm top contact.

ZnO recombination due to oxygen vacancies [63]. Nonetheless, at 40 mA, light is emitted at a peak of about 405 nm and with a FWHM around 40 nm.

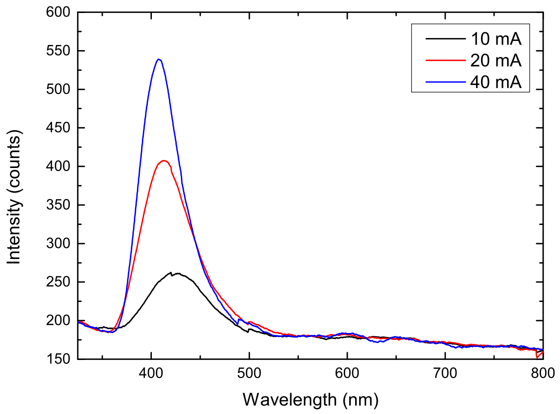

Fig. 4.7: Emission spectra of the blue nano-ZnO/GaN LED. A spectral blue shift is experienced at high injection currents.

This high value of FWHM is not a drawback when thinking to white LEDs: a higher content of wavelengths contributes to increase the CRI of the final device. In spite of what reported by several authors, there is also no yellow luminescence, typical of trapped impurities or oxygen vacancies, indicating that there is a very low defect content in the nanorods grown [64, 65, 66]. In Fig. 4.8, the emission spectrum of the device with the incorporated PMMA layer is reported.

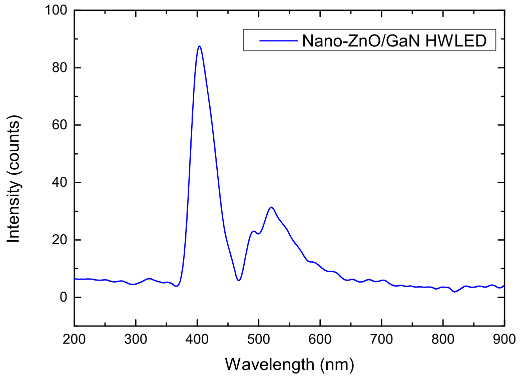

Fig. 4.8: Emission spectrum of the nano-ZnO/GaN HWLED.

The broad band in the range between 500 nm and 600 nm is clearly due to the emission of the Lumogen dye: the peak at 490 nm, partially re-absorbed by the dye itself, and the peak at 530 nm can also be found in Fig. 3.32. The power emitted at 400 nm is measured with a Newport Power Meter (mod. 1815-C) and a silicon photodetector (mod. 818-UV): the recorded value is 0.8 μW and the resulting luminous flux is 0.013 lm. Despite the low optical power, the chromaticity coordinates for this HWLED are (0.25;0.31) which puts the emission very close to the equal energy point (see Fig. 4.9) with a CCT of 12049 K and a CRI of 69: for an undoped ZnO-based device, the results are very promising.

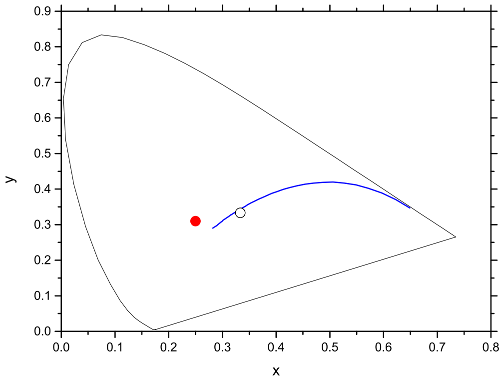

Fig. 4.9: Chromaticity coordinates of nano-ZnO/GaN HWLED's emission: the hollow point is the equal energy point, the red point is the emission color.

4.2 GaN/InGaN HWLED

4.2.1 Device Fabrication

The GaN/InGaN-on-sapphire wafer supplied by NOVAGAN Sàrl contains high-brightness LED that are specifically tuned, with quantum wells, to emit blue light at 450 nm. The device are grown in a mesa configuration and coated with the most appropriate metal for each semiconductor side (Ti/Au for *n*-GaN and Ni/Au for *p*-GaN). In Fig. 4.10 is shown one sixth of a 2” processed wafer.

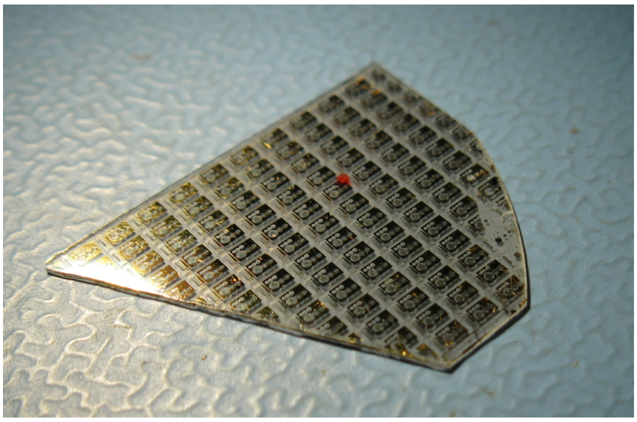

Fig. 4.10: NOVAGAN GaN/InGaN-on-sapphire chip of 2” wafer.

The wafer is spin-coated with the chuck speed ramping up at 1250 rpm for 30 s. After the coating phase is complete, the OCL is visually inspected. The layer appears translucent and well dried, thus there is no need to place the device in the oven (this phase is needed when the solvent does not dry completely even after the spin-coating). The sample appears as shown in Fig. 4.11.

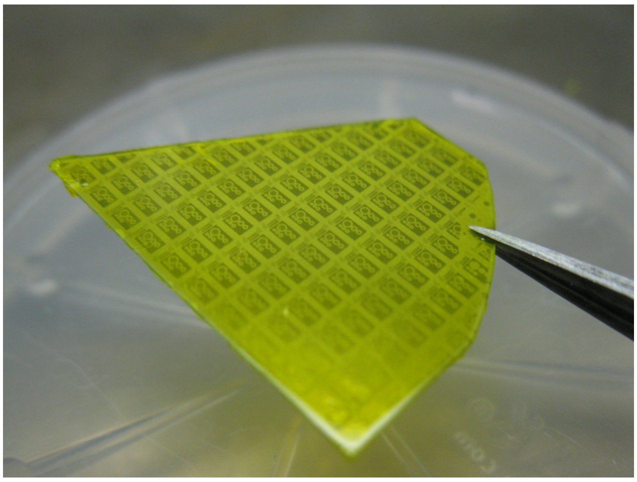

Fig. 4.11: Coated GaN/InGaN HWLEDs.

4.2.2 Characterization and Analysis

The sample is placed on the probe station and its light is captured while the current of the device is monitored by a power supply. All of the photometric parameters are taken at 20 mA. The emission spectrum is shown in Fig. 4.12.

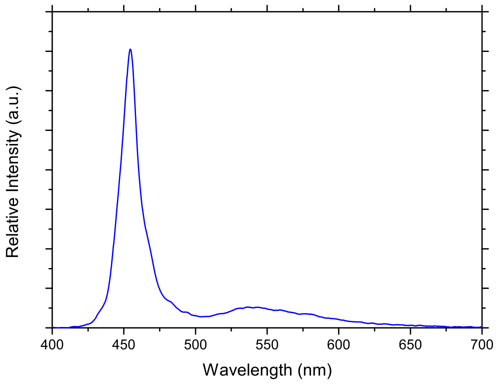

Fig. 4.12: Emission spectrum of the spin-coated GaN/InGaN HWLED.

A very weak band appears in the broad band between 500 nm and 600 nm, whereas the source pump at 450 nm is still clearly visible and mostly un-converted. The luminescence of the dye is so weak that even the emission peaks are quenched in such a configuration. The luminous flux measured is 4.80 lm and the luminous efficacy is 64.19 lm/W whereas, undere these conditions, the CCT and the CRI are not even measurable since the values have no physical meaning. In fact the point (0.19;0.14) is still too close to the border of the CIE 1931 color space. In Fig. 4.13, the chromaticity diagram of this HWLED is reported.

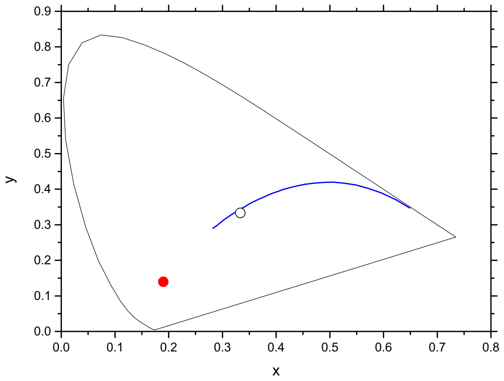

Fig. 4.13: Chromaticity coordinates of the spin-coated GaN/InGaN HWLED.

Since the frequency down-conversion was very poor, the OCL is washed away with an acetone bath, the wafer is rinsed with distilled water and a new sample with two successive spin coating is prepared. Extra-care needs to be taken when performing multiple coating since, when pouring the solution on the sample that was already spin-coated once, the liquid solvent slowly dissolves the underlying layer, therefore introducing an un-controlled variable. For this reason, after the first deposition, pouring the solution for the second time must be rapidly done. Then the output spectrum and the chromaticity coordinates of the HWLED twicely spin-coated are captured (Figg. 4.14 and 4.15).

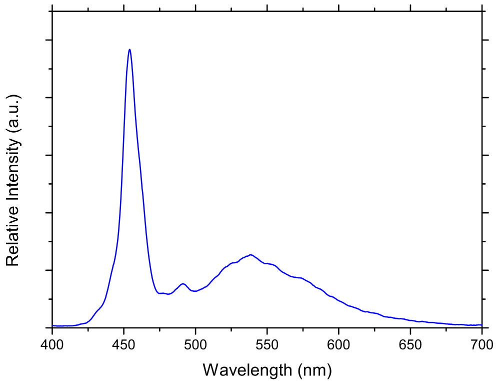

Fig. 4.14: Emission spectrum of the GaN/InGaN HWLED spin-coated twice.

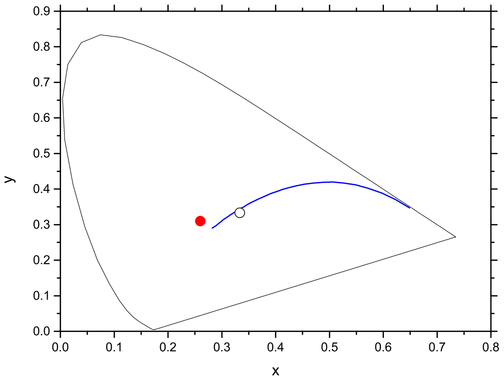

Fig. 4.15: Chromaticity coordinates of the GaN/InGaN HWLED spin-coated twice.

This time a considerable effect of excitation of the Lumogen is perceptible in both diagrams. The luminous flux raised 6.98 lm and the luminous efficacy has a value of 95.89 lm/W. The coordinates of the point move towards (0.26;0.31), whereas the computed CCT is 11456 K and the CRI is 71. Interestingly, the chromaticity coordinates of this device have a difference of only 0.01 on the x coordinate of the nano-ZnO/GaN HWLED tested previously, but here the CRI is 2 points higher. Though the numbers may not look impressive, the result is already comparable to most of the commercial low-power LEDs [67, 68, 69].

Of course, one could repeat the spin-coating deposition several times but this could represent a time-consuming process for the industry. In the large scale production of white LEDs, it is common to completely cover the blue LED by dipping it into the conversion phosphor resin. Therefore, this technique is as well discussed.

The OCL is again washed away in a bath of acetone and the wafer rinsed with distilled water, then the clean sample is dipped in the conversion solution and quickly taken out to dry at ambient conditions. After complete evaporation of the solvent, the contact side is gently cleaned with a sterilized cotton swab that was immersed in acetone (see Fig. 4.16).

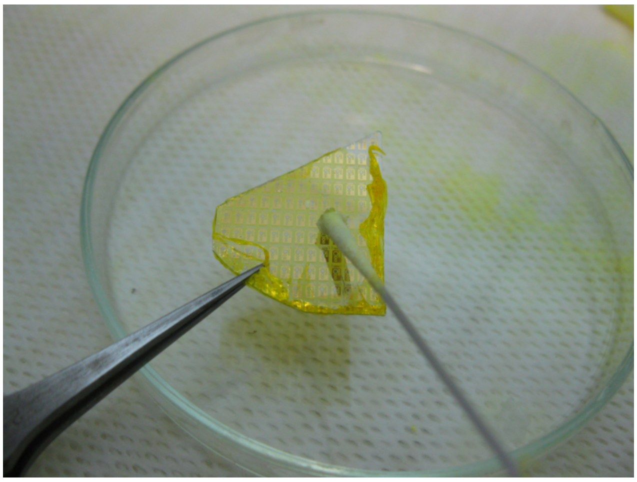

Fig. 4.16: The contact side of the HWLED is cleaned with a cotton swab immersed in acetone after dipping the wafer in the solution with the frequency down-conversion material.

At the end of the cleaning process, the output spectrum and the chromaticity coordinates are again recorded and plotted in Figg. 4.17 and 4.18.

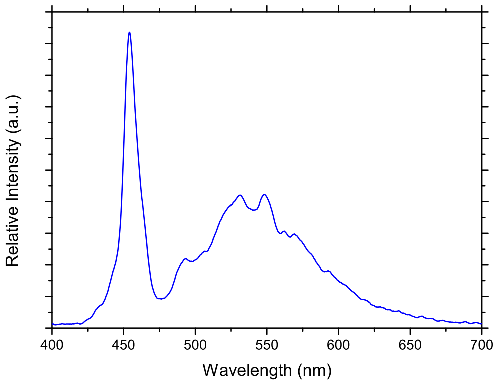

Fig. 4.17: Emission spectrum of the dip-coated GaN/InGaN HWLED.

A noticeable effect stands out in the emission spectrum: the shape of the luminescence curve of Lumogen is not particularly defined like in the previous cases. This is very probably due to the fact that the dip-coating process is not as uniform as the spin-coating, with the possibility that thick-deposited zones lie very close to thinner zones: not only this causes the spectrum to have an hardly predictable shape but also, most importantly, the binning of the HWLED is increased in such a manner that two devices next to each other in the same wafer could have a big difference in their color coordinates.

Nevertheless, the photometric parameters are outstanding: the best dip-coated result led to a luminous flux of 9,37 lm with a luminous efficacy of 118.23 lm/W [70]. Due to the high portion of electroluminescence in the region between 475 nm and 525 nm, the content of light-blu/green is very evident in the CIE color space: at the point (0.27;0.36), while the CCT decreased to a warmer temperature of 8414 K, the CRI decreased to 58.

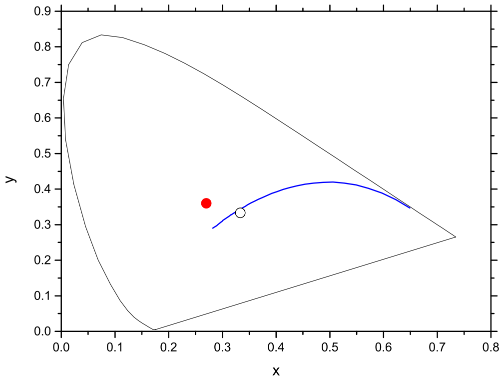

Fig. 4.18: Chromaticity coordinates of the dip-coated GaN/InGaN HWLED.

The technique surely brings the best photometric results but not certainly the best colorimetric ones. The table below summarizes the results obtained for the GaN/InGaN HWLED.

Tab. 4.1: Photometric and colorimetric parameters of the GaN/InGaN HWLEDs analyzed.

Deposition Method	Luminous Flux (lm)	Luminous Efficacy (lm/W)	Chromaticity Coordinates	CCT (K)	CRI
Single spin-coating	4.80	64.19	(0.19;0.14)	-	-
Double spin-coating	6.98	95.89	(0.26;0.31)	11456	71
Dip-coating	9.37	118.23	(0.27;0.36)	8414	58

As a matter of fact, the HWLEDs produced so far have been lacking in CRI and since the audience of the LED show is very large, some customers may consider this unacceptable.

Higher color-rendering index values can in general be obtained with a warmer white. So, just like inorganic red phosphors can be added to the formulation of the typical Ce:YAG, it is natural to ask whether the addition of a red organic dye could help in obtaining a warm HWLED. To this purpose, the F Red 305 is the corresponding perylene-based dye of the Lumogen family by BASF.

A careful inspection of the absorption/emission curves of Fig. 4.19 reveals that the emission of the yellow dye well overlaps with the absorption of the red one. This suggests that, just by choosing the amount of dyes to be mixed, one could tune the emission of the HWLED, obtaining a double frequency down-conversion process: one from blue to yellow and the other from yellow to red.

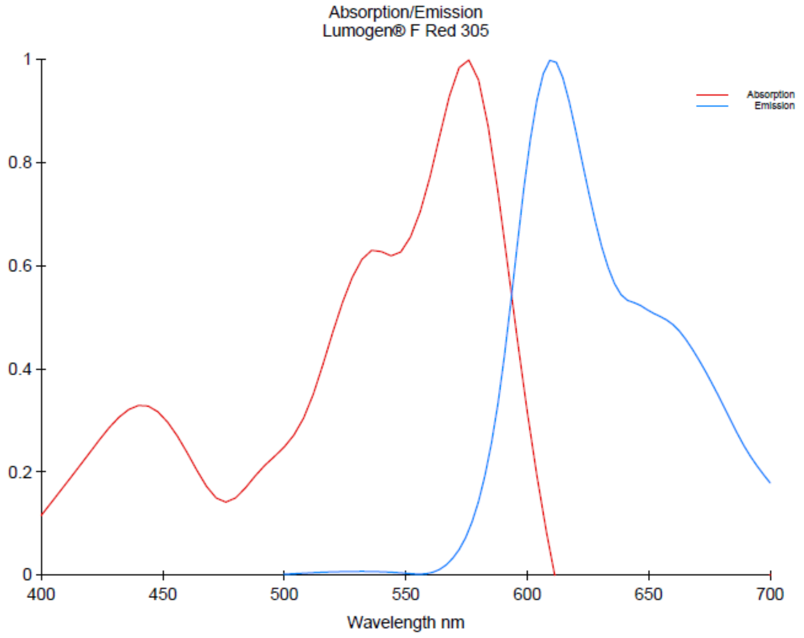

Fig. 4.19: Absorption and emission spectra of Lumogen F Red 305. *(source: BASF Lumogen F Red 305 Technical Datahseet)*.

In order to exploit the effect of the concentration of the organic dyes, four coating solutions with different red to yellow ratio were prepared: for the solutions MIX1, MIX2, MIX3, MIX4, the concentration of Lumogen Yellow was kept at 0.5 g/L whereas the Lumogen Red was added respectively to reach concentrations of 0.05 g/L, 0.1 g/L, 0.2 g/L, 0.5 g/L.

In the first experiment, the HWLEDs are dip-coated in the solutions. The spectra and the chromatic point in Figg. 4.20 and 4.21 labeled as W1 correspond to the HWLED dip-coated in solution MIX1, whereas the one labeled W2 correspond to the HWLED dip-coated in solution MIX2, and so on. A self-constructed dip-coater is used for these experiments to improve the reproducibility of the results.

The results show that the emission of the HWLEDs contains also the luminescence of the Lumogen Red and this is confirmed by the widened broad band peaked at 600 nm; still, the spectra are missing some yellow component since the chromaticity coordinates lie too much under the planckian locus. The values of CCT and the CRI are summarized in Table 4.2.

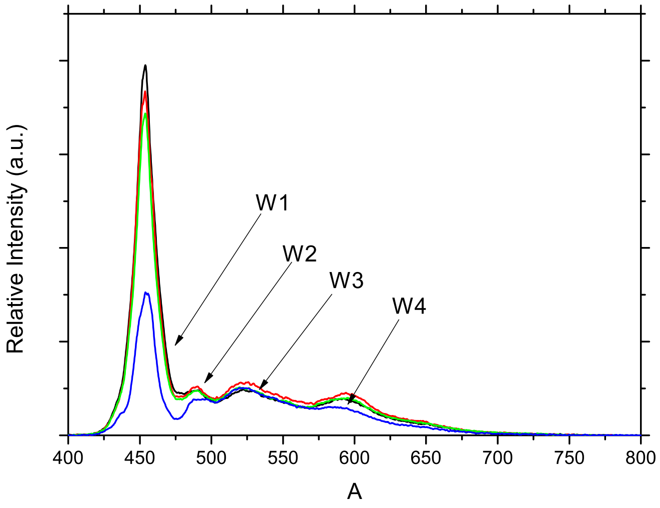

Fig. 4.20: Emission spectra of the GaN/InGaN HWLEDs dip-coated in the mixed dyes solutions.

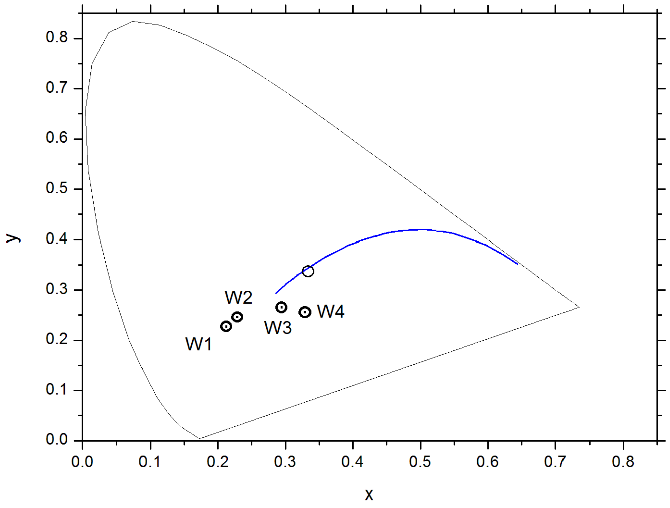

Fig. 4.21: Chromaticity coordinates of the GaN/InGaN HWLEDs dip-coated in the mixed dyes solutions.

Tab. 4.2: Correlated color temperature and CRI of light emitted by LEDs W1-W4.

Sample	W1	W2	W3	W4
CCT (K)	-	74660	9903	5293
CRI	-	85	86	63

In the next experiment, a first dip-coating was performed in a simple yellow solution, then a second dip-coating was made with the mixed dye solutions. The results are shown in Figg. 4.22 and 4.23 and summarized in Table 4.3.

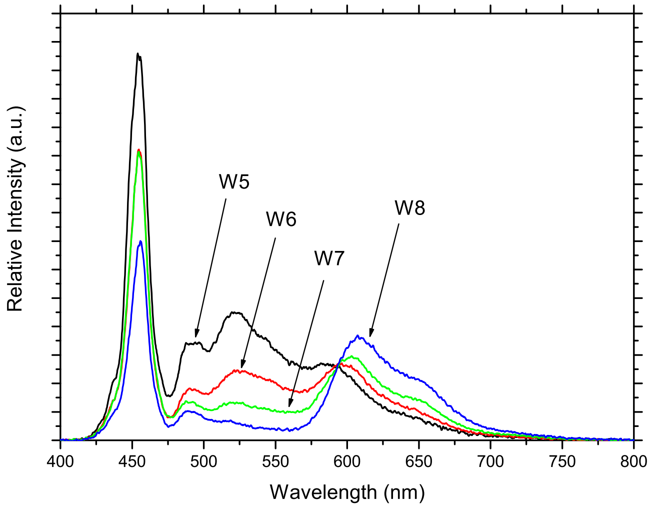

Fig. 4.22: Emission spectra of the GaN/InGaN HWLEDs dip-coated first in the yellow solution and then in the mixed dyes solutions.

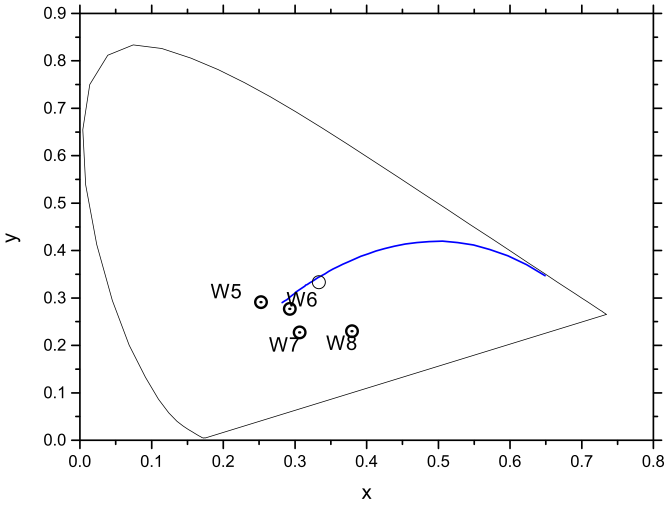

Fig. 4.23: Chromaticity coordinates of the GaN/InGaN HWLEDs dip-coated first in the yellow solution and then in the mixed dyes solutions.

Tab. 4.3: Correlated color temperature and CRI of light emitted by LEDs W5-W8.

Sample	W5	W6	W7	W8
CCT (K)	13523	9239	11491	2159
CRI	78	90	62	32

The obtained result is definitely acceptable for a cold white HWLED, especially considering W6 and its CRI of 90, but still not enough for a warm white one. In the last experiment, a first dip-coating in the yellow solution and two successive dip-coatings in the mixed dyes solutions were carried out. The results are shown in Figg. 4.24 and 4.25 and summarized in Table 4.4.

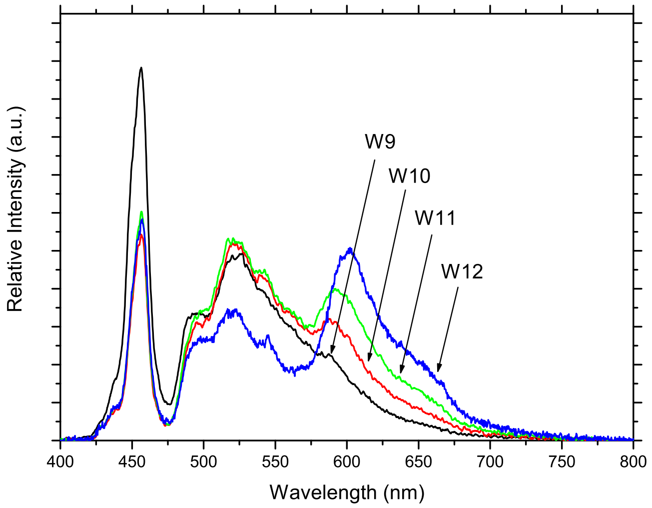

Fig. 4.24: Emission spectra of the GaN/InGaN HWLEDs dip-coated first in the yellow solution and then twice in the mixed dyes solutions.

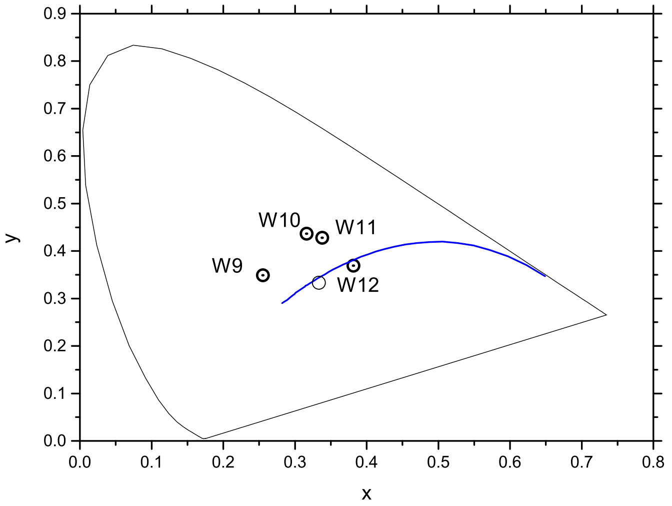

Fig. 4.25: Chromaticity coordinates of the GaN/InGaN HWLEDs dip-coated first in the yellow solution and then twice in the mixed dyes solutions.

The final results show that though the CCT of the HWLEDs effectively decreased, also the CRI can suffer a little if the distance of the cromaticity coordinate of the LED's emission to the standard illuminant is high. The performances of the HWLED

Tab. 4.4: Correlated color temperature and CRI of light emitted by LEDs W9-W12.

Sample	W9	W10	W11	W12
CCT (K)	9587	5966	5369	3912
CRI	64	66	76	87

W12 show that a clever distribution of the mixing of the dyes and of the thicknesses of the OCLs can lead to optimal results in terms of tuning of color temperature [71].

It must be pointed out that the parameters that can be set by the dip-coater are the velocity and the acceleration of the extraction of the sample in the solution, but there was no control on any kind of tilting of the sample. That said, the spectra are quite correlated and show congruent data that support the theory concerning the benefits of adopting organic dyes as good substitutes for traditional phosphors.

5

Stability of the Organic Conversion Layer

One of the major obstacles that limit the use of organic compounds for lighting purposes is the limited stability of the luminescent materials [72, 73]. Quantum structures or the use of nanoparticles introduced in the polymer matrices of the OCL are promising techniques [74] but their high cost make these solutions not much prone to the large scale production.

It is well known that organic compounds suffer from low chemical stability. The UV photodegradation of dyes is a widely documented process but also embedding polymers can exhibit significant bleaching caused by chemicophysical agents [75, 76, 77]. Since PMMA is one the most widely used polymers for these applications, its stability needs to be investigated. In this chapter the results of the degradation of the OCL under prolonged irradiation of the pump source are presented.

5.1 Spectral Degradation and Color Shift of HWLEDs

The stability of white light-emitting diodes is a problem that can be of an importance that goes beyond mere aesthetic issues. In some applications, like in museums or hospitals, mantaining a constant color is required since objects are evaluated by their color. It is also quite curious that the standards for the life time of luminaires give indications for the lumen output of SSL sources and do not specify any color stability parameter.

However, the degradation of an HWLED is quite noticeable when analyzing the emission spectra and the corresponding color shift. For the emission in Fig. 5.2, the light output of the HWLED is monitored using the setup in in Fig. 5.1 during 210 minutes of constant driving current at 20 mA. The charge-coupled device (CCD) of the spectrometer senses a relative intensity change of the 450-nm emission peak from 1500 to 6500 photon counts. The fluorescence of the dye remains almost unchanged, meaning that Lumogen becomes less sensitive to the increasing intensity of the pump source. Moreover, not only does the dye visually bleach but the PMMA itself could be affected by the exposure to the source [78, 79]. The reasons for this degradation can be ascribed to thermal and optical stresses and they will be carefully analyzed in sections 5.2.1 and 5.2.2.

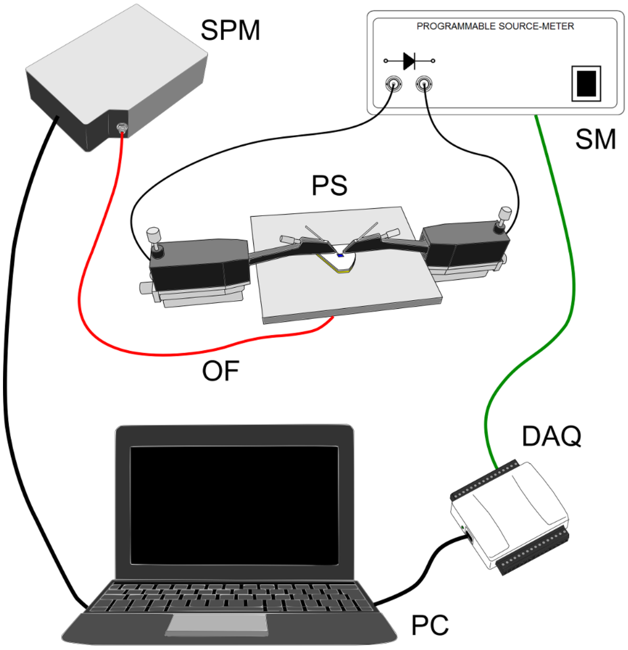

Fig. 5.1: Experimental setup used for the optical characterization of the HWLED. The metal contacts of the LED are probed with two micromanipulators on a probe station (PS) connected to a programmable source meter unit (SM). A laptop (PC) acquires the V–I characteristics of the diode through a USB interface (DAQ) while the light output of the LED is recorded with an optical fiber (OF) connected to a USB spectrometer (SPM); the source meter unit is able to perform programmable constant current driving.

The CIE (x;y) chromatic coordinates of the HWLED (0.30;0.39) moved towards the point at (0.21;0.23) (see Figg. 5.3 and 5.4).

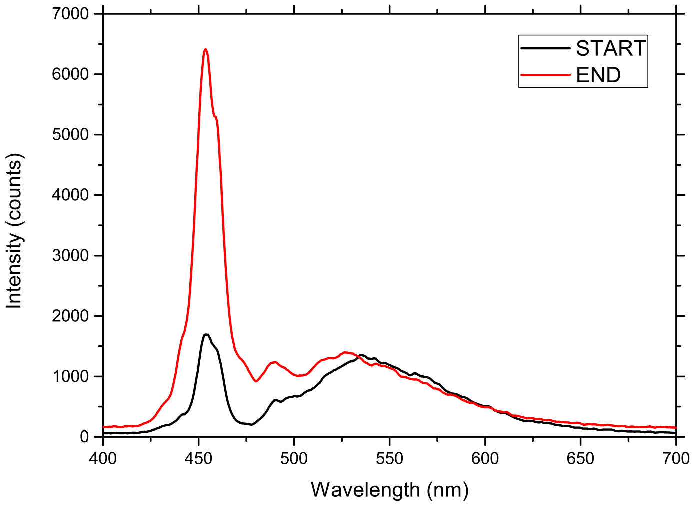

Fig. 5.2: Emission spectra of the HWLED collected during an optical stability test consisting of 210 min of constant driving current operation.

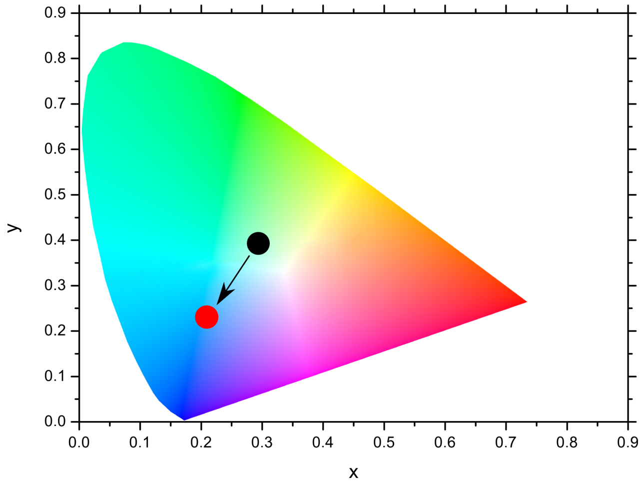

Fig. 5.3: Chromaticity shift of the HWLED color emission in the CIE plot.

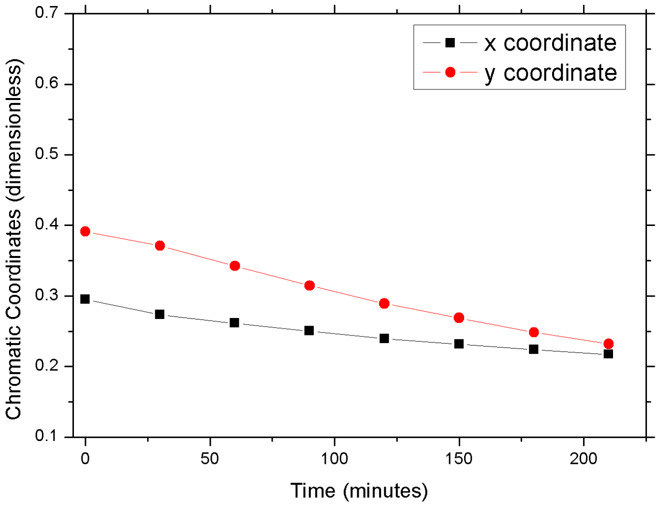

Fig. 5.4: The variation of chromaticity coordinates (x;y) of the HWLED as a function of time.

5.2 Stability Issues

5.2.1 Thermal Stability

The purpose of the thermal stability test is to exclude any connection between the degradation of the organic coating and the operating temperature at the interface between the conversion layer and the sapphire side of the HWLED. The theory is supported by the fact that sapphire has a high thermal conductivity (40 W/m·K at 25°C), so the heat from the low-power LED can flow through the substrate in the flip-chip configuration. While direct measurement on the diode is a very hard task, the value of the temperature is extrapolated using an experiment.

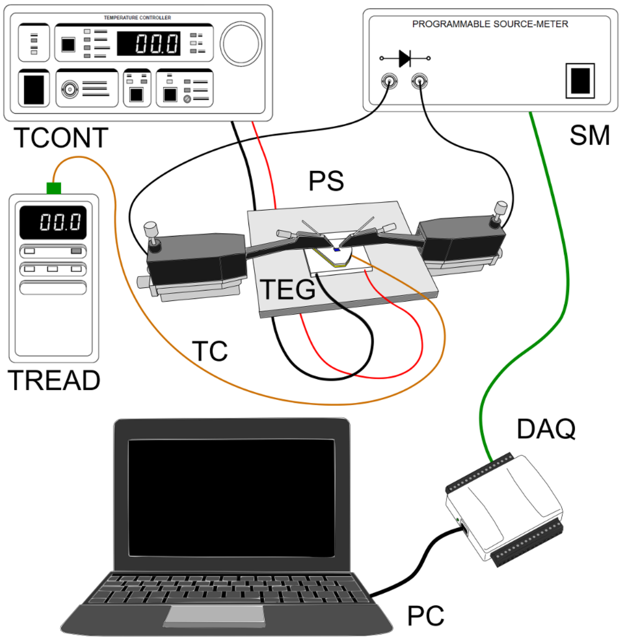

Fig. 5.5: Experimental setup used for the thermal characterization of the HWLED. The wafer is positioned on a thermoelectric generator (TEG) driven by a specific controller (TCONT) while the temperature of the sapphire substrate is monitored with a thermocouple (TC) connected to a digital reader (TREAD).

The V–I characteristics of the bare blue LED are plotted when heating the wafer from ambient temperature (25°C) to 45°C, 50°C, 70°C, and 80°C using a thermoelectric generator (TEG) connected to a Newport 325 temperature controller (see Fig. 5.5); the set of curves is then compared with the V–I characteristic resulting from a stress test on the LED when lit for 1 h. Since the curve of the diode after the stress test lies above the curve plotted at 25°C and well below the one at 45°C (see the dashed curve in Fig. 5.6), it is possible to reasonably confirm that any organic degradation cannot be ascribable to the rise in temperature at the interface between the PMMA and the sapphire.

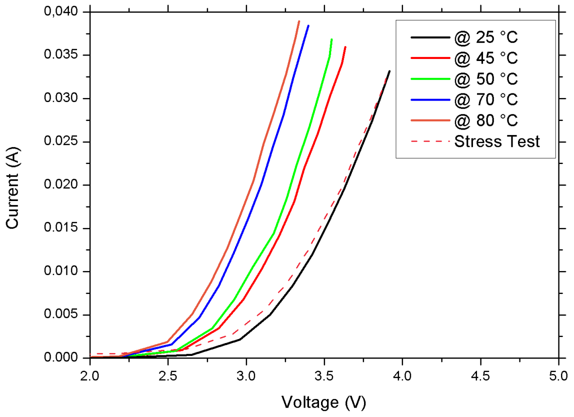

Fig. 5.6: V–I characteristic plots of the blue LED recorded with increasing operating temperature set by an external thermoelectric generator.

5.2.2 Optical Stability

To further investigate whether the light of the LED interacts with the polymer, a film of PMMA is prepared without addition of the dye and then exposed to the blue light for 100 h. The UV–VIS spectrum reported in Fig. 5.7 shows about a 3% change in the absorption around 450 nm. To obtain more information, FT-IR analysis was performed.

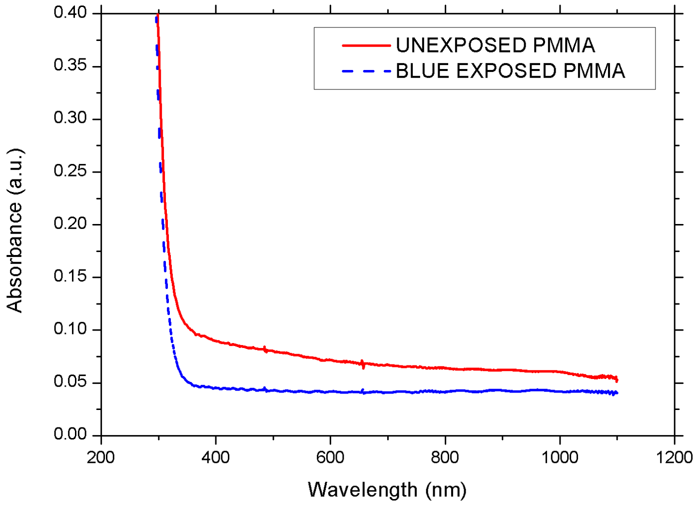

Fig. 5.7: UV–VIS absorption spectrum of two samples: the red solid curve represents the absorbance of an unexposed PMMA membrane; the blue dashed curve is the spectrum of a membrane exposed for 100 h to the blue light.

The pattern in Fig. 5.8 has an inset showing the magnified wavenumber region where the difference between the spectra is more prominent. No position modification is evidenced, but the peak located at 1735 cm^{-1} (stretching of COO– of ester group) shows an intensity variation which corresponds to a modification in some esteric groups of the PMMA's entanglement. A consequence of this change is also demonstrated by a less evident lowering of the bands from 1150 cm^{-1} to 1270 cm^{-1} and from 1350 cm^{-1} to 1500 cm^{-1}, which correspond to C–O and C–H stretching. This variation is consistent with literature [80].

Thus, a weak degradation phenomenon in the polymer also occurs due to decomposition of the ester group activated by the LED visible light.

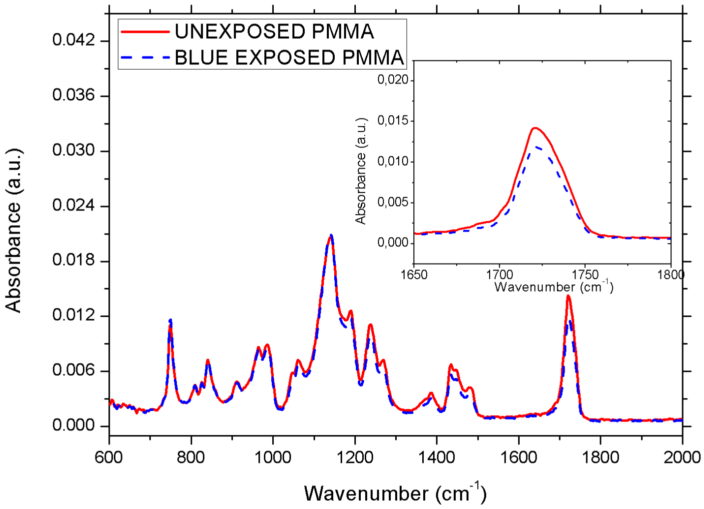

Fig. 5.8: FT-IR spectrum of a PMMA membrane. The dashed curve in the inset shows a magnified portion of the IR spectrum around 1730 cm^{-1}, indicating that the absorbance of the COO– group lowers when the PMMA film is exposed to the blue light of the LED with respect to an unexposed polymer film.

5.3 Improving the Stability of Organic Fluorescent Coatings in HWLEDs

In this section, three methods for improving the stability of the conversion layer are presented. The first deals with UV curing of the solution containing PMMA; the second method uses a polymer with different average molecular weight; the third method makes use of a different polymer concentration in the prepared solution.

The curing process generally involves modification of the structure of the polymer that eventually acts as a protective matrix for the dye. Changing the composition of the solution using a polymer with higher M_W, or preparing a more concentrated one, slows down the process of photooxidation of the polymer chain.

The curing time, the choice of a different PMMA, and a higher concentration value of the solution are chosen as optimum values for the experiments to be performed. All of the tests are conducted for 210 min at 20 mA constant current. For each method, the emission spectra recorded at the beginning and end of each test are reported. Table 5.1 summarizes the shift of the chromatic coordinates of the HWLEDs for the three methods proposed.

5.3.1 PMMA UV Curing

A solution is prepared by dissolving PMMA powder in ethyl acetate; after stirring, the solution is cured with a UV lamp for 1 h. In the following step, the dye is incorporated and the conversion layer spin-coated onto the wafer. After the treatment, a noticeable stabilization effect is clearly visible, since both the spectra growth and the variation in the CIE chromatic coordinates are reduced. Fig. 5.10 shows the emission spectrum, which reveals that the organic layer is less sensitive to the pump source: the wavelength peak at 450 nm shows a smaller change in intensity, while the chromatic coordinates exhibit a variation Δ(x;y) equal to -(0.03;0.08) (Fig. 5.11). The UV light modifies the structure of the polymer in a way that protects the incorporated dye. The drawing in Fig. 5.9 shows the key steps involved in the process adopted.

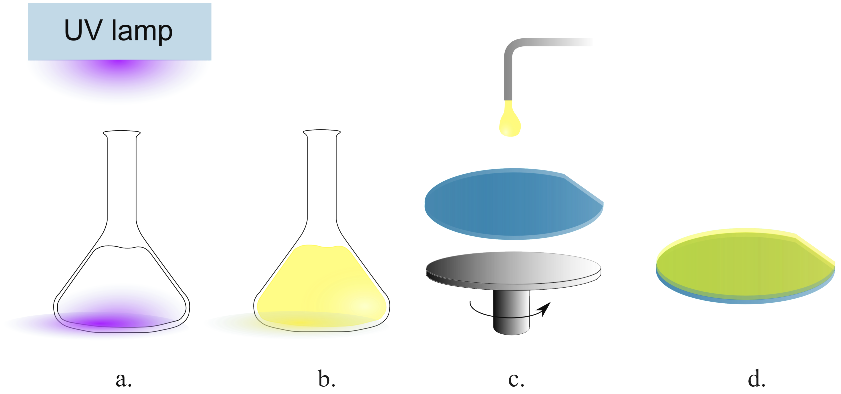

Fig. 5.9: Steps involved in the proposed process for improvement of the stability of PMMA in HWLEDs: (a) UV exposure, (b) incorporation of yellow dye, (c) spin-coating of the conversion layer, and (d) finished coated wafer.

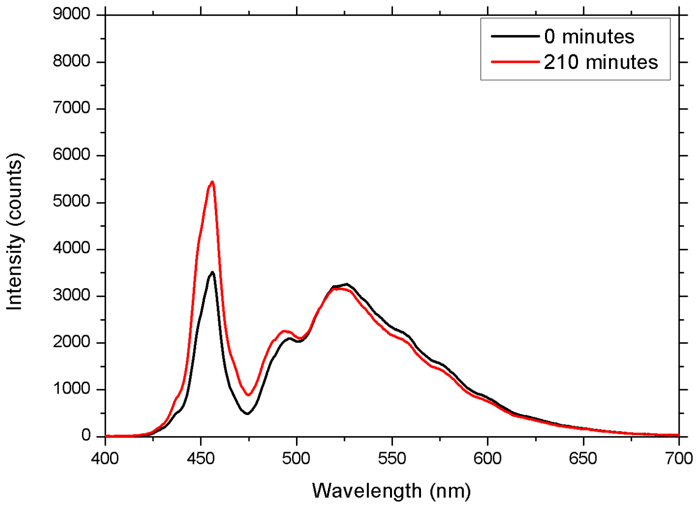

Fig. 5.10: Spectra of HWLEDs prepared using an UV-cured PMMA.

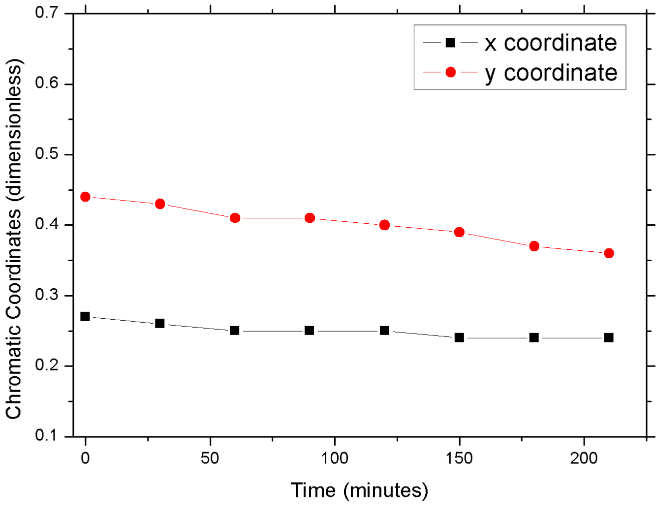

Fig. 5.11: Chromaticity coordinates, as a function of time, of HWLEDs prepared using an UV-cured PMMA.

5.3.2 Using a PMMA with Different M_W

A new solution is prepared using PMMA with average molecular weight M_W=996,000. The concentration of the solution is kept at 11% (w/w). The chromatic coordinates are more stable with respect to the case of the UV-curing method: the measured Δ(x;y) shift is -(0.01;0.04) (Fig. 5.12), while the recorded spectra revealed a small change in the emission of the HWLED (Fig. 5.13). This method is effective, but the experimental procedure showed difficulties since incorporation of the dye is very time consuming for the solution with a long-chain polymer dissolved in it.

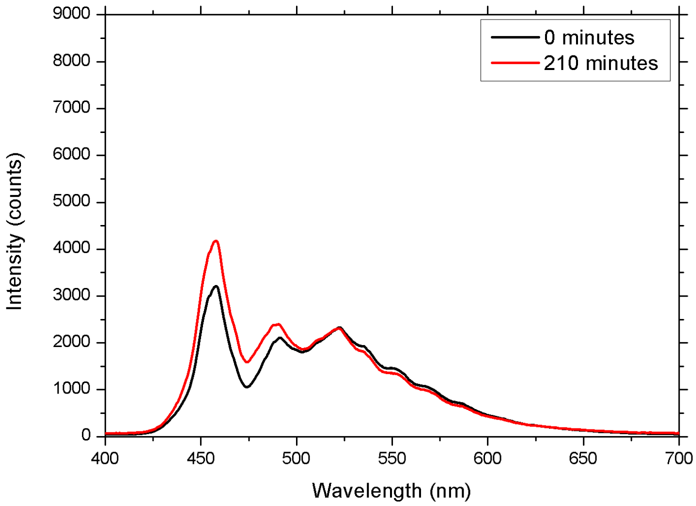

Fig. 5.12: Spectra of HWLEDs prepared using a PMMA with higher M_W.

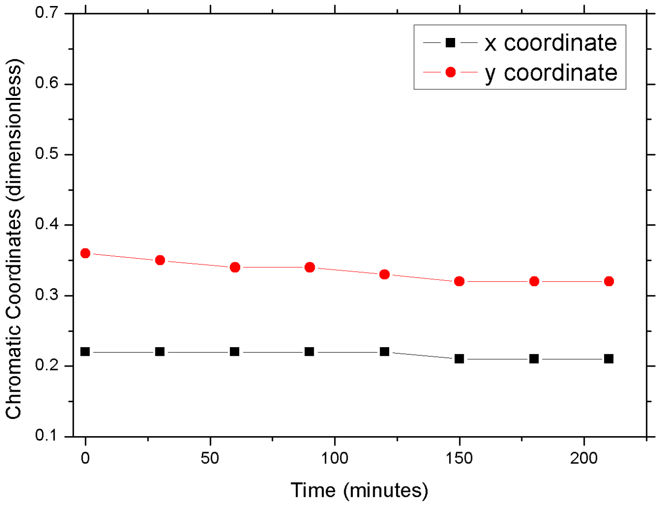

Fig. 5.13: Chromaticity coordinates, as a function of time, of HWLEDs prepared using a PMMA with higher M_W.

5.3.3 Changing the Solution Concentration

The last method for improving the stability of the conversion layer also makes use of PMMA with $M_W = 350{,}000$, but the concentration of the solution is raised to 18% (w/w). Fig. 5.14 shows the results for the emission spectra, revealing almost no change. For this last case, the chromatic shift Δ(x;y) is equal to -(0.01;0.02) (Fig. 5.15). Though this method proved to be the best of the three proposed, spin-coating a high-viscosity polymer solution is a complex task that hardly yields results in terms of the perfectly reproducible spectra.

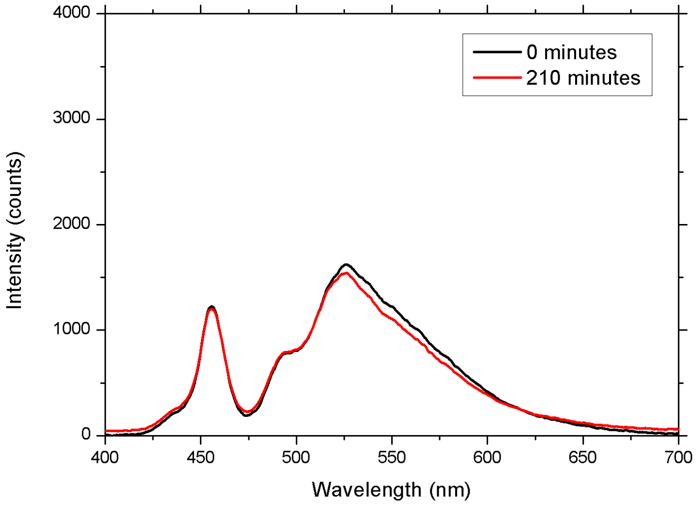

Fig. 5.14: Spectra of HWLEDs prepared using a more concentrated solution.

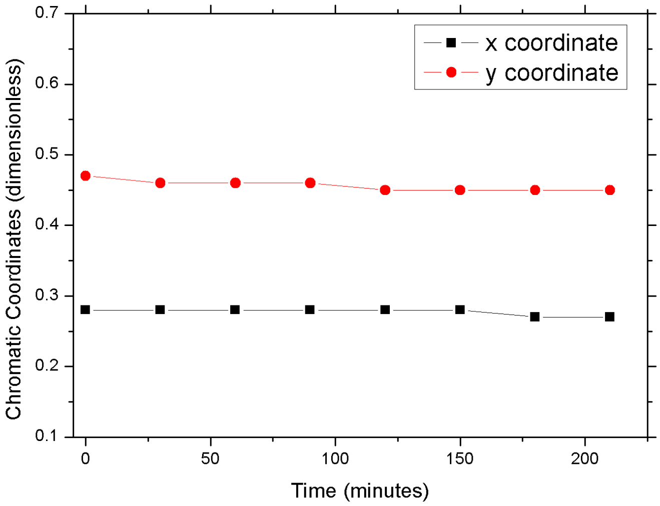

Fig. 5.15: Chromaticity coordinates, as a function of time, of HWLEDs prepared using a more concentrated solution.

Therefore, all three methods proved to be effective concerning the emission spectra and the shift in the CIE chromatic coordinates during 210 min of constant drive.

Tab. 5.1: Shift of chromatic coordinates of white light emitted by LEDs using the three proposed methods.

Method	Δ(x;y)
UV curing	-(0.03;0.08)
High-M_W polymer	-(0.01;0.04)
High-concentration solution	-(0.01;0.02)

Conclusions

6

The goal of this research was to analyze in deep detail the solutions proposed to valorize the Hybrid White Light-Emitting Diode technology. LEDs are optoelectronics devices based on the emission properties of semiconductors that can be engineered enough to fully replace any kind of luminaire in the future, and impose the value of SSL in the market both for economical and for energy saving reasons. The diffusion of more and more efficient sources pushes continuously the researchers to explore new ideas applied to material science.

In this work, two main subjects were studied. First, organic dyes that, when compared with conventional inorganic phosphors for color conversion in white LED, show their advantages for the high conversion efficiency. Second, re-designing the blue sources with the use of nanostructures, obtained with a low-cost technique, which leaves enough space to further improvements of the performances of the devices.

At first, the dissertation presented the materials investigated: GaN and ZnO, the former being the most diffuse III-V compound (together with its alloys) that with its remarkable optical properties leads the market of blue and white LEDs, and the latter being a promising candidate as an allied material to nitride semiconductors. The second chapter explained the theory behind the light-emitting diode technology, with definitions useful for the understanding of the content of this work, and the motivations beyond the development of HWLEDs, especially when nanostructured.

In chapter three, the experimental section dedicated to the development of the materials used in this work is detailed along with the description of the physical properties of the materials. For the GaN section, the MOVPE growth of *p*-type semiconductor was described. The morphological characterization of some samples grown at CNRS-CRHEA in Valbonne (France) was performed with AFM and optical microscope, and also the electrical characterization methods using C-V measurements and Hall Effect were presented. The investigation was followed by the analysis of low-temperature PL of *p*-GaN. In the ZnO section, extensive information were given concerning the growth mechanism of ZnO nanorods on various type of substrates. The SEM and XRD analyses of the material grown on GaN thin films show that a well-aligned structure can be achieved with the hydrothermal growth, a low-temperature acqueous chemical growth technique, without making use of seed or nucleation layers. The results obtained show the potential of this technique: nanostructuring heterojunction devices at low-cost is possible and the growth parameter can be controlled to obtain the desired density of nanostructures. The chapter ended with the details on the preparation of the organic conversion layer making use of PMMA and Lumogen F Yellow, a perylene-based dye.

Chapter four showed the results of two working devices. The first, a nanostructured ZnO/GaN-based diode, showed blue/violet light output at 405 nm with a peaked emission band. Proof of the realization of the junction was given with the I-V curves, obtained for several devices tested, which followed a rectifying behaviour. When combined with the organic conversion layer, a cold white emission was achieved with impressive chromaticity coordinates (0.25;0.31) on the CIE 1931 plot. On the other hand, the output power of the HWLED was quite low: this effect was attributed to the absence of doping in ZnO and to the choice of the metals adopted for the GaN contact that did not allow proper electrical injection. The second device was obtained using low-power high-brightness GaN/InGaN blue LEDs provided by NOVAGAN Sàrl, a spin-off of the of the École Polytechnique Fédérale de Lausanne (Switzerland). The devices were coated with the organic conversion layer following different techniques: record values of luminous flux and luminous efficacy of 9.37 lm and 118.23 lm/W respectively were achieved, obtaining a HWLED with chromaticity coordinates of (0.27;0.36). The low CRI recorded was a problem that was eventually solved with the adoption of a mix of yellow and red Lumogen dyes: the best device obtained with this technique showed a CRI of 90, whereas the “warmest” HWLED had a CCT of 3912 K.

Chapter five explored the degradation of the organic coating, while showing that almost 4 hours of continuous current drive severly degraded the color performances of the device. A series of experiments were conducted to explore on the thermal and optical stability of the dye and the encapsulating matrix, showing that the visible light of the blue LED pump source can affect the photostability of the coating. Three effective methods were also proposed to improve the stability of the conversion layer, each one with its advantages and drawbacks.

So far, much research on nanoscale LEDs has been done but there are still several aspects that need to be explored. The numerous possibilities offered by the material engineering show that this field is continuously evolving, producing always more efficient structures. Much effort in this direction is still under way in the Thin Films Laboratory of the Università degli Studi di Palermo, where I could spend three years of fascinating research on material deposition and growth for optoelectronics and photonics applications.

Bibliography

[1] G. Zissis and P. Bertoldi. *2014 Update on the Status of LED Market*. JRC Science and Policy Reports JRC92971. EU Joint Research Centre, 2014.

[2] Collaborating Labeling and Appliance Standards Program (CLASP). *Estimating potential additional energy savings from upcoming revisions to existing regulations under the ecodesign and energy labelling directives*. CLASP review. European Council for an Energy Efficient Economy, 2013.

[3] D. Persano Adorno and S. Pokutnyi. *Advances in Semiconductor Research: Physics of Nanosystems, Spintronics and Technological Applications*. Nova Science Publishers, 2014.

[4] H. Morkoç and Ü. Özgür. *Zinc oxide: fundamentals, materials and device technology*. John Wiley & Sons, 2008.

[5] S. Nakamura, T. Mukai, and M. Senoh. “Candela-class high-brightness InGaN/AlGaN double-heterostructure blue-light-emitting diodes”. In: *Applied Physics Letters* 64.13 (1994), pp. 1687–1689.

[6] S. Nakamura and G. Fasol. *The Blue Laser Diode*. Springer-Verlag, 1997.

[7] K. S. Gibson and E. P. T. Tyndall. “Visibility of radiant energy”. In: *Scientific Papers of the Bureau of Standards* 19 (1923), pp. 131–191.

[8] L. T. Sharpe, A. Stockman, W. Jagla, and H. Jägle. “A luminous efficiency function, $V^*(\lambda)$, for daylight adaptation”. In: *Journal of Vision* 5.11 (2005), p. 3.

[9] B. Saunders. “Revisiting basic color terms”. In: *Journal of the Royal Anthropological Institute* 6.1 (2000), pp. 81–99.

[10] B. Berlin and P. Kay. *Basic color terms*. 1969.

[11] E. F. Schubert. *Light-Emitting Diodes*. Cambridge University Press, 2006.

[12] CIE. “Colorimetry”. In: *CIE Pub* 15.3 (2004).

[13] CIE Colorimetry. “Official Recommendations of the International Commission on Illumination”. In: *Commission Internationale de l’Èclairage* (1976).

[14] G. E. Moore. “Cramming more components onto integrated circuits”. In: *Electronics* 38.8 (1965), p. 114.

[15] R. Haitz. “Another semiconductor revolution: this time it’s lighting!” In: *Advances in Solid State Physics*. Springer, 2003, pp. 35–50.

[16] B. Kramer. *Advances in Solid State Physics*. Springer Science, 2001.

[17] A. De Almeida, B. Santos, B. Paolo, and M. Quicheron. “Solid state lighting review–Potential and challenges in Europe”. In: *Renewable and Sustainable Energy Reviews* 34 (2014), pp. 30–48.

[18] W. A. Thornton. “Luminosity and color-rendering capability of white light”. In: *Journal of the Optical Society of America* 61.9 (1971), pp. 1155–1163.

[19] C. R. Ronda. *Luminescence: From Theory to Applications*. John Wiley & Sons, 2007.

[20] P. Pust, V. Weiler, C. Hecht, et al. “Narrow-band red-emitting $Sr[LiAl_3N_4]:Eu^{2+}$ as a next-generation LED-phosphor material”. In: *Nature materials* 13.9 (2014), pp. 891–896.

[21] L. Vayssieres et al. “Growth of arrayed nanorods and nanowires of ZnO from aqueous solutions”. In: *Advanced Materials* 15.5 (2003), pp. 464–466.

[22] M. C. Tamargo. *II-VI Semiconductor Materials and their Applications*. Vol. 12. CRC Press, 2002.

[23] *The Nobel Prize in Physics 2014*. `http://www.nobelprize.org/nobel_prizes/physics/laureates/2014/`.

[24] J. Piprek. *Nitride Semiconductor Devices: Principles and Simulation*. John Wiley & Sons, 2007.

[25] P. Mottier. *LED for Lighting Applications*. Vol. 134. John Wiley & Sons, 2010.

[26] H. Amano, N. Sawaki, I. Akasaki, and Y. Toyoda. “Metalorganic vapor phase epitaxial growth of a high quality GaN film using an AlN buffer layer”. In: *Applied Physics Letters* 48.5 (1986), pp. 353–355.

[27] S. Brochen, J. Brault, S. Chenot, et al. “Dependence of the Mg-related acceptor ionization energy with the acceptor concentration in p-type GaN layers grown by molecular beam epitaxy”. In: *Applied Physics Letters* 103.3 (2013), p. 032102.

[28] M. A. Reshchikov and H. Morkoç. “Luminescence properties of defects in GaN”. In: *Journal of applied physics* 97.6 (2005), p. 061301.

[29] M. Leroux, N. Grandjean, B. Beaumont, et al. “Temperature quenching of photoluminescence intensities in undoped and doped GaN”. In: *Journal of Applied Physics* 86.7 (1999), pp. 3721–3728.

[30] C. W. Bunn. “The lattice-dimensions of zinc oxide”. In: *Proceedings of the Physical Society* 47.5 (1935), p. 835.

[31] E. Mollwo. “Die wirkung von wasserstoff auf die leitfähigkeit und lumineszenz von zinkoxydkristallen”. In: *Zeitschrift für Physik* 138.3-4 (1954), pp. 478–488.

[32] A. E. Tsurkan, N. D. Fedotova, L. V. Kicherman, and P. G. Pas’ ko. “Injection electroluminescence in n-ZnO-p-ZnTe heterojunctions”. In: *Semiconductors* 6 (1975), p. 1183.

[33] L. J. Brillson. “Chemical reaction and charge redistribution at metal–semiconductor interfaces”. In: *Journal of Vacuum Science & Technology* 15.4 (1978), pp. 1378–1383.

[34] Z. W. Pan, Z. R. Dai, and Z. L. Wang. “Nanobelts of semiconducting oxides”. In: *Science* 291.5510 (2001), pp. 1947–1949.

[35] X. Y. Kong, Y. Ding, R. Yang, and Z. L. Wang. “Single-crystal nanorings formed by epitaxial self-coiling of polar nanobelts”. In: *Science* 303.5662 (2004), pp. 1348–1351.

[36] X. Y. Kong and Z. L. Wang. “Spontaneous polarization-induced nanohelixes, nanosprings, and nanorings of piezoelectric nanobelts”. In: *Nano Letters* 3.12 (2003), pp. 1625–1631.

[37] C. F. Klingshirn, A. Waag, A. Hoffmann, and J. Geurts. *Zinc oxide: from fundamental properties towards novel applications*. Vol. 120. Springer Science & Business Media, 2010.

[38] Z. L. Wang. *Piezotronics and Piezo-Phototronics*. Springer Science & Business Media, 2012.

[39] P. Yang, H. Yan, S. Mao, et al. “Controlled growth of ZnO nanowires and their optical properties”. In: *Advanced Functional Materials* 12.5 (2002), p. 323.

[40] C. Kirchner, T. Gruber, F. Reuss, et al. “MOVPE growth of ZnO using various oxygen precursors”. In: *Journal of Crystal Growth* 248 (2003), pp. 20–24.

[41] L. Vayssieres, K. Keis, S. E. Lindquist, and A. Hagfeldt. “Purpose-built anisotropic metal oxide material: 3D highly oriented microrod array of ZnO”. In: *The Journal of Physical Chemistry B* 105.17 (2001), pp. 3350–3352.

[42] Y. Wang, X. Li, N. Wang, X. Quan, and Y. Chen. “Controllable synthesis of ZnO nanoflowers and their morphology-dependent photocatalytic activities”. In: *Separation and Purification Technology* 62.3 (2008), pp. 727–732.

[43] T. M. Shang, J. H. Sun, Q. F. Zhou, and M. Y. Guan. “Controlled synthesis of various morphologies of nanostructured zinc oxide: flower, nanoplate, and urchin”. In: *Crystal Research and Technology* 42.10 (2007), pp. 1002–1006.

[44] M. N. R. Ashfold, R. P. Doherty, N. G. Ndifor-Angwafor, D. J. Riley, and Y. Sun. “The kinetics of the hydrothermal growth of ZnO nanostructures”. In: *Thin Solid Films* 515.24 (2007), pp. 8679–8683.

[45] S. Baruah and J. Dutta. “Hydrothermal growth of ZnO nanostructures”. In: *Science and Technology of Advanced Materials* 10.1 (2009), p. 013001.

[46] A. Sugunan, H. C. Warad, M. Boman, and J. Dutta. “Zinc oxide nanowires in chemical bath on seeded substrates: role of hexamine”. In: *Journal of Sol-Gel Science and Technology* 39.1 (2006), pp. 49–56.

[47] L. E Greene, M. Law, D. H. Tan, et al. “General route to vertical ZnO nanowire arrays using textured ZnO seeds”. In: *Nano Letters* 5.7 (2005), pp. 1231–1236.

[48] L. W. Ji, S. M. Peng, J. S. Wu, et al. “Effect of seed layer on the growth of well-aligned ZnO nanowires”. In: *Journal of Physics and Chemistry of Solids* 70.10 (2009), pp. 1359–1362.

[49] C. Y. Kung, S. L. Young, M. C. Kao, et al. “Thickness effect of sputtered ZnO seed layer on the electrical properties of Li-doped ZnO nanorods and application on the UV photodetector”. In: *Nanoelectronics Conference (INEC), 2013 IEEE 5th International*. IEEE. 2013, pp. 417–420.

[50] K. A. Wahid, W. Y. Lee, H. W. Lee, et al. “Effect of seed annealing temperature and growth duration on hydrothermal ZnO nanorod structures and their electrical characteristics”. In: *Applied Surface Science* 283 (2013), pp. 629–635.

[51] D. Yun, X. Xia, S. Zhang, et al. “ZnO nanorod arrays with different densities in hybrid photovoltaic devices: Fabrication and the density effect on performance”. In: *Chemical Physics Letters* 516.1 (2011), pp. 92–95.

[52] H. Xu, H. Wang, Y. C. Zhang, et al. “Hydrothermal synthesis of zinc oxide powders with controllable morphology”. In: *Ceramics International* 30.1 (2004), pp. 93–97.

[53] H. Y. Ku and L. C. Scala. “Polymeric electron beam resists”. In: *Journal of The Electrochemical Society* 116.7 (1969), pp. 980–985.

[54] J. E. Mark. *Polymer Data Handbook*. Vol. 27. Oxford university press New York, 2009.

[55] I. Y. Evchuk, R. I. Musii, R. G. Makitra, and R. E. Pristanskii. “Solubility of polymethyl methacrylate in organic solvents”. In: *Russian Journal of Applied Chemistry* 78.10 (2005), pp. 1576–1580.

[56] R. F. Kubin and A. N. Fletcher. “Fluorescence quantum yields of some rhodamine dyes”. In: *Journal of Luminescence* 27.4 (1983), pp. 455–462.

[57] T. Jüstel, H. Nikol, and C. Ronda. “New developments in the field of luminescent materials for lighting and displays”. In: *Angewandte Chemie International Edition* 37.22 (1998), pp. 3084–3103.

[58] BASF SE. *Lumogen F Collector Dyes - Technical Information*. 1997.

[59] e2v technologies ltd. *Technical Note on UV Conversion Coatings: LUMOGEN (also known as LUMILUX, LIUMOGEN AND LUMIGEN)*. 2003.

[60] A. F. Mansour, M. G. El-Shaarawy, S. M. El-Bashir, M. K. El-Mansy, and M. Hammam. “Optical study of perylene dye doped poly (methyl methacrylate) as fluorescent solar collector”. In: *Polymer International* 51.5 (2002), pp. 393–397.

[61] L. Shamsuddin, S. S. MdIzah, and K. Mohamed. “Comparative Study of PMMA 120K and 996K for Electron Beam Lithography Application”. In: *Australian Journal of Basic and Applied Sciences* 15.8 (2014), pp. 55–58.

[62] D. F. Croxall, R. C. C. Ward, C. A. Wallace, and R. C. Kell. “Hydrothermal growth and investigation of Li-doped zinc oxide crystals of high purity and perfection”. In: *Journal of Crystal Growth* 22.2 (1974), pp. 117–124.

[63] L. E. Greene, M. Law, J. Goldberger, et al. “Low-temperature wafer-scale production of ZnO nanowire arrays”. In: *Angewandte Chemie International Edition* 42.26 (2003), pp. 3031–3034.

[64] X. Wang, J. Cole, and H. O. Jacobs. “Electroluminescence of ZnO nanowire/p-GaN heterojunction light emitting diodes”. In: *Proceedings of 2007 NSTI Nanotechnology Conference*. Vol. 4. Citeseer. 2007, pp. 526–529.

[65] J. T. Chen, W. C. Lai, C. H. Chen, et al. “Electroluminescence of ZnO nanocrystal in sputtered ZnO-SiO 2 nanocomposite light-emitting devices”. In: *Optics Express* 19.12 (2011), pp. 11873–11879.

[66] L. Zhang, Q. Li, C. Qu, et al. “White electroluminescence from ZnO nanorods/p-GaN heterojunction light-emitting diodes under reverse bias”. In: *Journal of Optics* 15.2 (2013), p. 025003.

[67] OSRAM Opto Semiconductors. *OSRAM TOPLED long life LUW T6SG Datasheet*. 2010.

[68] Nichia Corporation. *Specifications for white LED NHSW157AT*. 2005.

[69] CREE LED Light. *SMD LED Model LM1-EWN1-01-N2 Datasheet*. 2005.

[70] F. Caruso, M. Mosca, R. Macaluso, E. Feltin, and C. Calı. “Generation of white LED light by frequency downconversion using perylene-based dye”. In: *Electronics Letters* 48.22 (2012), pp. 1417–1419.

[71] M. Mosca, F. Caruso, L. Zambito, et al. “Warm white LED light by frequency downconversion of mixed yellow and red Lumogen”. In: *SPIE Microtechnologies*. International Society for Optics and Photonics. 2013, pp. 87670L–87670L.

[72] A. F. Mansour. “Optical efficiency and optical properties of luminescent solar concentrators”. In: *Polymer Testing* 17.5 (1998), pp. 333–343.

[73] A. V. Deshpande and E. B. Namdas. “Correlation between lasing and photophysical performance of dyes in polymethylmethacrylate”. In: *Journal of Luminescence* 91.1 (2000), pp. 25–31.

[74] P. Wang, S. M. Zakeeruddin, P. Comte, I. Exnar, and M. Grätzel. “Gelation of ionic liquid-based electrolytes with silica nanoparticles for quasi-solid-state dye-sensitized solar cells”. In: *Journal of the American Chemical Society* 125.5 (2003), pp. 1166–1167.

[75] M. Kopietz, M. D. Lechner, D. G. Steinmeier, et al. “Light-induced refractive index changes in polymethylmethacrylate (PMMA) blocks”. In: *Polymer Photochemistry* 5.1 (1984), pp. 109–119.

[76] J. O. Choi, J. A. Moore, J. C. Corelli, J. P. Silverman, and H. Bakhru. “Degradation of poly (methylmethacrylate) by deep ultraviolet, x-ray, electron beam, and proton beam irradiations”. In: *Journal of Vacuum Science & Technology B* 6.6 (1988), pp. 2286–2289.

[77] A. Torikai, M. Ohno, and K. Fueki. “Photodegradation of poly (methyl methacrylate) by monochromatic light: Quantum yield, effect of wavelengths, and light intensity”. In: *Journal of Applied Polymer Science* 41.5-6 (1990), pp. 1023–1032.

[78] B. Dickens, J. W. Martin, and D. Waksman. “Thermal and photolytic degradation of plates of poly (methyl methacrylate) containing monomer”. In: *Polymer* 25.5 (1984), pp. 706–715.

[79] P. Cacioli, G. Moad, E. Rizzardo, A. K. Serelis, and D. H. Solomon. “The use of model compounds in interpreting the thermal degradation of poly (methy methacrylate)”. In: *Polymer Bulletin* 11.4 (1984), pp. 325–328.

[80] P. Henzi, K. Bade, D. G. Rabus, and J. Mohr. “Modification of polymethylmethacrylate by deep ultraviolet radiation and bromination for photonic applications”. In: *Journal of Vacuum Science & Technology B* 24.4 (2006), pp. 1755–1761.

List of Figures

List of Tables

Appendix A

Scientific Activity

Publications on International Peer-Reviewed Journals

1. **F. Caruso**, M. Mosca, S. Rinella, R. Macaluso, C. Calì, F. Saiano, and E. Feltin. "Frequency-Downconversion Stability of PMMA Coatings in Hybrid White Light Emitting Diodes". *Journal of Electronic Materials*, vol. 45, issue 1, pp. 682-687, 2016. DOI: 10.1007/s11664-015-4173-y.

2. R. Macaluso, M. Mosca, V. Costanza, A. D'Angelo, G. Lullo, **F. Caruso**, C. Calì, F. Di Dranco, M. Santamaria, and F. Di Quarto. "Resistive switching behaviour in ZnO and VO_2 memristors grown by pulsed laser deposition". *Electronics Letters*, vol. 50, issue 4, pp. 262 – 263, 2014. DOI: 10.1049/el.2013.3175.

3. M. Mosca, R. Macaluso, G. Randazzo, M. Di Bella, **F. Caruso**, C. Calì, F. Di Franco, M. Santamaria, and F. Di Quarto. "Anodized Ti-Si alloy as gate oxide of electrochemically-fabricated organic field-effect transistors". *ECS Solid State Letters*, vol. 3, issue 1, P7 - P9, 2014. DOI: 10.1149/2.007401ssl.

4. **F. Caruso**, M. Mosca, R. Macaluso, E. Feltin and C. Calì, "Generation of white LED light by frequency down-conversion using a perylene-based dye". *Electronics Letters*, vol. 48, issue 22, pp. 1417 - 1419, 2012. DOI: 10.1049/el.2012.3084.

Publications on Other Journals

1. M. Mosca, **F. Caruso**, L. Zambito, R. Macaluso, C. Calì, E. Feltin, "Hybrid LEDs Pave Way to New Lighting Applications". *Photonics Spectra*, vol. 47, pp. 60 - 64, 2013. ISSN: 0731-1230.

Proceedings of National and International Conferences and Congresses

1. **F. Caruso**, M. Mosca, R. Macaluso, C. Calì, E. Feltin, “Well-Aligned Hydrothermally Synthesized Zinc Oxide Nanorods on p-GaN without a Seed Layer”, *IEEE 15th International Conference on Nanotechnology*, Book of Abstracts, Rome (Italy), July 27 – 30, 2015.

2. **F. Caruso**, M. Mosca, S. Rinella, R. Macaluso, C. Calì, F. Saiano, E. Feltin, “Stability improvement of PMMA and Lumogen® coatings for hybrid white LEDs”, *10th International Conference on Electroluminescence and Organic Optoelectronics*, Book of Abstracts, p. 180. Cologne (Germany), August 31 – September 3, 2014.

3. M. Mosca, **F. Caruso**, B. Seminara, L. Zambito, R. Macaluso, C. Calì, E. Feltin, “Warm white LEDs based on Lumogen® Red and Yellow”. *Proceedings of GE2013, 45th annual meeting of Italian Group of Electronics*, pp. 109 - 110. Udine (Italy), June 19 - 21, 2013. ISBN: 978-88-903069-3-8.

4. M. Mosca, **F. Caruso**, L. Zambito, B. Seminara, R. Macaluso, C. Calì, E. Feltin, “Warm white LED light by frequency down-conversion of mixed yellow and red Lumogen®”. *Proceedings of SPIE 8767, Integrated Photonics: Materials, Devices and Applications II*, 87670L-1 - 87670L-10, May 22, 2013. ISBN: 978-0-8194-9564-8.

5. M. Mosca, **F. Caruso**, L. Zambito, B. Seminara, R. Macaluso, C. Calì, E. Feltin, “Warm white LED light by frequency down-conversion of mixed perylene-based dyes”. *SPIE Microtechnologies Conference; Integrated Photonics: Materials, Devices and Applications*, Book of Abstracts, pp. 69 – 70. Grenoble (France), April 24 - 26, 2013.

6. M. Mosca, **F. Caruso**, R. Macaluso, C. Calì, E. Feltin, “White LED light obtained by frequency down-conversion of perylene-based dyes”. *Proceedings of GE2012, 44th annual meeting of Italian Group of Electronics*. Marina di Carrara (Italy), June 20 - 22, 2012. ISBN: 978-88-6741-012-5.

7. **F. Caruso**, M. Mosca, R. Macaluso, C. Calì, “Fabbricazione di LED bianchi tramite down-conversion di coloranti basati su perilene”. *Proceedings of Fotonica 2012 - 14esimo Convegno Nazionale delle Tecnologie Fotoniche*. Firenze (Italy), May 15 - 17, 2012. ISBN: 9788887237146.

Book Chapters

- M. Mosca, R. Macaluso, **F. Caruso**, V. Lo Muzzo, C. Calì, “The *p*-Type Doping of ZnO: Mirage or Reality?”, *Advances in Semiconductor Research: Physics of Nanosystems, Spintronics and Technological Applications*, Chapter 12, edited by D. Persano Adorno and S. Pokutnyi, Nova Science Publishers, New York, 2014. ISBN: 978-1-63321-788-1.

Research Period Spent Abroad

- May 2015 - October 2015: Internship at the *Equipe Nano* of the CNRS - Centre de Recherche sur l’Hétéro-Epitaxie et ses Application in Valbonne (France). Advisor: Dr. Jesús Zúñiga-Pérez.

Professional Qualifications

- Since September 2013: member of SPIE - the international society for optics and photonics.

- Since January 2014: member of IEEE - Institute of Electrical and Electronics Engineers.

- Since October 2014: member of AIGE - Associazione Italiana Gruppo Elettronica.